

See discussions, stats, and author profiles for this publication at: <https://www.researchgate.net/publication/267730899>

Quest for Nonaqueous Multivalent Secondary Batteries: Magnesium and Beyond

ARTICLE *in* CHEMICAL REVIEWS · OCTOBER 2014

Impact Factor: 46.57 · DOI: 10.1021/cr500049y · Source: PubMed

CITATIONS

31

READS

163

3 AUTHORS, INCLUDING:



John Muldoon

Toyota Research Institute of North America

23 PUBLICATIONS 1,324 CITATIONS

[SEE PROFILE](#)



Claudiu Bucur

Toyota Research Institute of North America

12 PUBLICATIONS 336 CITATIONS

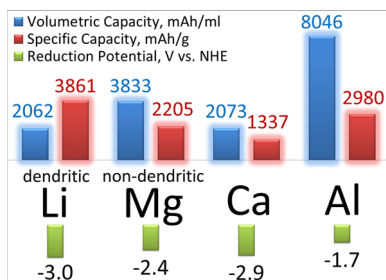
[SEE PROFILE](#)

Quest for Nonaqueous Multivalent Secondary Batteries: Magnesium and Beyond

John Muldoon,*[†] Claudiu B. Bucur,[†] and Thomas Gregory[‡]

[†]Toyota Research Institute of North America, 1555 Woodridge Avenue, Ann Arbor, Michigan 48105, United States

[‡]Borealis Technology Solutions LLC, Midland, Michigan 48642, United States



CONTENTS

1. Introduction
 2. Magnesium
 - 2.1. Electrolytes
 - 2.1.1. From Grignards to Magnesium Organo-haloaluminate Electrolytes
 - 2.1.2. Magnesium Organoborates
 - 2.1.3. Corrosive Nature of Magnesium Electrolytes
 - 2.1.4. Electrolytes with Magnesium Alloy Anodes
 - 2.1.5. Polymeric Gel Magnesium Electrolytes
 - 2.1.6. Ionic Liquids
 - 2.2. Cathodes
 - 2.2.1. Intercalation Cathodes
 - 2.2.2. Conversion Cathodes
 - 2.2.3. Mg Cathode Summary
 3. Calcium
 - 3.1. Electrochemistry of Ca Electrodes in SOCl_2
 - 3.2. Organic Solvents and Salts
 - 3.3. Challenges in Developing New Calcium Electrolytes
 4. Aluminum
 - 4.1. Electroplating Baths as Aluminum Electrolytes
 - 4.2. Cathodes for Rechargeable Aluminum Batteries
 5. Closing Remarks
- Author Information
- Corresponding Author
 - Notes
 - Biographies
- Acknowledgments
- Glossary
- References

A
B
B
B
E
G
I
I
L
M
M
Y
Z
AA
AA
AB
AB
AC
AC
AF
AG
AG
AG
AG
AG
AH
AH
AH

1. INTRODUCTION

Solar radiation provides direct energy input to the earth's biosphere sustaining both biological and physical processes. Monumental industrial progress was ushered in by the discovery of technologies which enabled the recycling and repurposing of a portion of this energy by combustion of fossilized carbon matter derived from living tissues. Through natural processes these fossil fuels sediment in the earth's crust over geological periods of time. As the rate of their exploitation surpasses the rate of their formation an overall decline in the availability of these reserves can be expected. Diversification of primary energy sources into alternative sources which are renewable over the time scale of their exploitation promises reduced environmental footprint and improved sustainability. Implementation of such technologies, including direct solar, hydroelectric, thermal, and wind energy capture, could mark the advent of a new industrial era. This transition will require implementation of strategies such as novel energy storage technologies to compensate the intermittent characteristics of such alternative energy generation technologies and provide power on demand or on schedules similar to those provided by existing electric grids.^{1–3}

Motive power represents an additional and a substantial opportunity for utilizing energy storage to minimize emissions of pollutants and greenhouse gases as well as substantially reduce fuel consumption. Toyota considers this a top priority and introduced the first-generation hybrid electric Prius in Japan in 1997. Currently, Toyota sells numerous hybrid models; consumer acceptance of this technology has resulted in global sales of 3.1 million hybrid electric vehicles (HEVs). As of March 2011, the reduced fuel consumption enabled by this hybrid technology has also reduced CO_2 emissions by 19 million tons. Plug-in hybrid electric vehicles (PHEV) and full electric vehicles (EV), which promise further fuel consumption and emission reductions, have recently been introduced by Toyota.⁴ Keys to increasing the market acceptance of these vehicle technologies are reduced cost and increased range under electric power which will require further advances in battery technology. In particular, development of batteries with improved energy density and cost per unit of stored energy vs existing commercially available Li-ion batteries is essential. Development of post-lithium-ion battery technologies is considered to be a promising pathway to achieving these goals.^{5–9} Post-lithium-ion batteries (PLIB) can be defined as

Special Issue: 2014 Batteries

Received: January 28, 2014

batteries with a higher theoretical energy density than existing lithium-ion batteries containing a carbon anode and a lithium metal oxide cathode (~2000 Wh/L based on active materials). Thus, development of PLIB's may require the substitution of lithiated graphite or alloy-based anodes with pure metal anodes. Lithium metal is considered to be a strong candidate due its high volumetric capacity of 2062 mAh/mL and highly negative reduction potential of -3.04 V vs SHE (Figure 1). However,

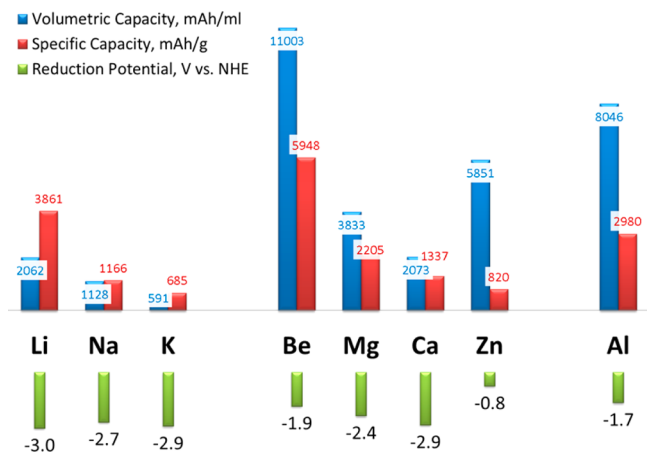


Figure 1. Capacities and reductive potentials for various metal anodes.

successful commercialization of rechargeable batteries containing lithium metal anodes has been hampered by the inherent instability of lithium metal, especially during the charge cycle when lithium metal is redeposited at the anode.^{3,10,11} Dendritic deposition of lithium metal can result in short circuits leading to internal heating and subsequent thermal runaway due to exothermic chemical reactions involving battery components. Recent approaches to stabilize the lithium metal anode and avoid dendrite formation include development of new electrolytes or additives^{12–15} which promote more uniform lithium electrodeposition. In particular, development of electrolyte additives such as chlorosilanes, chlorophosphines, and chloroboranes, which appear to form protective layers on the lithium anode surface through reaction with Li, represents a significant advance in this area. These protective layers apparently stabilize electrochemical cycling of lithium metal.^{10,16–19}

Magnesium is an alkaline earth metal which has nearly double the volumetric capacity (3832 mAh/mL) of lithium with a very negative reduction potential of -2.4 V vs SHE. The volumetric energy density of a battery pack becomes important when there is a limited volume for mounting it. A high volumetric energy density is more desirable for mobile devices (such as vehicles or assistive robots) than for stationary energy storage. The more portable the device (such as personal electronics), the less space is available for its battery and the volumetric energy density plays a crucial role. In addition, magnesium metal anodes do not appear to be plagued by dendrite formation to the same degree as lithium.^{20,21} Additionally, air exposure is much less of a safety and processing issue with magnesium than it is with lithium. Magnesium is also far more abundant in the earth's crust, resulting in wider availability and much lower cost. Use of alkali metals such as lithium in batteries is enabled by formation of a passive layer via reaction with the electrolyte to form a solid electrolyte interface which is blocking to electrons but not to the alkali metal cations. This allows transport of lithium ions

between the anode and the electrolyte without substantial degradation of either component. The alkaline earth metals, however, tend to form analogous passivation films through which cations diffuse sluggishly or not at all.²² Although this would be expected to hamper magnesium electrode performance especially during the charge cycle, effective magnesium electrodeposition was achieved from ethereal solutions of Grignard reagents as early as 1927, demonstrating the critical use of Mg metal anodes.²³

Research in lithium-ion cathodes has evolved toward attempts to achieve two-electron reduction at a single metal redox center.^{24–28} This offers the promise of doubling the capacity of current cathode materials but has to overcome the challenge of inserting two lithium cations for every transition metal center in the cathode material. This is not trivial due to the volume expansion resulting from insertion of two lithium cations. Interestingly, two-electron reduction can be achieved by insertion of a single divalent magnesium cation which has a similar radius to a monovalent lithium cation (ionic radius of Li^+ is 0.9 Å and of Mg^{2+} 0.86 Å), thus circumventing the excessive volume expansion problem. However, the higher charge density of magnesium cations poses solid-state diffusion challenges. A battery containing a calcium anode may have some advantages over a battery containing a magnesium anode due to the more negative reductive potential of calcium (~ 500 mV more negative). In addition, the ionic radius of the calcium cation (Ca^{2+}) is 33% (1.14 Å) larger while carrying the same charge. This lower charge density may allow faster solid-state diffusion in cathodes. However, due to the lack of suitable electrolytes, reversible cycling of a calcium metal anode has not been reported. Interestingly, volumetric capacities higher than magnesium or calcium can be achieved by denser multivalent metals such as aluminum and zinc. Unfortunately, their reduction potentials are significantly less negative. The reduction potential of zinc is 2.2 V more positive than lithium, and most zinc electrochemistry is aqueous and outside the scope of this paper which discusses nonaqueous electrochemistries of multivalent metals.^{29–32} While the reduction potential of aluminum is -1.7 V vs SHE, its volumetric capacity (8045 mAh/mL) is nearly four times higher than lithium. Unlike calcium, electrodeposition of aluminum has a rich history due to the well-established aluminum electroplating industry. While offering impressive Coulombic efficiencies close to 100%, aluminum electrolyte baths are often corrosive, which hinders discovery of high-voltage cathodes. There are however several reports of rechargeable aluminum batteries operating below 1 V which are presented in this review.

Most of the research efforts on rechargeable multivalent batteries have focused on nonaqueous magnesium electrochemistry. In this review we highlight recent progress on the development of both electrolytes and cathodes for magnesium batteries. In addition, we discuss progress and give our insight toward rechargeable calcium and aluminum batteries.

2. MAGNESIUM

2.1. Electrolytes

2.1.1. From Grignards to Magnesium Organohaloaluminate Electrolytes. Reports of effective magnesium electrodeposition from Grignard reagents in ethereal solutions date back to the early part of the 20th century and have periodically appeared in the literature ever since.^{23,33–40} In an attempt to enhance the stability of the electroplating baths based on

Grignards, in 1957 Connor et al. investigated the electro-deposition of magnesium from magnesium borohydride $Mg(BH_4)_2$ generated in situ by reaction of $MgBr_2$ and $LiBH_4$.³⁶ Unfortunately, boron and magnesium codeposit in a 1:9 ratio.³⁶ Use of $Mg(BH_4)_2$ as an electrolyte for magnesium batteries has been recently demonstrated by Mohtadi et al.⁴¹ The electrochemical performance of $Mg(BH_4)_2$ in glyme is superior to that in THF, and surprisingly, addition of $LiBH_4$ dramatically enhances the current densities of magnesium deposition. In contrast to the impure magnesium deposit obtained from the in-situ reaction of $MgBr_2$ and $LiBH_4$ reported by Connor, XRD analysis shows pure magnesium metal deposition when high-grade magnesium borohydride is used. Unfortunately, the oxidative stability of $Mg(BH_4)_2$ has been reported as being similar to that of Grignard solutions. Early reports of Connor et al. also include evaluation of concentrated solutions of $MgBr_2$ and in-situ-generated $Mg(AlH_4)_2$ from reaction of $Li(AlH_4)$ and $MgCl_2$ in a molar ratio of 2:1. The surprising reversibility of magnesium deposition from a 2.5 M solution of $MgBr_2$ has also been recently reported by Abe et al.^{42,43} Other reports of magnesium deposition from boron-based compounds came in 1971 from Brenner, who evaluated electroplating from magnesium decaborane generated from the reaction of a lithium decaborane complex with $MgCl_2$ in THF.³⁷ Since Brenner's electrolyte based on a boron hydride cluster was evaluated as an electroplating bath, its oxidative stability was not reported.

One of the obstacles in developing high-voltage rechargeable magnesium batteries is moving beyond the oxidative stability of Grignards such as ethylmagnesium bromide ($EtMgBr$) and butylmagnesium chloride ($BuMgCl$) which have an oxidative stability of 1.3 V vs Mg. The low oxidative stability of Grignard solutions limits the choice of available cathodes. In 1990, Gregory et al. synthesized the electrolyte $Mg(B(C_4H_9)_4)_2$ from reaction of dibutylmagnesium and the Lewis acid tri-*n*-butylborane, which showed enhanced oxidative stability versus $BuMgBr$.⁴⁴ It was assumed that the character of the Lewis acid could be a factor in improving the voltage stability. Gregory also evaluated magnesium deposit quality by spiking of alkyl Grignards such as ethylmagnesium chloride ($EtMgCl$) and methylmagnesium chloride ($MeMgCl$) with aluminum trichloride ($AlCl_3$) to enhance electrochemical plating. In addition, Gregory evaluated the magnesium organoborate electrolyte $Mg(B(C_4H_9)_4)_2$ with several cathodes such as Co_3O_4 , Mn_2O_3 , RuO_2 , and ZrS_2 . In the same year, Mayer investigated the electrodeposition of magnesium from organometallic electrolytes.⁴⁵ Mayer's initial attempt at formulating magnesium plating electrolytes was to evaluate complexes of dialkylmagnesium (R_2Mg) and metal fluorides such as sodium fluoride with 2 equivalent of dibutylmagnesium (Bu_2Mg). This solution showed no magnesium deposition. However, when alkylaluminum Lewis acids were slowly added to the mixture, the solution showed good conductivity and deposition of pure magnesium was observed (>99%). Mayer concluded that electrolytes containing a molar ratio of aluminum alkyls such as tri-isobutylaluminum (iso- $(C_4H_9)_3Al$) or triethylaluminum ($AlEt_3$) to R_2Mg such as Bu_2Mg of 3.5:1 or less deposited essentially pure magnesium. Following on this observation, Aurbach et al. investigated the Coulombic efficiency and oxidative stability of electrolytes as a function of different combinations and ratios of organomagnesium compounds (R_2Mg) to Lewis acids. Surprisingly, no magnesium deposition was obtained from THF solutions of dialkylmagnesium Lewis

bases in combination with a wide variety of Lewis acids (BPh_2Cl , $BPhCl_2$, $B[(CH_3)_2N]$, BEt_3 , BBr_3 , BF_3 , $SbCl_3$, $SbCl_5$, PPh_3 , PEt_2Cl , $AsPh_3$, $FeCl_3$, and TeF_3).⁴⁶ However, reaction of 1 equivalent of dibutylmagnesium and 2 equivalent of ethylaluminum chloride in-situ generated magnesium organohaloaluminate with a given formula of $Mg(AlCl_2BuEt)_2$ (designated DCC). This electrolyte exhibited an electrochemical stability window of 2.4 V and 100% Coulombic efficiency (Figure 2) for reversible deposition of magnesium.^{47,48}

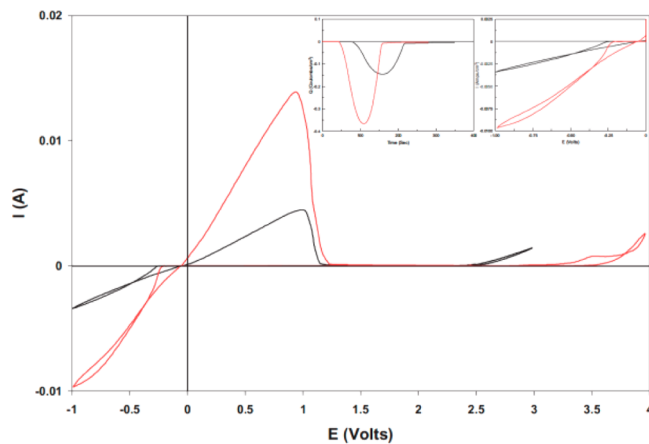


Figure 2. Comparison between the voltammetric behavior of THF solutions containing 0.25 M of the reaction product between 1:2 $MgBu_2$ and $AlCl_2Et$ (DCC) and 0.4 M of the reaction product between 1:2 $AlCl_3$ and $PhMgCl$ (designated APC) as indicated; 25 $mV\ s^{-1}$, Pt wire working electrode, 25 $^{\circ}C$. (Right insert) Enlargement of the cyclic voltammograms near 0 V vs Mg reference electrode, comparing the overpotential for Mg deposition in the two solutions. (Left insert) Charge balance upon typical Mg deposition–dissolution cycles in these solutions (100% cycling efficiency of Mg deposition). Reprinted with permission from ref 48. Copyright 2007 WILEY-VCH Verlag GmbH & Co. KGaA, Weinheim.

To facilitate analysis of the structure of this DCC electrolyte, single crystals of the solute were precipitated from a THF solution by addition of hexane. However, dissolution of the precipitated crystal $(Mg_2(\mu-Cl)_3\cdot 6THF)(EtAlCl_3)$ in THF did not result in an electrochemically active solution.^{46,49,50}

Aurbach concluded that cleavage of the relatively weak Al–C bond in DCC electrolyte via β -H elimination limits the electrochemical window and is thus the main weakness of DCC. Substitution of the ethyl groups on the Lewis acid with a methyl or phenyl group, which excludes β -H elimination as a possible oxidation route, was found to enlarge the electrochemical stability window. In particular, a magnesium organohaloaluminate called APC generated in situ via reaction of 1 equivalent of $AlCl_3$ with 2 equivalent of $PhMgCl$ displayed a significantly broader electrochemical stability window of 3.3 V vs Mg on a Pt working electrode and a Coulombic efficiency of 100% for Mg deposition/dissolution (Figure 3). Additionally, this electrolyte possesses a specific conductivity of 2 mS/cm . NMR, FTIR, and Raman spectroscopy studies reveal that the solution consists of a mixture of THF-coordinated Mg complexes including $MgCl_2$, $MgCl^+$, $Mg_2Cl_3^+$, Ph_2Mg , and $PhMgCl$.⁵¹ One can assume that the key step in formation of the magnesium organohaloaluminate APC is transmetalation of the phenyl group from Mg to Al to yield the $PhAlCl_3^-$ anion. A proposed route to account for formation of other anions

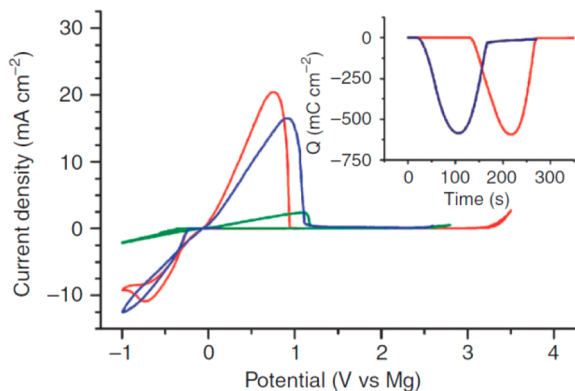


Figure 3. Cyclic voltammograms of HMDSMgCl (green), the reaction product generated *in situ* from a 3:1 mixture of HMDSMgCl to AlCl_3 (blue), and the crystal obtained from a 3:1 mixture of HMDSMgCl to AlCl_3 (designated GEN1) (red). (Inset) Charge balance during deposition and subsequent dissolution of Mg. Reprinted with permission from ref 52. Copyright 2011 Nature Publishing Group.

present in solution of general structure $\text{Ph}_{4-n}\text{AlCl}_n^-$ could involve reactions of PhAlCl_3^- with the nucleophilic PhMgCl or diphenylmagnesium (Ph_2Mg). Unfortunately, although the *in-situ*-generated magnesium organohaloaluminates reported so far exhibit high Coulombic efficiencies, they contain nucleophilic equilibrium products such as Ph_2Mg and are air sensitive, therefore precluding their use with electrophilic, high-capacity cathode active materials such as sulfur or oxygen. This represents a significant limitation since, for example, elemental sulfur can provide capacities as high as five times the capacity of existing Li-ion cathode materials based on transition metal oxides or phosphates.⁷ Despite its electrochemical stability, a 2:1 mixture of PhMgCl and AlCl_3 in THF has nevertheless demonstrated incompatibility with an electrophilic sulfur cathode. Direct reaction between this electrolyte and sulfur to form phenyl disulfide and biphenyl sulfide was confirmed via gas chromatography–mass spectroscopy analysis.⁵²

A promising approach to eliminating the reactivity between electrophilic cathode materials and *in-situ*-generated nucleophilic magnesium organohaloaluminates involves use of non-nucleophilic Hauser bases as electrolytes. For example, potassium hexamethyldisilazide is a non-nucleophilic base, so the corresponding Hauser base (hexamethyldisilazide magnesium chloride) (HMDSMgCl) would be expected to exhibit compatibility with electrophilic sulfur. In addition, reversible magnesium deposition has been demonstrated from solutions of HMDSMgCl at current densities similar to those achieved with Grignard reagent-based electrolytes.⁵³ Similar to the previous work of Aurbach et al., addition of AlCl_3 to solutions of HMDSMgCl was found to increase the current density for magnesium deposition by a factor of 7. However, AlCl_3 addition did not result in improvement of the voltage stability of HMDSMgCl-containing electrolytes (Figure 3).

Crystallization of the product of the reaction between HMDSMgCl and AlCl_3 was accomplished by slow diffusion of hexane. This material was identified as crystalline $(\text{Mg}_2(\mu\text{-Cl})_3\cdot6\text{THF})(\text{HMDSAlCl}_3)$ by single-crystal X-ray diffraction (Figure 4a).

The cation was comprised of two octahedrally coordinated Mg centers which were bridged by three chlorine atoms. The three remaining coordination sites on each Mg center were associated with the oxygen of THF solvent. The anion was

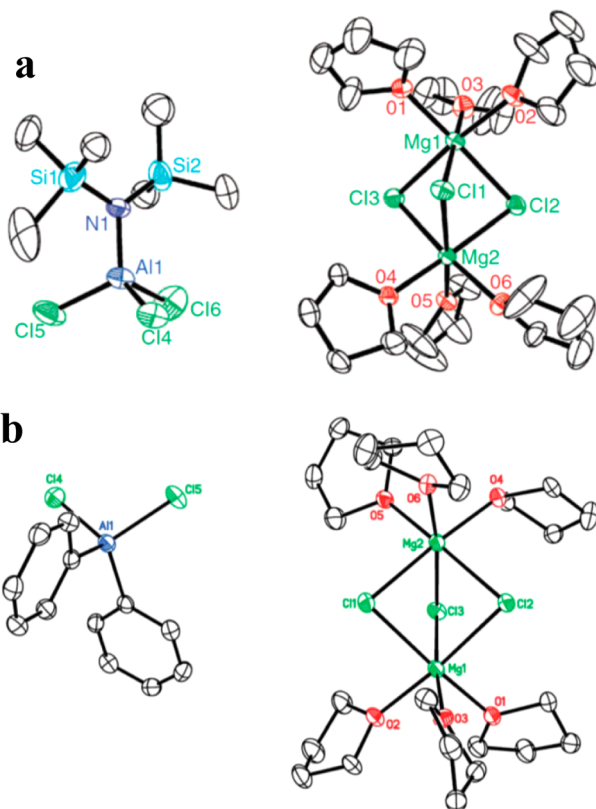


Figure 4. (a) ORTEP plot (25% thermal probability ellipsoids) of crystallized product, $(\text{Mg}_2(\mu\text{-Cl})_3\cdot6\text{THF})(\text{HMDSAlCl}_3)$ (GEN1). Hydrogen atoms, THF of crystallization, and second component of disorder are omitted for clarity. Reprinted with permission from ref 52. Copyright 2011 Nature Publishing Group. (b) ORTEP plot (25% thermal probability ellipsoids) of $(\text{Mg}_2(\mu\text{-Cl})_3\cdot6\text{THF})(\text{Ph}_2\text{AlCl}_2)$ (APC); 50% thermal probability ellipsoids; hydrogen atoms omitted for clarity. Reprinted with permission from ref 9. Copyright 2012 Royal Society of Chemistry.

comprised of an Al atom tetrahedrally coordinated by one HMDS group and three chlorides. This crystal was found to be electrochemically active in solution; preparation of the electrolyte solution from crystallized material improved both the voltage stability and the Coulombic efficiency vs the *in-situ*-generated electrolyte formed from reaction of a 3:1 mixture of HMDSMgCl and AlCl_3 . NMR and mass spectrometry analysis of the crystalline electrolyte (hereafter referred to as GEN1) confirmed that the major product is $(\text{Mg}_2(\mu\text{-Cl})_3\cdot6\text{THF})(\text{HMDSAlCl}_3)$ and the minor product $(\text{Mg}_2(\mu\text{-Cl})_3\cdot6\text{THF})(\text{HMDS}_2\text{AlCl}_2)$.⁵² Chemical stability of GEN1 was indicated by the fact that no loss in electrochemical performance was observed even after 1 year of storage in the glovebox.

Demonstration of the desired electrochemical activity of crystallized electrolyte GEN1 prompted the synthesis and experimental investigation of crystallized products obtained from *in-situ*-generated magnesium organohaloaluminates previously reported by Aurbach et al.⁴⁸ It was found that, in contrast to previous reports on crystallized DCC, crystallized $(\text{Mg}_2(\mu\text{-Cl})_3\cdot6\text{THF})(\text{EtAlCl}_3)$ obtained from reaction of *n*-butylmagnesium and ethylaluminum chloride was, in fact, electrochemically active (Figure 5).⁵² Similarly, the electrochemical activity of the crystallized reaction product between PhMgCl and AlCl_3 at a 2:1 ratio was also confirmed. Crystallization of the *in-situ*-generated electrolyte APC yields

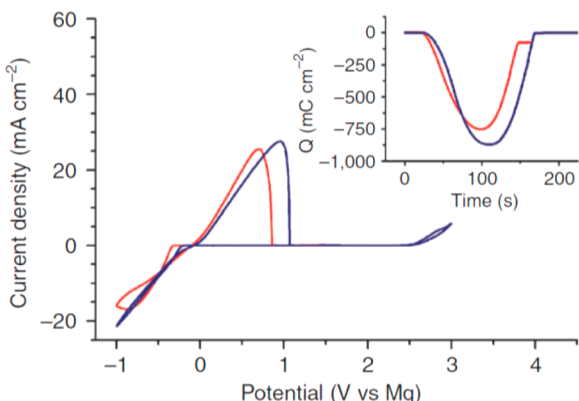


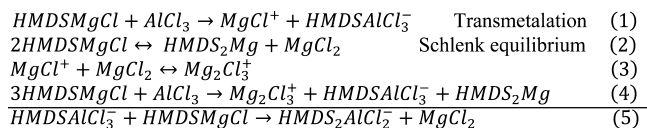
Figure 5. Cyclic voltammograms of 0.4 M THF solution of the reaction product generated *in situ* from a 2:1 mixture of Bu_2Mg to EtAlCl_2 (DCC) (blue) and the crystal obtained from a 2:1 mixture of Bu_2Mg to EtAlCl_2 (crystallized DCC) (red). Scan rate is 0.025 V s^{-1} . Reprinted with permission from ref 52. Copyright 2011 Nature Publishing Group.

a compound with general formula $(\text{Mg}_2(\mu\text{-Cl})_3\cdot 6\text{THF})\cdot (\text{Ph}_n\text{AlCl}_{4-n})$ ($n = 1\text{--}4$). The predominant product of this reaction was identified as $(\text{Mg}_2(\mu\text{-Cl})_3\cdot 6\text{THF})(\text{Ph}_2\text{AlCl}_2)$ by single-crystal X-ray diffraction (Figure 4b).

The cation $(\text{Mg}_2(\mu\text{-Cl})_3\cdot 6\text{THF})^+$ has been identified in all of the electrochemically active, crystallized magnesium organohaloaluminates, suggesting that it is the primary electrochemically active species generated from reaction between an organomagnesium compound and a Lewis acid. However, the equilibrium between the magnesium cations $(\text{Mg}_2(\mu\text{-Cl})_3\cdot 6\text{THF})^+$ and $\text{MgCl}_2/\text{MgCl}^+$ can conceivably affect the Mg electrochemistry in these solutions, and thus, the assumption that the $(\text{Mg}_2(\mu\text{-Cl})_3\cdot 6\text{THF})^+$ cation is solely responsible for magnesium deposition cannot be made with complete confidence. For example, X-ray absorption near edge structure (XANES) results indicate that the presence of a Mg species besides the Mg dimer is required before deposition of Mg occurs. The exact structure of the electrochemically active species thus remains unknown.⁵⁴

Scheme 1 shows the proposed steps in formation of GEN1.⁵² The first step involves transmetalation of the HMDS group

Scheme 1. Proposed key steps in the formation of GEN1.⁵²



from Mg to Al to yield the HMDSAlCl_3^- anion (eq 1, Scheme 1). Formation of the cation $(\text{Mg}_2(\mu\text{-Cl})_3\cdot 6\text{THF})^+$ is likely due to rapid reaction between MgCl^+ and MgCl_2 (eq 3, Scheme 1). MgCl_2 is formed *in situ* via the Schlenk equilibrium (eq 2, Scheme 1), and its depletion via reaction 3 (Scheme 1) drives the equilibrium to the right, forming additional $(\text{HMDS})_2\text{Mg}$. Recently, Zhao-Karger et al. synthesized GEN1 by reaction of $(\text{HMDS})_2\text{Mg}$ and AlCl_3 in a 1:2 ratio.⁵⁵ A proposed pathway to account for the minor product $(\text{Mg}_2(\mu\text{-Cl})_3\cdot 6\text{THF})\cdot (\text{HMDS}_2\text{AlCl}_3)$ involves further reaction of HMDSMgCl with the HMDSAlCl_3^- anion (eq 5, Scheme 1).

Similar to GEN1, crystallization of *in-situ*-generated magnesium organohaloaluminates such as DCC and APC

results in removal of their nucleophilic components. For example, solutions of the magnesium organohaloaluminate generated from reaction of a 2:1 ratio of PhMgCl and AlCl_3 (APC) contain the nucleophilic components PhMgCl and Ph_2Mg which are the reason for the reactivity of this electrolyte with elemental sulfur. Crystallization of APC removes these nucleophilic components, yielding an electrolyte, which does not react with sulfur to form biphenyl sulfide and phenyl disulfide as observed with the *in-situ*-generated organomagnesium electrolyte. NMR studies clearly demonstrate that GEN1 also has no reactivity with sulfur, and no change is observed in the ^{33}S NMR spectrum of elemental sulfur in the presence of these crystallized electrolytes even after 1 week.⁵² Thus, it is apparent that crystallized magnesium organohaloaluminate electrolytes are non-nucleophilic, whereas *in-situ*-generated magnesium organohaloaluminate electrolytes are nucleophilic and incompatible with electrophilic cathode materials such as sulfur. Further evidence for the electrochemical activity of magnesium cations coordinated with chlorine atoms and ether molecules has been reported by Doe et al., who have recently shown that *in-situ* reaction between MgCl_2 and AlCl_3 yields an electrolyte with a voltage stability of 3.1 V vs Mg and a Coulombic efficiency of 99%.⁵⁶ However, this electrolyte has not been crystallized or structurally characterized. A significant limitation of this inorganic electrolyte is a dramatically lower current density for Mg electrodeposition than that obtained with magnesium organohaloaluminates. This may be due to reduced solution conductivity in the absence of complex aluminum anions. Recently, Liu et al. prepared electrolytes with oxidative stabilities of up 3.4 V vs Mg and Coulombic efficiencies of up to 100% via reaction of MgCl_2 with aluminum Lewis acids such as AlEtCl_2 , AlPh_3 , and AlCl_3 .⁵⁷

2.1.2. Magnesium Organoborates. The electrochemically active cation in all of the crystallized magnesium organohaloaluminate electrolytes prepared thus far is $[(\text{Mg}_2(\mu\text{-Cl})_3\cdot 6\text{THF})]^+$. Thus, apparent stability differences between electrolytes are likely due to their unique anions. In the case of APC, both the crystallized and the *in-situ*-generated electrolyte contain a complex mixture of anions of the structure $(\text{AlPh}_n\text{Cl}_{4-n})^-$ ($n = 1\text{--}4$). Recently, Aurbach utilized DFT calculations to estimate the oxidative stability of the components of the *in-situ*-generated magnesium organohaloaluminate electrolyte obtained via reaction of PhMgCl with AlCl_3 using the IEFPCM model to include solvent influences.⁵¹ Studies of this electrolyte system in our lab show that the voltage stability can range anywhere between 2.9 and 3.2 V depending upon the reaction time and the ratio of the PhMgCl to AlCl_3 . This voltage stability was very difficult to control presumably due to the different ratios of the anions in both the crystallized and the *in-situ*-generated electrolyte. A proposed route to account for formation of other anions present in solution of the general structure $\text{Ph}_n\text{AlCl}_{4-n}^-$ could involve reactions of PhAlCl_3^- with the nucleophilic PhMgCl or Ph_2Mg . In order to eliminate nucleophilic substitution it would be essential to start with Al Lewis acids of the structure R_3Al , where R is aromatic. A possible strategy to extend the voltage stability beyond APC would be to move to fluorinated aluminates. Unfortunately, an attempt to crystallize 4-fluorophenyllithium resulted in an explosion. On the basis of our results and literature reports fluorinated aryl metal reagents have a tendency to be explosive and should be handled with caution.⁵⁸ In addition, nonfluorinated trialkyl- and triarylalu-

minimum Lewis acids are highly reactive with air and water, can result in spontaneous and uncontrollable fires, and should be handled by experienced organometallic chemists. In contrast, the triphenylboron Lewis acid is air and moisture stable, and the corresponding fluorinated tetraarylborates are nonexplosive.

DFT calculations have been shown to be useful in the screening of electrolyte candidates by estimation of their oxidative and reductive stability.⁹ The maximum cathode voltage is limited by the oxidative stability of an electrolyte which may be estimated from the calculated highest occupied molecular orbital (HOMO) energy as the oxidation reaction involves removal of an electron from this orbital. The oxidative stability of the electrolyte increases as the HOMO energy becomes more negative. Similarly, the reductive stability of the electrolyte has important implications for its behavior at the anode. A low reductive stability of the anion and/or the solvent may favor electrolyte decomposition reactions at the anode surface. Such reactions can result in formation of an electronically insulating surface layer on the anode which does not conduct magnesium ions. The reductive stability can be estimated from the lowest unoccupied molecular orbital (LUMO) energy, as reduction involves addition of an electron to this orbital. In this case, increased reductive stability is predicted by a more positive LUMO energy. Due to the presence of ionic components in electrolyte solutions, Hocking et al. demonstrated that gas-phase DFT calculations do not correlate well with experimental trends unless solvation corrections are included.⁵⁹ Table 1 summarizes the calculated

Table 1. Summary of HOMO and LUMO Energy Levels for the Anion Component of the Crystallized Electrolytes^a

electrolyte	anion	HOMO (eV)	LUMO (eV)
1	$(\text{HMDS})_2\text{AlCl}_2^-$		
	$(\text{HMDS})\text{AlCl}_3^-$	-5.670	0.061
2	Ph_4Al^-	-5.384	0.182
	Ph_3AlCl^-	-5.678	0.047
	$\text{Ph}_2\text{AlCl}_2^-$	-6.045	0.058
	PhAlCl_3^-	-6.402	-0.062
	Cl_4Al^-	-6.742	-1.384
3	Ph_4B^-	-4.819	-0.536
4	$(\text{C}_6\text{F}_5)_3\text{BPh}^-$	-5.559	-0.422

^aReprinted with permission from ref 9. Copyright 2012 Royal Society of Chemistry. ^bThe structural flexibility of $(\text{HMDS})_2\text{AlCl}_2^-$ makes its geometry difficult to optimize.

HOMO and LUMO energy levels for a number of magnesium electrolytes. Since an electrolyte typically includes multiple components, it is important to note that the oxidative stability of the electrolyte is governed by the species with the most positive HOMO energy.

These DFT calculations predict the following order for electrolyte stability based on anion HOMO energy: 4 (GEN3: $(\text{Mg}_2(\mu\text{-Cl})_3\text{-}6\text{THF})[\text{B}(\text{C}_6\text{F}_5)_3\text{Ph}]$) > 2 (APC) > 3 (GEN2: $(\text{Mg}_2(\mu\text{-Cl})_3\text{-}6\text{THF})(\text{BPh}_4)$) > 1 (GEN1).⁹ In order to investigate the correlation between these theoretical calculations and experimental results, synthesis and characterization of both nonfluorinated GEN2 ($\text{Mg}_2(\mu\text{-Cl})_3\text{-}6\text{THF})(\text{BPh}_4)$) and fluorinated GEN3 ($\text{Mg}_2(\mu\text{-Cl})_3\text{-}6\text{THF})[\text{B}(\text{C}_6\text{F}_5)_3\text{Ph}$) magnesium organoborate electrolytes containing the $(\text{Mg}_2(\mu\text{-Cl})_3\text{-}6\text{THF})^+$ cation were accomplished. GEN2 electrolyte was prepared via reaction of triphenylboron with 3 equivalent of PhMgCl , and GEN3 was synthesized by replacing triphenylbor-

on with tris(pentafluorophenyl)borane, $B(C_6F_5)_3$, as the Lewis acid. Structures of GEN2 and GEN3 were confirmed by single-crystal X-ray diffraction (Figure 6).⁶⁰

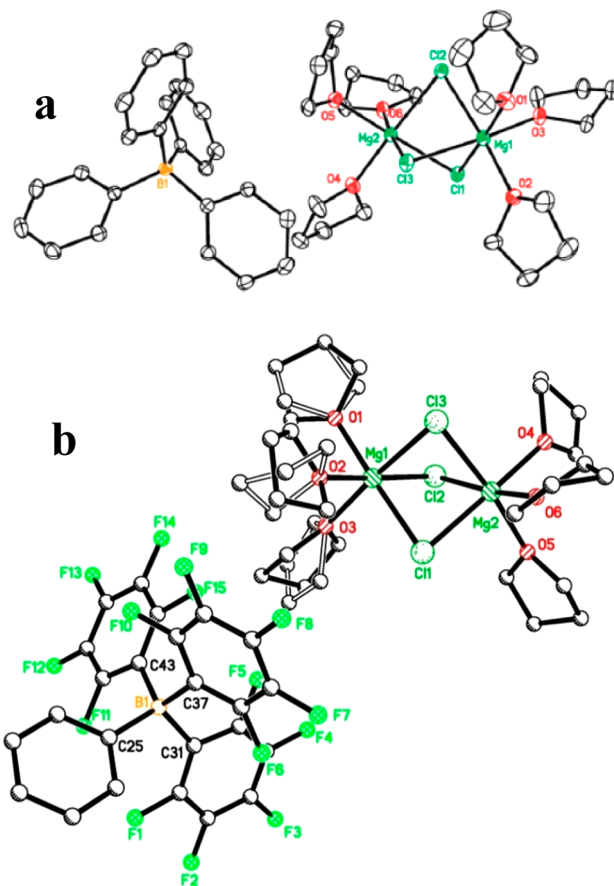


Figure 6. (a) Structure of the crystallized products 3 and 4. ORTEP plot (25% thermal probability ellipsoids) of $(\text{Mg}_2(\mu\text{-Cl})_3\cdot6\text{THF})\cdot(\text{BPh}_4)$. Hydrogen atoms, THF of crystallization, and second component of disorder are omitted for clarity. Reprinted with permission from ref 9. Copyright 2012 Royal Society of Chemistry. (b) ORTEP plot (25% thermal probability ellipsoids) of $(\text{Mg}(\mu\text{-Cl})_3\cdot6\text{THF})\cdot[\text{B}(\text{C}_6\text{F}_5)_3\text{Ph}]$; hydrogen atoms omitted for clarity.

Electrochemical stability of these magnesium electrolytes was determined using a Pt working electrode. Electrolytes GEN1, APC, GEN2, and GEN3 yielded oxidative stabilities of 3.2, 3.3, 2.6, and 3.7 V vs Mg, respectively (Figure 7). On the basis of the DFT results, the oxidative stability of crystallized APC is limited by the anion with the most positive HOMO energy, which is the $(\text{AlPh}_4)^-$ anion. The oxidative stability of GEN2 with $(\text{BPh}_4)^-$ anion is at most 0.6 V lower than that of APC. Therefore, the oxidative stability of the aluminates tends to be at most 0.6 V higher than those of the borates with identical functionalities. However, since fluorinated aluminates can exhibit explosive behavior but fluorinated borates are readily synthesized, the highest reported oxidative stability to date belongs to GEN3 with a voltage stability of 3.7 V vs Mg.⁹ This is due to fluorination of the aromatic rings, which extends the oxidative stability of the magnesium organoborate electrolytes beyond what can be safely achieved with magnesium organohaloaluminates.

Following initial reports on the electrochemical performance of magnesium organoborates generated from reaction of boron

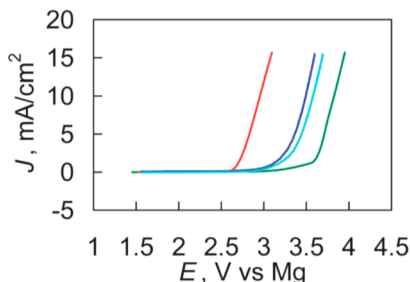


Figure 7. Linear scan voltammograms depicting typical voltage stability of $(\text{Mg}_2(\mu\text{-Cl})_3\cdot6\text{THF})(\text{HMDS}_n\text{AlCl}_{4-n})$ ($n = 1, 2$) (GEN1) (blue), $(\text{Mg}_2(\mu\text{-Cl})_3\cdot6\text{THF})(\text{Ph}_n\text{AlCl}_{4-n})$ ($n = 1\text{--}4$) (crystallized APC) (turquoise), $(\text{Mg}_2(\mu\text{-Cl})_3\cdot6\text{THF})(\text{BPh}_4)$ (GEN2) (red), and $(\text{Mg}_2(\mu\text{-Cl})_3\cdot6\text{THF})[\text{B}(\text{C}_6\text{F}_5)_3\text{Ph}]$ (GEN3) (green) on a Pt working electrode with a surface area of 0.02 cm^2 . Scan rate for all scans is 25 mV s^{-1} ; magnesium reference and counter electrodes are used at a temperature of 21°C . Reprinted with permission from ref 9. Copyright 2012 Royal Society of Chemistry.

based Lewis acids and Grignards, Guo et al. reported the synthesis of a magnesium organoborate from reaction of tris(3,5-dimethylphenyl)boron and PhMgCl.⁶¹ The air stability of this magnesium organoborate was investigated. Surprisingly, on exposure to air for a few hours Guo observed that magnesium deposition and dissolution could still be achieved from the in-situ mixture of tris(3,5-dimethylphenylboron) and PhMgCl. Wang et al. recently reported the synthesis of magnesium electrolytes from ROMgCl salts such as 2-*tert*-butyl-4-methyl-phenolate magnesium chloride with AlCl₃.⁶² Figure 8 shows the voltammograms of this class of electrolytes.

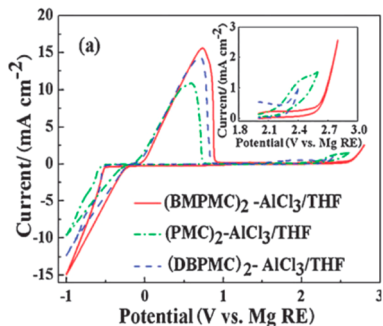


Figure 8. Typical steady-state voltammograms of Pt electrodes in different electrolytes in which a reversible Mg deposition–dissolution process is performed: (red) 0.5 M $(\text{BMPMC})_2\text{-AlCl}_3/\text{THF}$, where BMPMC stands for [2-*tert*-butyl-4-methylphenolate magnesium chloride, (green) 0.5 M $(\text{PMC})_2\text{-AlCl}_3/\text{THF}$, where PMC stands for phenolate magnesium chloride, and (blue) $(\text{DBPMC})_2\text{-AlCl}_3/\text{THF}$, where DBPMC stands for 2,6-di-*tert*-butyl-phenolate magnesium chloride. Reprinted with permission from ref 62. Copyright 2012 Royal Society of Chemistry.

The voltage stability is around 2.6 V vs Mg, and the authors show highly reversible magnesium deposition and dissolution. The air stability of these electrolytes was also evaluated, and they were reported to show reversible magnesium deposition even after several hours of exposure. Interestingly, this contradicts the findings in our laboratory about the air stability of magnesium organoborates containing the cation $(\text{Mg}_2(\mu\text{-Cl})_3\cdot6\text{THF})^+$. GEN3 dissolved in dry THF and placed on the benchtop for 24 h showed no capability for magnesium deposition or dissolution.

In our lab, we investigated the air stability of the in-situ electrolyte formed from reaction of $\text{B}(\text{C}_6\text{F}_5)_3$ with 3 equivalent of PhMgCl by exposure to air for several days. On crystallization of the air-exposed in-situ electrolyte we observed formation of a magnesium trimer cation bridged by phenoxides and chlorides (Figure 9). Presumably, the phenoxides are formed from reaction of PhMgCl with oxygen followed by subsequent reactions with moisture in the air. The anion $[\text{B}(\text{C}_6\text{F}_5)_3\text{Ph}]^-$ was air stable.

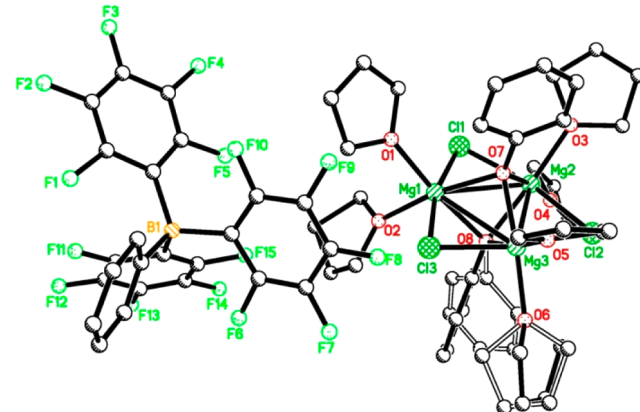


Figure 9. ORTEP plot (25% thermal probability ellipsoids) of $(\text{Mg}_3(\mu\text{-Cl})_3(\mu\text{-OPh})_2\cdot6\text{THF})[\text{B}(\text{C}_6\text{F}_5)_3\text{Ph}]$; hydrogen atoms omitted for clarity.

2.1.3. Corrosive Nature of Magnesium Electrolytes. Zhao et al. reported a dependence of the measured oxidative stability of Grignard reagents on the type of working electrode used.⁶³ Pellion Technologies reported a similar observation for the oxidative stability of in-situ-generated magnesium organohaloaluminate electrolytes vs working electrode material.⁶⁴ It is plausible that this result from Pellion was influenced by corrosion of the metal electrodes by PhMgCl, which Aurbach et al. identified in in-situ-generated APC electrolyte. As noted above, crystallization results in removal of byproducts and yields a pure magnesium organohaloaluminate and thus may result in electrolytes with improved stability. This hypothesis was tested by determining the oxidative stability of a crystallized electrolyte at various working electrode materials. Results of these experiments are shown in Figure 10, which shows the oxidative stability of GEN1 on several working electrodes. Most notably, the voltage stability on stainless steel, which is often used in fabrication of coin cells, is depressed to 2.2 V vs Mg due to corrosion of the stainless steel. It is worth noting that GEN1 has properties similar to those of crystallized APC. The corrosive nature of DCC has also been investigated and reported.^{65,66}

Metal corrosion can be indicated by current density hysteresis during cyclic oxidative stability tests and decreased oxidative stability on less noble working electrodes.⁹ Therefore, corrosion of metal cell components by magnesium organohaloaluminate electrolytes apparently limits charging in a coin cell battery configuration to under 2.2 V when the casing and current collectors are constructed from less noble metals such as stainless steel, aluminum, and nickel.

Thus, successful operation of coin cells (or other cell configurations which utilize similar metal components) above 2.2 V requires development of a new generation of high-performance magnesium electrolytes which do not promote

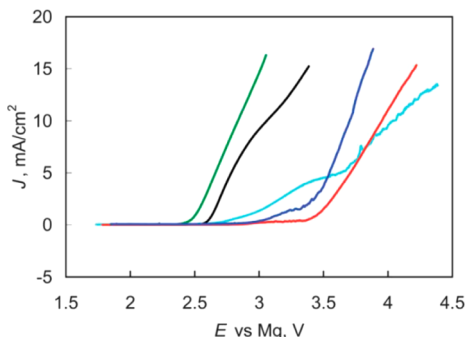


Figure 10. Linear scan voltammograms of $(\text{Mg}_2(\mu\text{-Cl})_3\cdot 6\text{THF})\cdot (\text{HMDS}_n\text{AlCl}_{4-n})$ ($n = 1, 2$) (GEN1) with a scan rate of 25 mV s^{-1} depicting characteristic voltage stabilities on various working electrodes (green, stainless steel; black, Ni; blue, Pt; turquoise, Au; red, glassy carbon) with areas of 0.02 cm^2 and a magnesium reference and counter electrode at a temperature of 21°C . Reprinted with permission from ref 9. Copyright 2012 Royal Society of Chemistry.

corrosion of the metal components. A plausible explanation for the metal corrosion observed using magnesium organohaloaluminates is the presence of halides in the cation and anion components of the electrolyte. In particular, preliminary results demonstrate that the anion has a dramatic effect on electrolyte corrosion behavior. For example, the magnesium organoborate electrolyte GEN2 with a halogen-free anion BPh_4^- exhibits reduced corrosivity as evidenced by the same measured oxidative stability (2.6 V vs Mg) on both stainless steel and Pt electrodes, which represents a 400 mV improvement vs crystallized APC and GEN1 on stainless steel. In addition, cyclic voltammograms of GEN2 using a stainless steel working electrode do not exhibit hysteresis (Figure 11a). In order to enhance the oxidative stability of GEN2 use of fluorinated Lewis acids such as $\text{B}(\text{C}_6\text{F}_5)_3$ was considered. As previously noted, reaction of $\text{B}(\text{C}_6\text{F}_5)_3$ with PhMgCl results in

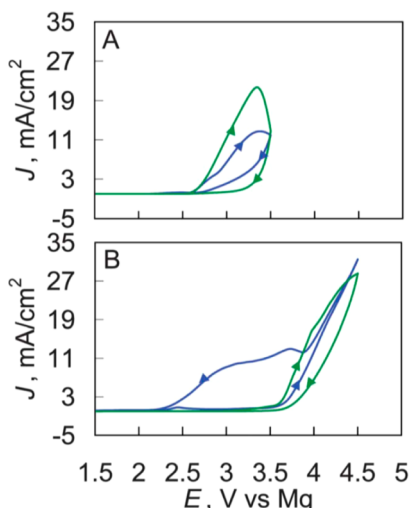


Figure 11. Cyclic voltammograms of $(\text{Mg}_2(\mu\text{-Cl})_3\cdot 6\text{THF})(\text{BPh}_4^-)$ (GEN2) (A) and $(\text{Mg}_2(\mu\text{-Cl})_3\cdot 6\text{THF})[\text{B}(\text{C}_6\text{F}_5)_3\text{Ph}]$ (GEN3) (B) on platinum (green) and stainless steel (blue) working electrodes with an area of 0.02 cm^2 at a temperature of 21°C . Clockwise arrows designate passivation, while counterclockwise arrows denote hysteresis. Scan rate is 25 mV s^{-1} , and the counter and reference electrodes are both magnesium. Reprinted with permission from ref 9. Copyright 2012 Royal Society of Chemistry.

formation of GEN3, which has an oxidative stability of 3.7 V vs Mg on Pt as determined by a linear scan voltammogram between OCV and 4.5 V vs Mg (Figure 11b). Unfortunately, during the reverse scan back to OCV GEN3 exhibits hysteresis and a stability of 2.2 V vs Mg on a stainless steel working electrode, indicative of corrosive behavior

Magnesium organoborates based on a naked magnesium cation ($\text{Mg}\cdot 6\text{THF})^{2+}$ partnered with a halide-free anion may eliminate the corrosive nature previously observed with magnesium organohaloaluminates and magnesium organoborates containing the magnesium dimer ($\text{Mg}_2(\mu\text{-Cl})_3\cdot 6\text{THF})^+$ cation. Our initial results in this area demonstrate a novel approach to synthesize magnesium organoborates through an ion-exchange pathway.⁶⁷ An interesting non-coordinating anion, tetrakis[3,5-bis(trifluoromethyl)phenyl]borate (BAr_F), was synthesized by Kobayashi et al. as a sodium salt and has demonstrated excellent stability.^{68,69} Its oxidative stability vs Mg is estimated to be 4.5 V . The corresponding magnesium salt $\text{Mg}(\text{BAr}_F)_2$ is therefore a useful model compound to evaluate the corrosivity of nonchlorinated magnesium organoborates at high potentials (above 3.0 V) vs Mg. Preparation of $\text{Mg}(\text{BAr}_F)_2$ is achieved by ion exchange between magnesium chloride (MgCl_2) and $\text{Ag}(\text{BAr}_F)$ (eq 6).



$\text{Mg}(\text{BAr}_F)_2$ exhibits a very high oxidative stability (in excess of 4.5 V vs Mg) on a stainless steel working electrode. This appears to validate the hypothesis that magnesium organoborates which do not contain chlorides in either the cation or the anion should exhibit reduced corrosivity. However, in order for $\text{Mg}(\text{BAr}_F)_2$ to function acceptably as an electrolyte in a rechargeable Mg battery, its reductive stability window must be shifted such that no reduction of the anion occurs at potentials more positive than the magnesium deposition overpotential.

Ideally, the electrode material used for electrolyte stability studies should be completely inert, and a prime candidate for high-voltage oxidative stability tests is glassy carbon, which has demonstrated the desired behavior in solutions of magnesium organohaloaluminates. Pt working electrodes, which are commonly used in such studies, still suffer from a low level of pitting corrosion at high positive potentials. However, Pt working electrodes are apparently better suited for Coulombic efficiency characterization of the Mg deposition/dissolution redox reactions, yielding higher efficiencies for that operation than those typically obtained with glassy carbon electrodes. Therefore, proper experimental conditions involving use of Pt and glassy carbon electrodes are necessary to ensure that electrochemical experiments characterize redox events pertaining solely to the magnesium electrolyte rather than reactions between the electrolyte and electrodes.

While Pt and glassy carbon appear to be inherently inert with respect to magnesium electrolytes in the potential range of interest, another approach to obtaining useful working electrodes would be to identify electrode materials which form passive surface layers that prevent further electrolyte/electrode reactions. Cheng et al. recently reported that molybdenum and tungsten are electrochemically stable ($>2.8 \text{ V vs Mg}$) through formation of such passive surface layers.⁷⁰ This suggests that materials which form such passive layers may be useful as both working electrodes in electrochemical studies involving magnesium electrolytes and current collectors in magnesium batteries.

2.1.4. Electrolytes with Magnesium Alloy Anodes. Mg has a standard reduction potential of -2.356 V vs SHE, which is 644 mV less negative than Li, and thus, one might expect that Mg deposition from organic solutions of Mg salts would be relatively straightforward. However, as noted above, the unique electrochemistry of Mg prohibits its reversible deposition in aprotic solvents (excluding ethers) containing ionic salts which are currently commercially available such as magnesium bis(trifluoromethane)sulfonimide ($\text{Mg}(\text{TFSI})_2$) or magnesium perchlorate (MgClO_4).⁴⁶ Additionally, reduction of components of these electrolytes results in formation of a surface layer which is apparently nonconductive with respect to both electrons and magnesium ions and thus inhibits Mg deposition. While this occurs on pure Mg surfaces, use of electrode materials which readily form alloys with Mg appears to represent a means to avoid such limitations. For example, while electrolytes composed of $\text{Mg}(\text{TFSI})_2$ /acetonitrile (ACN) result in formation of an inert passive layer upon reduction on a magnesium metal anode, Arthur et al. recently showed the electrochemical magnesiation and demagnesiation of a bismuth anode by a $\text{Mg}(\text{TFSI})_2$ /ACN solution (Figure 12a).⁷¹

Shao et al. developed a high-performance nanostructured anode based on bismuth nanotubes which delivered a high reversible specific capacity of 350 mAh/g and excellent stability (7.7% capacity fade after 200 cycles) along with high

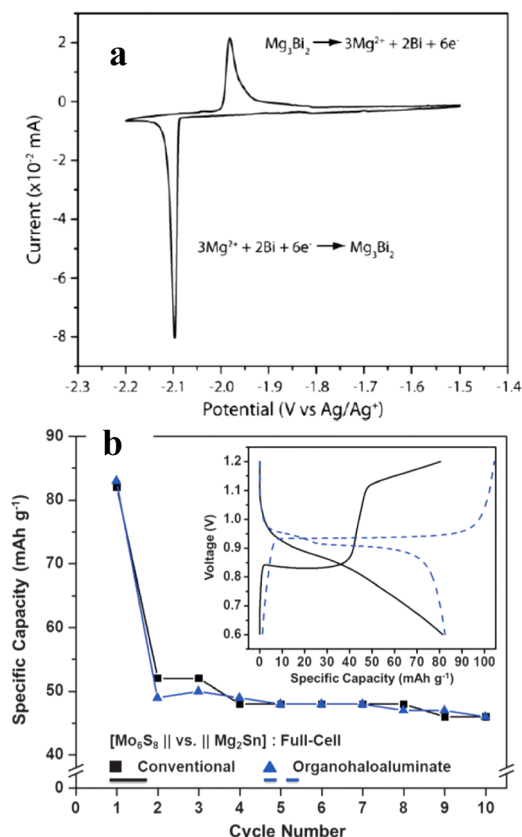


Figure 12. (a) Galvanostatic discharge of Bi, Sb, $\text{Bi}_{0.88}\text{Sb}_{0.12}$, and $\text{Bi}_{0.55}\text{Sb}_{0.45}$ anodes at a 0.01 C rate. Reprinted with permission from ref 71. Copyright 2012 Elsevier. (b) First 10 cycles for a $[\text{Mo}_6\text{S}_8$ —conventional electrolyte— Mg_2Sn] full cell (black) and a $[\text{Mo}_6\text{S}_8$ —organohaloaluminate electrolyte— Mg_2Sn] full cell (blue); (inset) first cycle voltage profiles for each full cell. Reprinted with permission from ref 73. Copyright 2012 Royal Society of Chemistry.

Coulombic efficiency. This nanostructured bismuth electrode was tested in a half cell with magnesium metal, utilizing a $\text{Mg}(\text{BH}_4)_2/\text{LiBH}_4$ /diglyme electrolyte which is compatible with magnesium metal. The authors state that these nanostructures can accommodate the large volume change which occurs during charge/discharge cycles without losing electrical conductivity and possess significantly reduced diffusion lengths for Mg^{2+} ions. The high rate performance of the electrode made from nanotubes dramatically improves the discharge rate previously reported by Arthur et al. for bismuth anodes. Figure 13 summarizes the cyclic voltammetry of magnesium insertion and deinsertion of bismuth as well as cycling stability and rate performance.⁷² This work emphasizes the importance of nanotechnology for dramatically enhancing the rate performance of electrode materials. Another material which can form alloys with Mg is tin, and Singh et al. was able to show that a tin anode could deliver higher capacity (903 mAh/g) and lower magnesium insertion and extraction voltage (0.15 V/ 0.2 V vs Mg) than those previously reported for bismuth (384 mAh/g, 0.23 V/ 0.32 V).⁷³ In order to highlight the compatibility and performance of the tin anode with a $\text{Mg}(\text{TFSI})_2$ electrolyte, a battery containing a premagnesiated tin anode (Mg_2Sn) and a Chevrel phase molybdenum sulfide cathode was cycled; its performance was compared to that of a cell using a magnesium organohaloaluminate electrolyte with the same electrodes (Figure 12b).

However, one of the major challenges with using alloys is severe expansion during magnesiation and pulverization during demagnesiation. It is possible that the volume changes during the alloying and dealloying processes result in rupture of the passivating film, which then renders the anode electrochemically active. Nanostructured alloy anodes, which are more resistant to pulverization, may benefit from this phenomenon. Interestingly, the reversible but sluggish magnesium electrodeposition from $\text{Mg}(\text{TFSI})_2/\text{DME}$ on magnesium metal has been reported⁷⁴ with a low Coulombic efficiency of $\sim 35\%$. This report was reproduced in our lab. The fact that cells using this electrolyte and alloy anodes have demonstrated greatly improved performance vs similar cells using pure Mg anodes appears to indicate that alloy anodes are useful with a wider range of electrolytes than pure Mg.

2.1.5. Polymeric Gel Magnesium Electrolytes. Polymeric battery electrolytes typically refer to viscous or free-standing gels composed of a polymer, an alkali salt, a plasticizer usually in the form of an organic solvent, and various additives. These polymeric gels can be formed into thin films to compensate for their lower conductivities vs liquid electrolytes. In addition, they are advantageous over solid-state battery electrolytes because they are soft and conform to solid surfaces, resulting in better interfacial contact with various electrode materials. Use of gel polymer electrolytes also avoids the problem of cell leakage. One of the initial polymers to be investigated as a Li^+ conductor was poly(ethylene oxide) (PEO). PEO complexes with alkali metal salts were first reported by Fenton⁷⁵ et al. in 1973 and demonstrated by Armand⁷⁶ to have reasonably high ionic conductivities for monovalent alkali cations in 1979. Soon thereafter, Linford and Farrington independently studied the conductivities of divalent alkali metals in PEO-based polymeric gels with hopes of developing either electrolytes for novel batteries with a multivalent anode or purely anionic conductors in cases where divalent cations have very low transference numbers compared to their monovalent anions.^{77–79} Both goals were

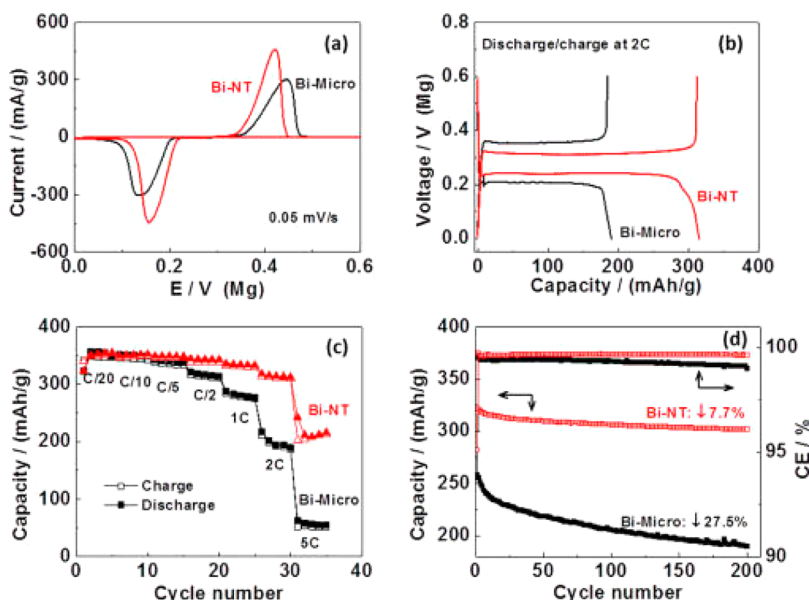


Figure 13. (a) Cyclic voltammograms of Mg insertion/deinsertion in bismuth; (b) discharge/charge profile of a Mg–Bi cell; (c) rate performance of a Mg–Bi cell; (d) cycling stability and Coulombic efficiency (CE) of bismuth electrode for reversible Mg insertion/deinsertion. Cell configuration: Mg/0.1 M $\text{Mg}(\text{BH}_4)_2$ –1.5 M LiBH_4 –diglyme/Bi. Reprinted with permission from ref 72. Copyright 2014 American Chemical Society.

equally attractive. They investigated gel complexes with salts such as magnesium chloride (MgCl_2), $\text{Mg}(\text{ClO}_4)_2$, and magnesium thiocyanate ($\text{Mg}(\text{SCN})_2$), and they reported no evidence of a significant transport number for Mg^{2+} (>0.005). It is interesting to note that the conductivity of MgCl_2 in PEO is comparable to that of lithium trifluoromethanesulfonate (LiCF_3SO_3) in PEO from 80 to 150 °C. For example, the complex PEO12-/Mg(ClO_4)₂ has a conductivity in the range of 10^{-5} S/cm at 30 °C. A survey of all divalent metals complexed with PEO was published by Sequiera in 1990.⁸⁰

In an attempt to improve the low conductivities of MgCl_2 in PEO, Ikeda et al. employed a technique reported by Abraham in 1995 of reinforcing a photo-cross-linked poly(ethylene glycol) diacrylate (PEGDA) with a microporous membrane such as Celgard.⁸¹ A magnesium trifluoromethanesulfonate ($\text{Mg}(\text{CF}_3\text{SO}_3)_2$) salt was impregnated with PEGDA and plasticized by various combinations of ethylene carbonate (EC), propylene carbonate (PC), and tetra(ethylene glycol) diacrylate (TEGDA).⁸² A 1 mol % $\text{Mg}(\text{CF}_3\text{SO}_3)_2$ gel has a conductivity of 2.1×10^{-4} S/cm at room temperature. Unfortunately, a full cell with a Mg metal anode, gel electrolyte, and tetramethylammonium iodide ((CH_3)₄NI) cathode attained less than 0.01% of theoretical capacity upon discharge. There were no reports on the reversibility of $\text{Mg}^0/\text{Mg}^{2+}$. With a similar goal in mind, Morita et al. used oligo(ethylene oxide)-grafted polymethacrylate (PEO–PMA) matrix with a poly(ethylene glycol) dimethyl ether (PEGDE) plasticizer and MgX_2 salts (X = TFSI⁻, CF_3SO_3^- , and ClO_4^-).⁸³ The $\text{Mg}(\text{TFSI})_2$ gel has a conductivity of 0.4 mS/cm, and 2% utilization of Mg is reported in a $\text{Mg}_{0.8}\text{V}_2\text{O}_5$ /polymeric gel/ V_2O_5 cell. Morita et al. also reported a conductivity of 1.1×10^{-4} S/cm at 20 °C from PEO–PMA dissolving the ionic liquid 1-ethyl-3-methylimidazolium bis(trifluoromethylsulfonyl)imide (EMITFSI) (50% by weight) with the magnesium salt ($\text{Mg}(\text{TFSI})_2$).⁸⁴ A different approach for improving gel polymer electrolytes was taken by Saito et al., who used PEG–borate esters as Lewis acids which interact and trap the ClO_4^- anion of a magnesium salt which frees up Mg^{2+}

and increases its transference number. While transference numbers for magnesium in polymer electrolytes have been previously unreported or very small, this value is reported to be as high as 0.36 by this approach. Total specific conductivities are also $\sim 10^{-3}$ S/cm.^{85,86} By varying the length of the PEG oligomers and the amount of boric acid added, Saito et al. increased the transference number of Mg^{2+} to 0.51 for PEG150/B₂O₃/Mg(ClO_4)₂.⁸⁷ A solvent-free class of PEG₄₀₀/ δ -MgCl₂ polymer electrolytes has been reported by Di Noto et al. as early as 1998 with room-temperature conductivities as high as 1.9×10^{-5} S/cm.⁸⁸ By monitoring molecular relaxations, Di Noto demonstrated that PEG400/(δ -MgCl₂)_x with $x \leq 0.120$, contains Mg^{2+} ions coordinated by the polyether oxygens and Cl⁻ anions coordinated by the terminal hydroxyls. For $x > 0.120$, [Mg–Cl]⁺ cations were detected in the bulk material. He also postulates that there are two different modes of magnesium-ion transport within this material: (1) interchain transfer, where the Mg^{2+} ion is coordinated by two different PEG400 chains, and (2) intrachain transfer, where the Mg^{2+} ion is coordinated by a single PEG chain. For each ion in the bulk material at least two types of coordination sites were predicted, indicated as A and C in Figure 14, each with a distinct relaxation phenomenon.^{89–91}

As noted above, the deposition/dissolution of magnesium from liquid solutions of commercial salts is sluggish ($\text{Mg}(\text{TFSI})_2$) or not observed (MgCl_2 , $\text{Mg}(\text{ClO}_4)_2$) due to a strong tendency for the surface of magnesium to become covered by a blocking passivation layer. By contrast, organic electrolytes containing Grignard reagents have been shown to be suitable for electrochemical magnesium deposition/stripping from ethereal solvents. On the basis of these reports, polymeric electrolyte systems with Grignard reagents dissolved in polymeric ethers were studied by Liebenow. A series of reports^{92–94} describe deposition/dissolution cyclic voltammograms akin to those typically observed with liquid magnesium electrolytes (Figure 15). In addition, Liebenow reports visible amounts of deposited magnesium on Ag, Ni, and Au electrodes from a free-standing EtMgBr–PEG–THF polymer electrolyte.

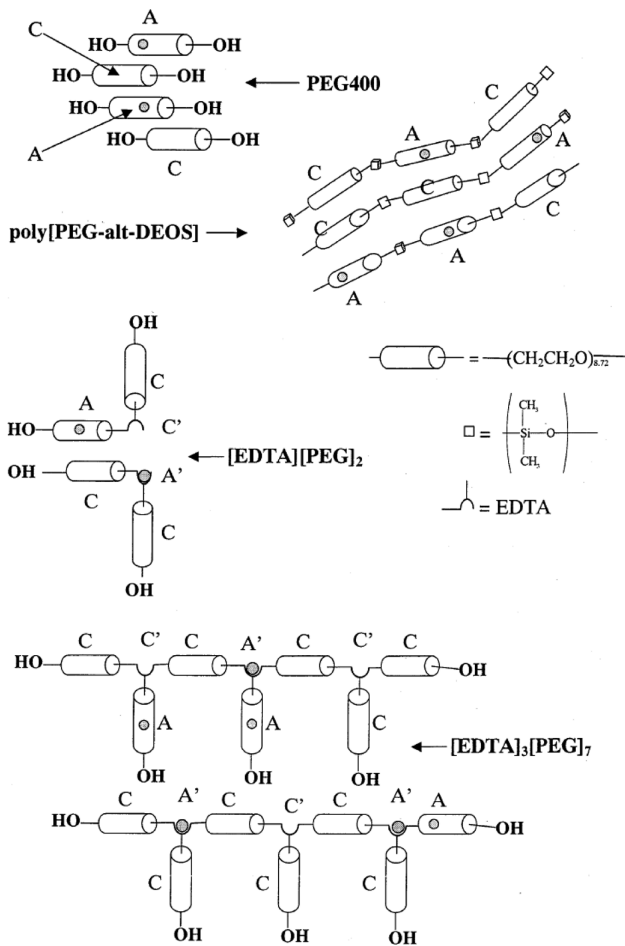


Figure 14. Schematic representation of the investigated PE materials. A and A' represent the sites coordinating a metal species (full site), and C and C' are all of the other sites which could coordinate a metal ion species (empty sites). A' and C' designate the sites present in the EDTA fragments. Reprinted with permission from ref 90. Copyright 2002 American Chemical Society.

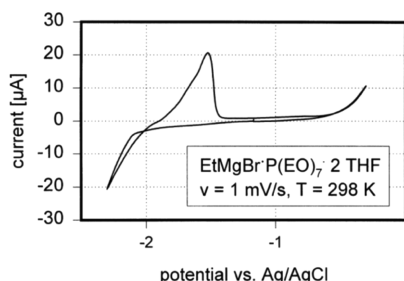
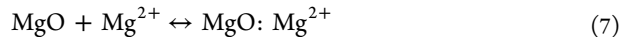


Figure 15. Cyclic voltammogram of EtMgBr-P(EO)₇-2THF, $v = 1 \text{ mV s}^{-1}$, working electrode nickel, potential vs Ag-AgCl, temperature 25 °C. Reprinted with permission from ref 93. Copyright 2000 Elsevier.

Conductivities at room temperature were reported around 0.5 mS/cm, 2 orders of magnitude higher than for previously reported “solvate-free” magnesium salts such as MgCl₂, Mg(ClO₄)₂, and Mg(SCN)₂.

Another class of polymers investigated for use in magnesium ion conducting gel polymer electrolytes has been poly(vinylidene fluoride-*co*-hexafluoropropylene) (PVDF-HFP). Oh et al. reported the conductivities of PVDF-HFP plasticized by EC:PC (1:1 ratio) containing Mg(ClO₄)₂ and stabilized by

high-purity silanized fumed silica.⁹⁵ Such fillers have the ability to preserve a porous structure in gel electrolytes, which maximizes the absorption of liquid electrolyte and reduces the risk of cell leakage. The ionic conductivity of this system is higher than those reported for the PEO systems. Incorporation of 12% SiO₂ provides a conductivity of 3.2 mS/cm at room temperature. Oh reports the decomposition voltage of the gel as greater than 4.3 V vs Mg, and 10 charge/discharge cycles are reported from a Mg/gel/V₂O₅ cell. The discharge voltage is 0.8 V, and capacities drop from 60 to 30 mAh/g. The authors rightly attribute the low capacities to reactions at the Mg/gel interface where surface films grow in thickness during cycling. A Mg(ClO₄)₂ liquid solution (in THF) does not electrochemically deposit or strip magnesium due to the presence of these films. Pandey et al. used the same gel matrix but with a magnesium oxide (MgO) dispersion. Pandey reported a conductivity of 6 mS cm⁻¹ with 10% MgO by weight and a 0.39 transference number for Mg²⁺.⁹⁶ The authors suggest that MgO interacts with magnesium as follows



MgO:Mg²⁺ forms a double layer in the filler-gel interfacial regions which induce a local electric field responsible for the enhanced Mg²⁺ ion mobility. Proof for the reversibility of the Mg/Mg²⁺ couple is suggested by a cyclic voltammogram which shows reduction and oxidation waves. There is however a 3 V separation between wave maxima (Figure 16). This is not

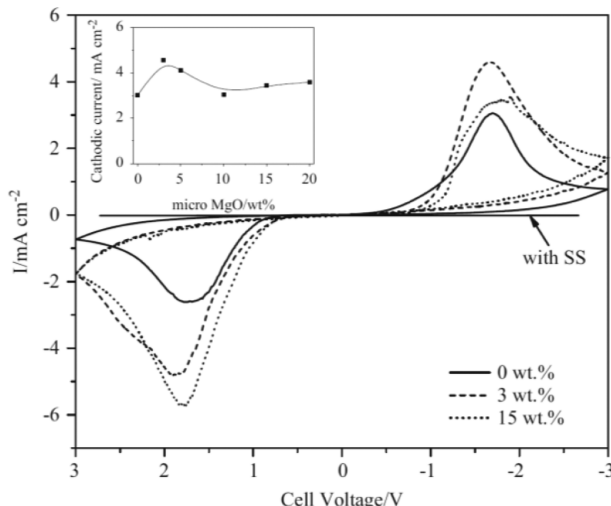


Figure 16. Cyclic voltammograms of cells: SS/composite gel film/SS and Mg/composite gel film/Mg with different MgO contents recorded at room temperature at a scan rate of 5 mV s⁻¹. (Inset) Variation of cathodic current as a function of MgO content. Reprinted with permission from ref 96. Copyright 2011 Elsevier.

typical for magnesium deposition/dissolution cyclic voltammograms reported in liquid solutions or in Liebenow's organomagnesium-based polymeric gels, where peak separation tends to be less than 1 V.

In addition, Mg(ClO₄)₂ is not compatible with magnesium metal in THF. Unfortunately, there is no indication of an observed magnesium deposit. The polymer electrolyte film is reported to be stable up to 3.5 V vs Mg. Interestingly, very high discharge capacities above 1000 mAh/g are reported for a Mg/gel/V₂O₅ cell at a rate of 0.2 mA cm⁻². Ten cycles are reported for a Mg-MWCNT/gel/V₂O₅ cell with capacities starting at

260 mAh/g at the same rate. The same group also reports an even higher conductivity of 1.1×10^{-2} S/cm at room temperature in an electrolyte of PVDF-HFP/Mg(ClO₄)₂/fumed silica filler.⁹⁷ A 0.3 transference number for Mg²⁺ is reported for 15% fumed silica by weight, and 10 cycles are reported in a Mg–MWCNT/gel/MoO₃ cathode cell with a starting capacity above 200 mAh/g at a rate of 0.1 mA cm⁻². The ionic liquid 1-ethyl-3-methylimidazolium trifluoromethanesulfonate (EMICF₃SO₃) has also been introduced as a gel matrix component, accompanied by Mg(TFSI)₂ and Mg-(CF₃SO₃)₂ salts.⁹⁸ A maximum conductivity of 4.8 mS/cm and a Mg²⁺ transport number of 0.26 have been observed. Promising results were obtained by Aurbach et al. from simple gels consisting of PVDF, DCC and tetraglyme as plasticizer.^{46,99} The reported conductivity at 25 °C was 3.7 mS/cm, and cells containing this gel, a magnesium anode, and Mo₆S₈ (Chevrel Phase) composite cathodes cycled very well over a temperature range of 0–80 °C. A discharge capacity value of 120 mAh/g was obtained, which is similar to the performance of liquid magnesium electrolyte DCC with the same electrodes. Other polymers have also been studied. Kumar et al. reports the use of polyacrylonitrile (PAN) with PC, EC plasticizers, and Mg(CF₃SO₃)₂. A high conductivity of 1.8 mS/cm is reported at room temperature.^{100,101}

2.1.6. Ionic Liquids. Due to its high negative standard potential, plating/dissolution of magnesium can only occur in aprotic solutions. However, electrolytes composed of existing commercial magnesium salts in aprotic solvents with high dielectric constants such as carbonates, esters, or acetonitrile have been reported to form dense passivating layers which are impermeable to the magnesium ion and block any deposition/dissolution.¹⁰² Successful plating/stripping has been shown from magnesium organohaloaluminates or magnesium organoborate salts which contain the (Mg₂(μ-Cl)₃·6THF)⁺ cation dissolved in etheric solvents.^{9,52} Ethers have a low dielectric constant, typically below 10, which restricts the solubility of magnesium salts (<0.5 M) as well as their ionic dissociation. It is desirable for a battery electrolyte to contain the electroactive salt in high concentrations (state of the art Li-ion electrolytes contain the LiPF₆ salt at concentrations above 1.0M) such that high conductivities and rapid charge/discharge rates can be achieved. In order to increase the solubility of currently available magnesium salts and diminish the volatile and flammable nature of ether based electrolytes, room-temperature ionic liquids (RTILS) have been considered as potential solvents for a variety of magnesium salts.

RTILs containing the tetrafluoroborate (BF₄⁻) anion have low melting points, low viscosity, and high ionic conductivity, and use of 1-n-butyl-3-methylimidazolium tetrafluoroborate (BMImBF₄) has been reported to allow magnesium electrodeposition from a 1 M solution of magnesium triflate (Mg(CF₃SO₃)₂). BMImBF₄ is stable on a platinum working electrode between -1 and 3 V vs Mg,¹⁰³ and deposition/dissolution of magnesium from the Mg(CF₃SO₃)₂ salt occurs with low currents within this electrochemical window (Figure 17). It is surprising that even though 100% Coulombic efficiency is reported, the plating/stripping process could not be repeated for more than 165 cycles due to strong voltage fluctuations. On the basis of EDS analysis, NuLi identified the presence of S and F (CF₃SO₃⁻ components) in the deposit along with Mg when the deposition takes place with a low charge density of 3.6 C/cm². This report infers that magnesium is deposited from this electrolyte system even though the anion

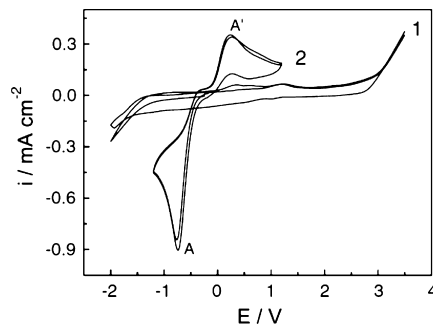


Figure 17. Typical cyclic voltammograms of BMImBF₄ without (curve 1) and with 1 M Mg(CF₃SO₃)₂ (curve 2) on platinum disk electrode at 50 mV/s. Reprinted with permission from ref 103. Copyright 2005 Elsevier.

of the magnesium salt (CF₃SO₃)⁻ reduces to form a film on the electrode. It is worth highlighting that Cheek et al. from the U.S. Naval Academy was unsuccessful in reproducing the findings of NuLi.¹⁰⁴ In addition, attempts in our lab to deposit magnesium from GEN1 dissolved in BMImBF₄ were unsuccessful. NuLi also reported reversible deposition of magnesium from a 1 M solution of Mg(CF₃SO₃)₂ in N-methyl-N-propylpiperidinium bis(trifluoromethane)sulfonimide (PP13TFSI) on a silver working electrode.¹⁰⁵ This was attributed to initial formation of Ag–Mg clusters which promote subsequent magnesium deposition. The bis(trifluoromethane)sulfonimide (TFSI⁻) anion exhibits a wider electrochemical window (4.5 V vs Mg on a Ag working electrode) than BMImBF₄. Unfortunately, the plating/stripping current potential response is sluggish, and complete dissolution (anodic current drop to zero) is not observed. It is again surprising that a 100% Coulombic efficiency is reported, but only 85 cycles could be obtained at a low rate of 0.1 mA/cm². While the TFSI⁻ anion shows great promise in terms of stability against oxidation, its reductive stability appears to be insufficient to support reversible magnesium deposition for a substantial number of cycles. Even magnesium deposition from a 1.0 M solution of Mg(TFSI)₂ in THF is sluggish, with a high overpotential of ~−1.0 V vs Mg and no dissolution visible on the first potential scan. Subsequent cycles improve the Coulombic efficiency to only ~35% on a Pt electrode. A small reduction wave is observed in this electrolyte before the onset of Mg deposition, which suggests that TFSI⁻ reduction could occur, decreasing the Coulombic efficiency of magnesium deposition/dissolution.

While RTILs can dissolve magnesium salts in high concentrations and exhibit low volatility and flammability, they are plagued by diminished conductivities and transference numbers for the electroactive species. This is due to higher viscosities than traditional organic solvents and the presence of ions in addition to magnesium which also migrate when an electric field is applied. In order to improve the conductivity, viscosities have been reduced by adding THF as a cosolvent. For example, Cheek et al. reports that 1 M PhMgBr in THF/1-butyl-1-methylpyrrolidinium triflate (BMPCF₃SO₃) can plate/stripg magnesium.¹⁰⁴ Morita's group reports that a 3:1 mixture of 1.0 M EtMgBr/THF:N,N-diethyl-N-methyl-N-(2-methoxyethyl)ammonium-bis(trifluoromethane)sulfonimide (DEMETFSI) has a conductivity of 7.44 mS/cm, and an order of magnitude increase in current density is observed in its current–potential curve vs that of 1.0 M EtMgBr/THF.¹⁰⁶ Optimization of the cation in imidazolium-based IL with a

TFSI⁻ anion further improves current densities.¹⁰⁷ Interestingly, he also reports that varying the ratio of TFSI⁻/bis(fluorosulfonyl)imide (FSI⁻) anions in the binary IL mixture MeMgBr/THF/[DEME⁺][TFSI⁻]_{0.5}[FSI⁻]_{0.5} also improves current densities (Figure 18).¹⁰⁸ In addition, GEN1 in [DEME⁺][TFSI⁻]_{0.5}[FSI⁻]_{0.5} was not electrochemically active, but activity was observed when THF was added.

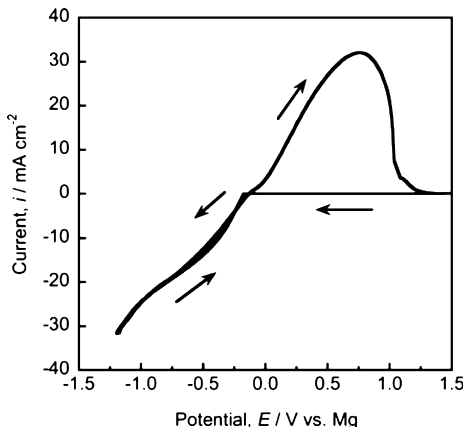


Figure 18. Cyclic voltammogram for Ni substrate in the electrolyte solution of MeMgBr/THF/[DEME⁺][TFSI⁻]_{0.5}[FSI⁻]_{0.5}. Reprinted with permission from ref 106. Copyright 2010 Elsevier.

Another class of RTILs in which magnesium stripping/plating has been demonstrated is that of binary molten electrolytes consisting of acetamide and Mg(ClO₄)₂ as reported by Narayanan et al.¹⁰⁹ A 0.17 mole fraction of Mg(ClO₄)₂ and 0.83 mole fraction of acetamide has an ionic conductivity on the order of several mS/cm at room temperature and a viscosity of 53 mPa·s (viscosity of BMIImBF₄ is 150 mPa·s). A cyclic voltammogram of the deposition/dissolution process in a symmetrical Mg/IL/Mg cell has been reported. Fifteen charge/discharge cycles are shown in a full battery with a magnesium metal anode, binary RTIL/Mg(ClO₄)₂ electrolyte, and γ-MnO₂ cathode. It is interesting to note that 1.0 M Mg(ClO₄)₂ in THF does not undergo plating/stripping on a Pt electrode. Due to acetamide being a protic solvent and the presence of the carbonyl functionality, the reported compatibility with magnesium would not be expected.

Derivatives of trihexyl(tetradecyl)phosphonium chloride [P_{6,6,6,14}][Cl] are also reported by Khoo et al. to dissolve magnesium through a hydrated SEI layer in a Mg–air primary battery.¹¹⁰ On the basis of the foregoing data, RTILs clearly represent an interesting solvent class and require further investigation to determine their true applicability in secondary magnesium batteries.

Interestingly, Higashi et al. recently demonstrated the molten salt Mg(BH₄)(NH₂) as an inorganic solid-state ion conductor for magnesium. This material exhibits ionic conductivity of 10⁻⁶ S/cm at 150 °C, and its electrochemical window is wider than 3 V. Unfortunately, the Coulombic efficiency is approximately 35%.¹¹¹ Other solid electrolytes which have been investigated are metal–organic frameworks (MOFs) doped with magnesium salts such as Mg(TFSI)₂. While the conductivity is 0.25 S/cm, little is known at this time about the electrochemical performance.¹¹²

2.2. Cathodes

A lithium metal anode can undergo a one-electron reduction, whereas a magnesium metal anode can undergo a two-electron reduction. Therefore, an ideal magnesium cathode is a compound that can undergo reversible intercalation of one magnesium ion per transition metal center (by a two-electron reduction of the transition metal) offering the promise of nearly double the capacity offered by existing lithium-ion cathodes. A number of compounds capable of reversible electrochemical intercalation of Mg²⁺ have been identified, although voltages, rates, and specific capacities have not typically reached levels seen with lithium ion cathodes. Relatively little work has been published on conversion cathodes such as oxygen or elemental sulfur coupled with magnesium metal anodes. In the following section we will survey the history of magnesium cathode development.

2.2.1. Intercalation Cathodes. **2.2.1.1. Initial Surveys.** In the early 1980s Gregory et al. evaluated the ability of a number of transition metal oxides, sulfides, and borides to intercalate Mg²⁺ ions.⁴⁴ Compounds were screened for possible Mg²⁺ intercalation by reduction with dibutylmagnesium. This approach is analogous to the early use of *n*-butyllithium solutions to screen compounds for Li⁺ intercalation. Atomic absorption spectroscopy was used to determine the magnesium composition. Open-circuit potentials (OCV) of cells containing the cathode candidates, an electrolyte composed of Mg(ClO₄)₂ in THF, and a magnesium metal anode were recorded (Table 2).

Table 2. Mg²⁺ Intercalation Capacity for Candidate Cathode Materials^a

host material	$E_{\text{Mg-cathode}}$ (V)	Mg:host (mole)	capacities calculated by chemical reduction (mAh/g _{host})
Co ₃ O ₄	2.28	0.80	222
Mn ₂ O ₃	2.40	0.66	224
Mn ₃ O ₄	2.40	0.66	154
MoO ₃	2.28	0.50	143
PbO ₂	3.10	0.25	56
Pb ₃ O ₄	3.10	0.25	20
RuO ₂	2.55	0.66	266
V ₂ O ₅	2.66	0.66	194
WO ₃	2.16	0.50	116
TiS ₂	1.63	0.15	157
VS ₂	1.71	0.34	154
ZrS ₂	2.60	0.66	228
MoB ₂	1.15	0.66	301
TiB ₂	1.25	0.42	324
ZrB ₂	1.20	0.66	313

^aMg²⁺ intercalation capacity for candidate cathode materials. Reprinted with permission from ref 44. Copyright 1990 The Electrochemical Society.

Similar to lithium systems, oxide-based cathodes yielded the highest OCVs. The exact nature of the valence change experienced by the transition metal in these intercalates was not directly determined. For example, a loading of 0.66 for magnesium intercalation into RuO₂ could be explained by reduction of 2/3 of the ruthenium from the IV to the III valence state and 1/3 to the II valence state. Alternatively, it is possible that the reduction is solely due to the Ru(IV)/Ru(II) transition. However, complete reduction of RuO₂ with Mg to form Ru and MgO is thermodynamically favorable and cannot

be discounted. The electrochemical behavior of RuO_2 cathode can be further understood by looking at the Mg–Ru–O phase diagram and $\text{Mg}|\text{RuO}_2$ discharge curve shown in Figure 19.

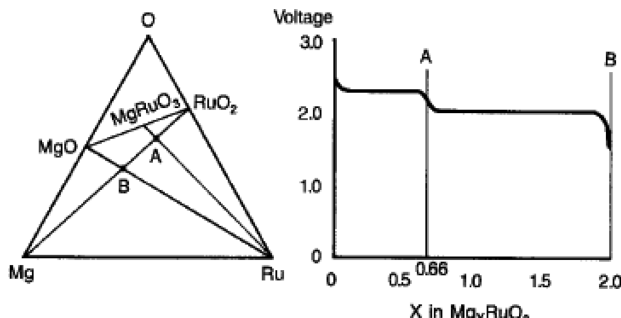


Figure 19. Mg–Ru–O phase diagram showing phase changes resulting from Mg insertion into RuO_2 . Reprinted with permission from ref 44. Copyright 1990 The Electrochemical Society.

As Mg is incorporated into the RuO_2 host material, the composition of the cathode moves from pure RuO_2 to the composition represented by point A in the phase diagram ($\text{Mg}_{0.66}\text{RuO}_2$) while exhibiting a relatively constant potential. Further addition of Mg moves the composition along the line from point A to point B. In this region of the phase diagram the stable phases include MgO and Ru. The voltage of the cell decreases with (likely) irreversible formation of MgO as a discharge product. When the ruthenium is fully reduced to Ru^0 further discharge is impossible. However, so long as the cell is not discharged beyond the composition represented by point A in the phase diagram the electrochemistry appears to be fully reversible, and a rechargeable battery can be operated. The relatively flat discharge curves also imply that the intercalate is in equilibrium with the host compound and that both are present in the cathode during cell discharge rather than having a situation where the entire host compound is being simultaneously reduced. This also appears to support a $\text{Ru(IV)}/\text{Ru(II)}$ reduction in the higher voltage plateau.

The only battery cycling behavior reported in this work was for the cell $\text{Mg}|0.25 \text{ M Mg[B(Bu}_2\text{Ph}_2\text{)]}_2\text{-THF/dimethoxyethane|Co}_3\text{O}_4$ (shown in Figure 20). Low open-circuit potential

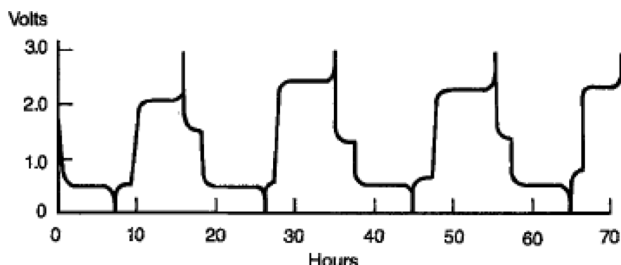


Figure 20. Cycling behavior of the cell $\text{Mg}|0.25 \text{ M Mg[B(Bu}_2\text{Ph}_2\text{)]}_2\text{-THF/dimethoxyethane|Co}_3\text{O}_4$. Reprinted with permission from ref 44. Copyright 1990 The Electrochemical Society.

(~1.5 V) and substantial polarization were observed, although the average cathode material utilization was 86%. It is noteworthy that results at Toyota R&D have shown magnesium organoborates containing a butyl group have a low voltage stability of 1.9 V due to β -H elimination.

A similar survey approach was reported by Bruce et al., who evaluated several transition metal oxides and sulfides for Mg^{2+}

insertion capacity via chemical intercalation using di-*n*-butyl magnesium and magnesium bis(2,6-di-*tert*-butylphenoxyde); in general, the phenoxide appeared to be inferior to the di-*n*-butyl magnesium for this purpose.¹¹³ Results from this work are summarized in Table 3.

Table 3. Chemical Intercalation of Mg into Various Host Materials^a

host material	Mg:host (mole)
TiS_2 (layered)	0.22
TiS_2 (cubic)	0.25
V_2O_5	0.10
V_6O_{13}	0.48
WO_3	0.08
MoO_3	0.05
$\gamma\text{-MnO}_2$	0.32
$\lambda\text{-MnO}_2$	0.09
$\beta\text{-MnO}_2$	0.02

^aReprinted with permission from ref 113. Copyright 1991 Royal Society of Chemistry.

The measured capacity of certain materials was clearly dependent on the crystal structure of the host material, especially for MnO_2 . Use of host materials with differing crystal structure, particle size, and porosity are possible explanations for the apparent discrepancies between results obtained in this work and those reported by others for compounds of equivalent composition.

Similarly, Novak and Desilvestro evaluated electrochemical intercalation of Mg^{2+} into TiS_2 , ZrS_2 , RuO_2 , Co_3O_4 , and V_2O_5 using an electrolyte of 1 M $\text{Mg}(\text{ClO}_4)_2/\text{ACN}$.¹¹⁴ Interestingly, they reported an improved performance when the electrolyte contained ~1 M H_2O and speculated that water molecules cointercalate with the Mg^{2+} cations and provide a smaller solvation shell than the organic solvent molecules. As a result, the charge distribution of the intercalated species could be improved and less pronounced structural changes in the host material could be observed. Even so, the authors reported irreversible, low capacities with TiS_2 (which was observed to undergo decomposition during electrochemical oxidation), ZrS_2 , RuO_2 , and Co_3O_4 . However, a first cycle capacity of >170 mAh/g for Mg^{2+} intercalation into V_2O_5 using 1 M $\text{Mg}(\text{ClO}_4)_2/\text{ACN}$ containing 1 M H_2O was measured. This Coulombic capacity declined rapidly in the first few cycles, stabilizing at about 50 mAh/g between cycles 10 and 20. This work focused on the behavior of the cathode materials in the wet electrolytes and did not discuss the behavior of the Mg counter electrode. However, it was noted that an electrolyte containing a significant concentration of water is likely to be impractical for use in a secondary Mg battery due to reactivity between water and the negative electrode.

2.2.1.2. Mg^{2+} Intercalation into Oxides. **2.2.1.2.1. Vanadium Oxides.** The promising results for Mg^{2+} intercalation into V_2O_5 obtained by Novak and Desilvestro led to additional investigations of vanadium oxides as possible cathode materials for secondary Mg batteries. Novak et al. synthesized a series of hydrated vanadium bronzes ($\text{MV}_3\text{O}_8 \cdot x\text{H}_2\text{O}$ where $\text{M} = \text{Li}, \text{Na}, \text{K}, \text{Ca}_{0.5}$, $\text{Mg}_{0.5}$, and $\text{V}_2\text{O}_5 \cdot y\text{H}_2\text{O}$ where y is typically up to 3).^{115–117} Use of organic solvent-based electrolytes containing significant amounts (1–2 M) of water were again found to yield specific capacities for Mg^{2+} intercalation significantly greater than those obtained with dry electrolytes. For example, the first

cycle specific capacity of NaV_3O_8 in “dry” $\text{Mg}(\text{ClO}_4)_2/\text{PC}$ was about 80 mAh/g, but with an ACN-based electrolyte containing 2 M H_2O a first cycle-specific capacity of 210 mAh/g was obtained. Use of a dry $\text{MgCl}_2/\text{AlCl}_3/1\text{-ethyl-3-methylimidazolium chloride}$ ionic liquid electrolyte enabled Mg^{2+} intercalation into $\text{Mg}(\text{V}_3\text{O}_8)_2$ with a first cycle-specific capacity of 150 mAh/g which declined to about 60 mAh/g after 50 cycles. The importance of the presence of H_2O in the cathode material structure was illustrated by the use of vanadium bronzes dried or synthesized at different temperatures which contained varying amounts of bound water; the measured specific capacity was found to decrease as the drying or synthesis temperature increased. Also, V_2O_5 xerogel which contained up to about 3 water molecules per V_2O_5 demonstrated first cycle capacities of about 170 mAh/g in both dry ACN and ionic liquid-based electrolytes. In order to address the issue of water reactivity in hydrated cathode materials the authors attempted to replace the lattice water molecules with solvent molecules such as DMSO but were unsuccessful due to the inability to produce materials with well-defined structures; these materials did not display electrochemical activity.

The effect of the water content of the electrolyte on Mg^{2+} intercalation into V_2O_5 was explored further by Yu and Zhang.¹¹⁸ They utilized the electrochemical cell $\text{Mg}(0.1 \text{ M } \text{Mg}(\text{ClO}_4)_2-x\text{M H}_2\text{O}-\text{PC})\text{V}_2\text{O}_5$ and found that the first cycle discharge capacity increased from 61.6 mAh/g when $x = 0$ to 158.6 mAh/g (corresponding to a $\text{Mg}:\text{V}_2\text{O}_5$ molar ratio of 0.53:1) when $x = 1.79 \text{ M H}_2\text{O}$. Capacity also faded rapidly with subsequent cycles, declining to 42.7 mAh/g by the ninth cycle. This was attributed in part to the irreversibility of the Mg electrode in this electrolyte; possible reduction in the water content of the electrolyte due to reaction with the Mg anode may have also played a role in this observation. The authors noted that low mobility of Mg^{2+} ions in passivation films formed on the Mg electrode surface due to reaction with water in the electrolyte would render the Mg electrode relatively inactive. The focus of the work was on the cathode, however, and characterization of surface films on the Mg electrode was not reported. Discharge curves at 0.3 mA/cm² exhibited two plateaus at about 1.35 and 0.8 V, although the second plateau appeared to be less distinct than the first plateau. The charge curve also exhibited two voltage plateaus. The impact of the water content of the electrolyte on the electrochemistry of Mg^{2+} insertion into V_2O_5 can be clearly seen in Figure 21, which shows cyclic voltammograms obtained using both dry and wet electrolytes.

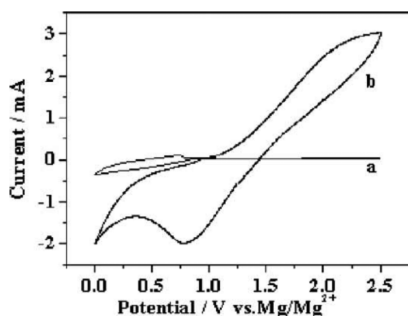


Figure 21. Cyclic voltammograms of V_2O_5 at a 1 mV/s scan rate in dry (scan a) and wet (scan b) electrolytes. Reprinted with permission from ref 118. Copyright 2004 Elsevier.

The shape of curve b in Figure 21 would suggest that there are substantial differences between the oxidation and the reduction reactions. The authors noted that irreversibility of one or both of the electrodes could contribute to this and speculated that formation of a passive film on the Mg counter electrode in particular may have influenced the apparent behavior of the V_2O_5 working electrode.

Electrochemical impedance spectroscopy indicated a decrease in both the contact capacitance and the resistance of the cathode as water is added to the electrolyte, while cell cycling resulted in increased solution and charge-transfer resistance. Color change of the V_2O_5 from yellow to black was also noted during discharge; phase changes were also confirmed with XRD.

These electrolytes composed of commercial salts such as $\text{Mg}(\text{ClO}_4)_2$ and polar solvents (excluding ethers) such as ACN or PC used to evaluate the cathodes are incompatible with a secondary magnesium metal anode. As a result, the cyclability reported for these cathodes with magnesium metal anodes is difficult to explain unless electrolyte decomposition was enabled by the use of a substantial excess of electrolyte.

Jiao et al. synthesized Cu-doped vanadium oxide nanotubes with electronic conductivity up to an order of magnitude higher than undoped material and increased interlayer spacing (3.67 vs 3.48 nm).¹¹⁹ First cycle discharge capacity at 10 mA/g current density was 120.2 vs <70 mAh/g for undoped material. Electrochemical impedance spectroscopy indicated a 35% decrease in charge transfer resistance for the doped vs undoped material. The electrolyte used in this work was DCC, which is capable of reversible Mg deposition/dissolution; thus, the cells constructed in this work were apparently capable of true reversible behavior at both electrodes, in contrast to much of the published work with Mg/vanadium oxide cells.

Nanoparticles of V_2O_5 were synthesized by Amatucci et al.¹²⁰ by a combustion flame/chemical vapor condensation process that produced primary particles on the order of 25 nm in diameter. This material was evaluated for its ability to electrochemically intercalate Li^+ , Mg^{2+} , Ca^{2+} , and Y^{3+} . Electrolytes mainly consisted of solutions of perchlorate salts of the target cation in PC, and the counter electrode utilized capacitive adsorption of perchlorate anion on activated carbon. Reversible capacities measured for cation intercalation into this nanocrystalline V_2O_5 material are shown in Table 4.

Table 4. Reversible Cation Intercalation into Nanocrystalline V_2O_5 ^a

cation	capacity (mAh/g _{host})
Li^+	140
Mg^{2+}	180
Ca^{2+}	200
Y^{3+}	260

^aData derived from ref 120.

Compared to Li^+ the polyvalent cations all exhibited significant charge/discharge voltage hysteresis; however, the nanocrystalline material still performed better in this regard than microcrystalline material.

Le et al. synthesized V_2O_5 aerogels via hydrogel synthesis followed by exchange of water with acetone and supercritical CO_2 drying.¹²¹ The resulting materials were evaluated for Mg^{2+} insertion capacity via chemical reduction with dibutylmagnesium and found to be capable of storing up to 2 mol of Mg per

V_2O_5 (589 mAh/g based on V_2O_5 formula weight). The volumetric capacity of the aerogel vs V_2O_5 xerogel was not discussed. The higher gravimetric capacity obtained for the aerogel vs xerogel was attributed to a greater interlayer spacing (1.25 nm via XRD vs 0.88 nm in xerogel). This increased interlayer spacing along with smaller pore wall dimensions was speculated to result in improved Mg^{2+} diffusivity in the aerogel vs the xerogel, leading to the increase in measured capacity. The measured capacity of the aerogel would result in a reduction of vanadium from the V to the III oxidation state.

Use of polymeric gel electrolytes instead of organic or ionic liquid electrolytes with V_2O_5 cathodes was evaluated by Morita et al.^{83,122} The cell $\text{Mgloligo}(\text{ethylene oxide})$ -grafted polymethacrylate/linear polyether/Mg trifluoromethane sulfonyl imide/ V_2O_5 exhibited a first cycle discharge capacity of about 100 mAh/g V_2O_5 but poor rechargeability, apparently due to high interfacial resistance at the Mg/polymeric electrolyte interface. Substitution of mixed EC/DMC for the polyether solvent and substitution of $\text{Mg}_x\text{V}_2\text{O}_5$ for Mg to construct a dual intercalation cell yielded a cell with recharge capability. The first cycle discharge capacity of this cell was 130 mA/g V_2O_5 , decreasing to about 60 mAh/g after 5 cycles. Degradation at the polymeric electrolyte/oxide interface and trapping of some intercalated Mg^{2+} in the oxide structure were cited as possible reasons for this capacity loss.

Electrochemical intercalation of Mg^{2+} into thin films of V_2O_5 was evaluated by Gershinsky et al. at very low current density in order to examine the fundamental properties of this material under conditions where slow solid-state diffusion of Mg^{2+} would have minimal impact on the results.¹²³ Vacuum-deposited 200 nm films of V_2O_5 on Pt substrates (20–50 nm primary particle size) were used as the cathode along with activated carbon cloth anodes (capable of reversible charge storage via double-layer capacitance rather than faradaic reactions) and electrolytes consisting of either 0.1 M magnesium bis(trifluoromethane sulfonyl)imide or 0.5 M $\text{Mg}(\text{ClO}_4)_2$ in dry ACN. Highly reversible electrochemical intercalation of Mg^{2+} into the V_2O_5 thin films was observed with a first cycle capacity of about 180 mAh/g, decreasing to a stable value of 150 mAh/g (corresponding to 0.5 mol of Mg per mole of V_2O_5) after 25 cycles.

A V_2O_5 /sulfur composite cathode material was prepared via a microwave water plasma technique by Inamoto et al. and exhibited discharge capacities as high as 300 mAh/g using an electrolyte of 0.3 M $\text{Mg}(\text{ClO}_4)_2$ in PC with 1.8 M H_2O added.¹²⁴ The first discharge exhibited two voltage plateaus; the second plateau at 1.0 V vs Mg (which disappeared in subsequent cycles) was attributed to sulfur oxidation, and S was identified in the electrolyte after cell disassembly. Addition of transition metal oxides to the V_2O_5 /S composite via ball milling to suppress S solubility was successful in increasing discharge capacity as shown in Table 5.

The V_2O_5 /S/ MnO_2 material appeared to develop an amorphous surface layer similar to a V_2O_5 xerogel and did not show distinct discharge or charge voltage plateaus unlike the other blends tested. Open-circuit voltage was >2 V, and typical discharge voltage declined from about 1.5 to 0.9 V, although the composite with NiO exhibited a slightly higher average discharge voltage. These reported capacities are impressive with respect to most other reported Mg battery cathode candidates; however, the fact that the electrolyte used was not capable of reversible deposition/dissolution of Mg and contained water must be taken into account when considering

Table 5. Effect of Metal Oxide Addition to V_2O_5 /S on Specific Capacity^a

metal oxide	second cycle discharge capacity (mAh/g)
MnO_2	420
MoO_3	320
Fe_2O_3	300
NiO	290
ZrO_2	230

^aData derived from ref 124.

these results. Verification using electrolytes compatible with both reversible Mg electrodes and sulfur cathodes would be a logical next step in evaluation of this cathode technology.

Although considerable variation in the reported Mg^{2+} intercalation capacity of V_2O_5 has appeared in the literature, the results of the fundamental studies of Gershinsky¹²³ appear to corroborate the results of a number of studies which yielded a measured capacity of approximately 150 mAh/g V_2O_5 . Slow solid-state diffusivity of Mg^{2+} due to its high charge density and strong interaction with the host material appears to have a strong limiting effect on the cell operating characteristics using this cathode active material. The structure of the material also appears to have an impact on its electrochemical performance.

While considerable effort has gone into measuring the electrochemical properties of Mg^{2+} intercalation into V_2O_5 , the mechanistic aspects of this reaction have received comparatively less attention. Gershinsky et al.¹²³ reported that the insertion and half-wave potentials for Mg^{2+} insertion into V_2O_5 are very close to those for Li^+ insertion into the same material, thus supporting a similar mechanism involving reduction of the vanadium metal centers. This was also supported by a color change from yellow to faint green upon Mg^{2+} insertion, indicative of a $\text{V}^{5+}/\text{V}^{3+}$ transition. Computation of dQ/dV curves from galvanostatic profiles indicated the existence of four different stages for Mg^{2+} insertion/deinsertion in V_2O_5 . These different stages were attributed to formation of different phases with distinct thermodynamic and kinetic behavior, although attempts to associate each process with a particular phase were not made. Raman and XRD analysis of V_2O_5 at different stages of Mg^{2+} insertion/deinsertion also indicated structural reversibility. XRD peak shifts for Mg^{2+} insertion were similar to those measured for Li^+ insertion, but new peaks observed for the magnesiated material have not been observed in lithiated material, indicating formation of a new phase. Demagnesiation resulted in a return to the pattern of pristine material. Similar XRD results were obtained by Yu and Zhang.¹¹⁸

2.2.1.2.2. Manganese Oxides. The early cathode material survey of Gregory et al.⁴⁴ identified Mn_2O_3 and Mn_3O_4 as having the ability to incorporate up to 0.66 mol of Mg per mole of host material via chemical reduction techniques, corresponding to specific capacities of 224 and 154 mAh/g of host material, respectively. The open-circuit voltage vs Mg in $\text{Mg}(\text{ClO}_4)_2/\text{THF}$ was reported as 2.40 V for both materials. Charge/discharge behavior was not reported. Most subsequent work with manganese oxides in Mg battery systems has utilized MnO_2 of varying crystal structures. The Mg–Mn–O phase diagram (Figure 22) shows that discharge of a $\text{Mg}|\text{MnO}_2$ cell would appear to proceed via single-phase formation of the Mg/ MnO_2 intercalate until a composition of MgMn_2O_4 is reached. Further discharge would be expected to result in irreversible disproportionation into a number of manganese (III,II) oxides and Mg–Mn–O species. The composition MgMn_2O_4

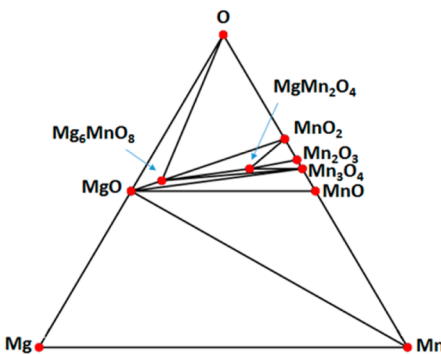


Figure 22. Mg–Mn–O phase diagram, constructed using the phase diagram app at www.materialsproject.org.

corresponds to a Mg loading of 0.5 Mg per host molecule and a specific capacity of 308 mAh/g MnO₂.

Manganese dioxide has been reported to function reversibly in a gel polymer electrolyte (polyacrylonitrile or poly(methyl methacrylate), PC, EC, Mg(CF₃SO₃)₂) secondary Mg battery.^{125,126} The reversible capacity was reported to be 20 mAh/g MnO₂ in the polyacrylonitrile-based electrolyte and 70 mAh/g in the PMMA-based electrolyte, which correspond to discharged cathode compositions of Mg_{0.065}Mn₂O₄ and Mg_{0.228}Mn₂O₄, respectively. The PAN-based electrolyte cell failed after 20 cycles due to increasing charge voltage. Failure modes cited were passivation of the Mg anode surface and poor rechargeability of the MnO₂ electrode. The nature of the surface film formed on the Mg electrode was not determined, although ac impedance data indicated that the resistance of this film was substantially higher than that of the GPE.

An evaluation of various MnO₂ crystal structures [Hollandite (2 × 2 tunnel), OMS-5 (4 × 2 tunnel), and Birnessite (layered)] determined that the Hollandite structure demonstrated the highest reversible capacity when incorporated into an electrode with acetylene black.¹²⁷ Average specific capacities over 8 cycles at 100 mA/g current density were Hollandite ≈ 140 mAh/g, OMS-5 – 95 mAh/g, and Birnessite ≈ 60 mAh/g. The discharge curves did not display well-defined voltage

plateaus, and significant voltage hysteresis was observed between charge and discharge cycles, possibly indicative of slow Mg²⁺ ion diffusion. A subsequent study by the same authors utilized hydrothermal synthesis to produce Hollandite with the empirical formula K_{0.14}MnO₂·xH₂O in a composite with acetylene black and sol–gel synthesis to produce pristine Hollandite MnO₂ which was physically mixed with acetylene black prior to incorporation into electrode structures using 15 wt % PTFE binder.¹²⁸ The presence of K⁺ and H₂O in the hydrothermally synthesized composite Hollandite/acetylene black is believed to impart improved structural stability to the material, and this material exhibited higher capacity than the sol–gel-synthesized material (210 vs 85 mAh/g first cycle discharge capacity at 100 mA/g MnO₂; ~140 vs ~60 mAh/g in cycles 2–8). However, the cell used in these studies was Mg|1 M Mg(ClO₄)₂–ACN|MnO₂ with a Ag/AgNO₃–Bu₄NClO₄–AN reference electrode. Since this electrolyte is incapable of reversible Mg deposition/dissolution, it is unclear what role if any that electrolyte decomposition products which could have formed at the anode may have played in the results obtained in this study. Nevertheless, conclusions from this study that first cycle capacity loss likely resulted from Mg²⁺ trapping in the cathode material and that the presence of water molecules in the structure of the hydrothermally synthesized material likely improved cycling performance of that material due to shielding of the charge on the inserted cations appear to be consistent with other studies.

Zhang et al. evaluated commercial Hollandite MnO₂ as a cathode in secondary Mg batteries using 0.2 M GEN1/THF electrolyte which is capable of reversible Mg deposition/dissolution.¹²⁹ The cathode composition was 70 wt % active material, 20 wt % carbon black, and 10 wt % PTFE. The first cycle discharge capacity was measured as 280 mAh/g MnO₂ at 36 μA/cm², corresponding to a loading of about 0.47 Mg per Mn or nearly the expected MgMn₂O₄ composition of a fully discharged cathode as per the phase diagram in Figure 22. Significant capacity fade was observed; by the sixth cycle the discharge capacity was <100 mAh/g. Figure 23 shows charge/discharge curves for the first 6 cycles, and XRD and XPS spectra of the positive electrode at different states of charge

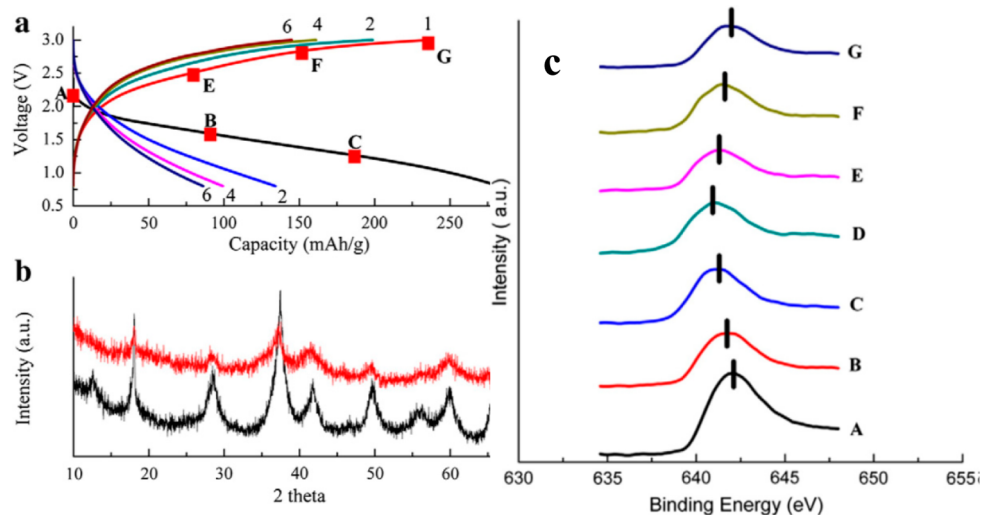


Figure 23. (a) Galvanostatic cycle of α -MnO₂ at 0.015 C rate. Red bars show the discharge/recharge states of the sample taken for XPS and XAS measurements. (b) XRD patterns of as-prepared α -MnO₂ electrode and fully discharged electrode. (c) XPS Mn 2p3/2 peaks of α -MnO₂ electrode with various electrochemical states as shown in panel a. Reprinted with permission from ref 129. Copyright 2012 Elsevier.

during both charge and discharge. The changes in binding energy of the Mn 2p3/2 peaks and the reversible shifts in peak position indicate reversible redox reactions of the MnO_2 .

Crystal structure instability due to Jahn–Teller distortion and Mn dissolution from the cathode material were cited as possible contributing factors to this behavior. The first cycle discharge capacity was also found to be dependent on cathode active material particle size; 280 mAh/g was measured with 20 nm average particle size MnO_2 vs 170 mAh/g for 100 nm particles, which may well be indicative of slow Mg^{2+} diffusion. XPS and XAS studies of the MnO_2 electrode at varying state of charge showed the expected changes in the Mn oxidation state and that some of the Mg inserted in the first discharge was not extracted in the subsequent charge cycle, leading to the observed irreversible capacity loss. Studies of the MnO_2 electrode via XRD and XANES revealed that the structure of the material recovered reversibly upon Mg deinsertion, but the recovery was incomplete, leading to some collapse of the tunnel structure. The authors speculated that methods for stabilizing the tunnel structure could potentially improve cycling performance of this cathode material. Techniques which have been employed to improve the performance of manganese oxide-based cathode materials in Li-ion batteries may also be potentially useful to reduce capacity fade and Mn dissolution in Mg batteries. Substitution of other transition metals for some of the Mn, electrolyte additives to suppress Mn dissolution, and use of composite cathode materials which blend another cathode material with Mn oxides are all potential techniques which could be explored. Sanchez and Pereira-Ramos¹³⁰ studied the electrochemical behavior of the mixed oxide $\text{Mn}_{2.15}\text{Co}_{0.37}\text{O}_4$ using an electrolyte of 0.1 M $\text{Mg}(\text{ClO}_4)_2$ /propylene carbonate and obtained a stable capacity of only about 30 mAh/g after 20 cycles. Capacity was primarily attributed to reduction of Mn^{4+} but believed to be limited by strong Coulombic repulsive interactions.

2.2.1.2.3. Other Oxides. As noted previously, results of Mg^{2+} chemical reduction experiments with MoO_3 were highly variable and thus inconclusive. Spahr et al. achieved electrochemical intercalation of Mg^{2+} into MoO_3 from ionic liquid (3 wt % MgCl_2 /41 wt % ethylmethyl imidazolium chloride/56 wt % AlCl_3) and wet organic (1 M $\text{Mg}(\text{ClO}_4)_2$ /ACN containing 3 mol % H_2O) electrolytes.¹³¹ No significant intercalation was observed using dry propylene carbonate-based electrolytes. Figure 24 shows specific capacity vs cycle number for Mg^{2+} intercalation into MoO_3 from the ionic liquid and wet organic electrolytes. A first cycle discharge capacity in the ionic liquid electrolyte of about 150 mAh/g (corresponding to an intercalant stoichiometry of $\text{Mg}_{0.38}\text{MoO}_3$) was measured, but the capacity faded to slightly above 50 mAh/g after 10 cycles. Use of the wet organic electrolyte, however, yielded 210 mAh/g in the first cycle and stabilized around 160 mAh/g after about 8 cycles.

Two potential explanations for the apparent capacity increase using the wet organic electrolyte were suggested. The first, solvation of Mg^{2+} with water molecules resulting in attenuation of the ion's strong polarization effect, has also been used to explain a similar effect observed with V_2O_5 .¹¹⁸ The second potential explanation involves parallel intercalation of H^+ along with Mg^{2+} . This phenomenon has also been observed in $\text{Mg}/\text{Mg}(\text{ClO}_4)_2/\text{AN}/\text{H}_2\text{OIV}_6\text{O}_{13}$ cells.

This work confirms that MoO_3 can reversibly intercalate significant amounts of Mg^{2+} ; however, these results were obtained via use of cyclic voltammetry at a 10 $\mu\text{V}/\text{s}$ scan rate

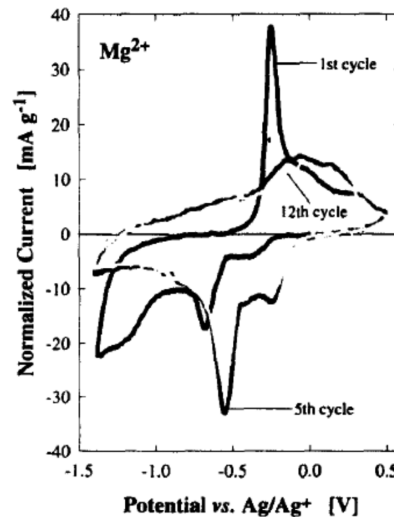


Figure 24. Electrochemical intercalation of Mg^{2+} into MoO_3 . Reprinted with permission from ref 131. Copyright 1995 Elsevier.

and galvanostatic cycling at a current density of 0.08 mA/cm², and thus, rate capability could not be determined.

Gershinski utilized MoO_3 thin films to study fundamental characteristics of Mg^{2+} intercalation and measured a reversible capacity of 210 mAh/g with 95% Coulombic reversibility over the first 10 cycles.¹²³ A dQ/dV plot of the discharge process showed two stages of intercalation at 1.80 and 1.74 V vs Mg/Mg²⁺. The electronic conductivity of the material was found to increase with increasing Mg loading, while deintercalation was speculated to lead to formation of Mg-deficient regions in the MoO_3 structure with low electronic conductivity, possibly leading to ion trapping and loss of capacity. The charge/discharge voltage hysteresis was greater for MoO_3 than that observed with V_2O_5 thin film electrodes, which was attributed to greater kinetic limitations with MoO_3 . Gershinski et al. did not evaluate these cathodes using electrolytes compatible with a magnesium metal anode which were previously reported from his laboratory.

RuO_2 is another compound which showed promise in both chemical and electrochemical Mg^{2+} intercalation screening experiments. Koch et al. constructed what may have been the first Mg-ion batteries using magnesiated graphite negative electrodes, RuO_2 positive electrodes, and an electrolyte containing 1 M $\text{Mg}(\text{ClO}_4)_2$ in 1:1:1 PC/EC/DMC.¹³² Although these cells were only cycled over a narrow positive electrode state of charge range, they did exhibit an open-circuit potential close to 2.5 V and sustained at least 200 cycles. Sutto and Duncan examined the electrochemical behavior of RuO_2 using an electrolyte of 1 M $\text{Mg}(\text{ClO}_4)_2$ in an ionic liquid (1,2-dimethyl-3-octylimidazolium bis(trifluoromethanesulfonyl)-imide, MMOITFSI).¹³³ A cyclic voltammogram of RuO_2 in this electrolyte at 0.1 mV/s (Figure 25a) showed an intercalation peak at about 4.3 V and a deintercalation peak at about 3.7 V. The higher intercalation voltage for Mg^{2+} vs Li^+ in RuO_2 was interpreted as being due to a greater energy barrier for intercalation of the more charge dense Mg^{2+} ion, while the deintercalation peak location was interpreted to indicate that Mg^{2+} is more tightly bound in RuO_2 than is Li^+ . Figure 25b shows the discharge capacity of RuO_2 in the Mg electrolyte as a function of cycle number at a C/3 discharge rate. The first cycle capacity of 101 mAh/g corresponds to a discharged stoichiometry of $\text{Mg}_{0.25}\text{RuO}_2$, and the observed capacity fade

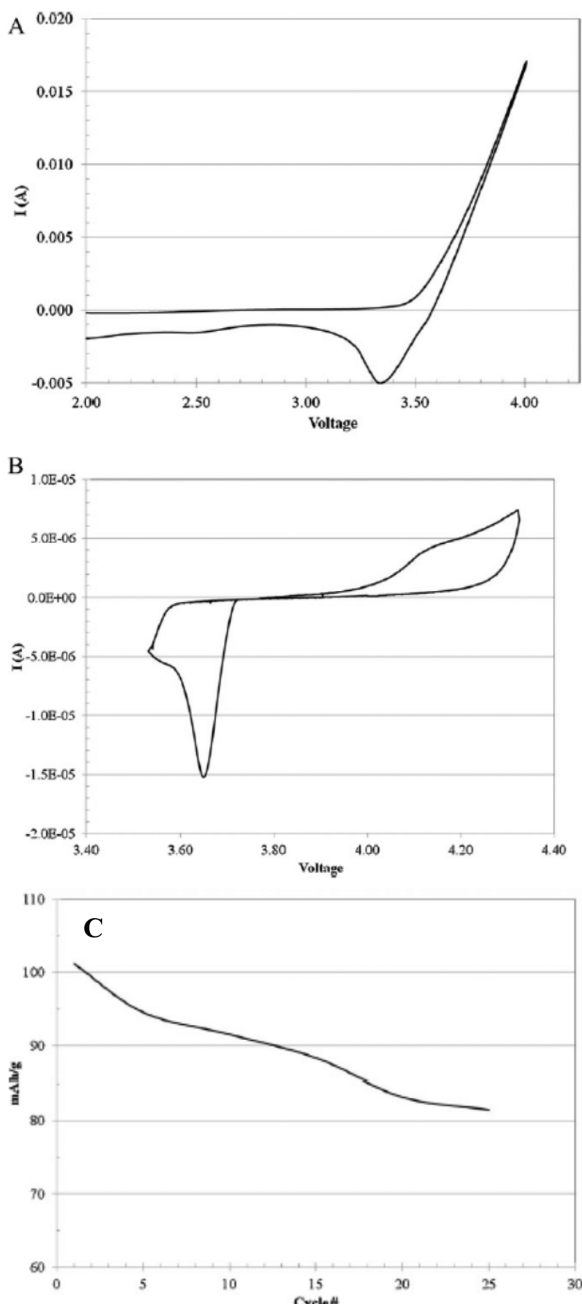


Figure 25. Cyclic voltammogram and specific capacity for Mg^{2+} intercalation/deintercalation in RuO_2 . Reprinted with permission from ref 133. Copyright 2012 Elsevier.

was attributed to the apparent poor reversibility of the electrode material.

Sutto and Duncan also evaluated the electrochemical performance of Co_3O_4 in ionic liquid electrolytes and obtained a maximum loading of $Mg_{0.33}Co_3O_4$ (74 mAh/g). Similar to their results with RuO_2 , rapid capacity fade was noted and attributed to difficulty in deintercalating Mg^{2+} .¹³⁴ However, in contrast to their results with RuO_2 , the voltammograms obtained for Co_3O showed much less peak separation and thus improved reversibility. It was also observed that deintercalation of Mg^{2+} from RuO_2 required a high applied potential. These observations were attributed to stronger interaction of Mg^{2+} with RuO_2 than with Co_3O_4 . Synthesis of a spinel-type magnesium cobalt oxide ($MgCo_2O_4$) by Kamioka

et al. via solid-state reactions between MgO and Co_3O_4 was unsuccessful, but a solution process starting with the metal nitrates did produce the desired structure, although Mg^{2+} mobility in that material appeared to be very limited.¹³⁵

In an attempt to develop cathode materials capable of Mg^{2+} intercalation at more positive potentials and thus create a Mg battery with higher cell voltage, Ichitsubo et al. utilized coprecipitation synthesis to produce $MgCo_2O_4$ (spinel structure) and $Mg_{0.67}Ni_{1.33}O_2$ (rock salt structure).¹³⁶ The cobalt spinel material generated an initial open-circuit voltage of 3.5 V vs Mg using an electrolyte of 1 M $Mg(ClO_4)_2$ in ACN, although voltage decay was seen which was attributed to structural relaxation and migration of Mg from the interior of the particles to the surface. The reported open-circuit voltage for the magnesium nickelate was 3.5–3.8 V. Specific capacities were not determined for these materials; however, commercially available $MgCo_2O_4$ appears to offer very low capacity (<15 mAh/g) and high polarization.¹³⁷

2.2.1.3. Mg^{2+} Intercalation into Molybdenum Sulfides and Selenides. The most extensively studied group of compounds for electrochemical Mg^{2+} intercalation is Chevrel phase $M_xMo_6T_8$, where M = metal and T = S, Se, or a combination of both. These materials consist of octahedral clusters of Mo atoms inside cubic anion frameworks and can be considered as consisting of stacks of Mo_6T_8 blocks. The Mo atoms exhibit variable valence, and the anionic framework is flexible with multidirectional paths for ionic diffusion and multiple types of cavities for inserted cations which enables intercalation of cations of different sizes. The Mo_6 clusters can sustain charge injection of up to 4 electrons, suggesting a theoretical capacity of up to 2 Mg^{2+} ions per Chevrel phase unit (129 mAh/g Mo_6S_8).¹³⁸ These are metastable compounds which are typically synthesized in the form of, for example, $CuMo_6S_8$ via high-temperature reaction of the elements in a sealed container followed by removal of the Cu via chemical or electrochemical leaching.¹³⁹ Aurbach et al. first reported the use of Mo_3S_4 as a reversible cathode material in the cell $Mg|DCCl|Mo_3S_4$.¹⁴⁰ Figure 26 shows a typical cell discharge curve obtained in this work along with a cyclic voltammogram of the cathode material and the crystal structure of the Chevrel phase material showing sites occupied by Mg^{2+} .

The two discharge plateaus correspond to Mg^{2+} insertion into the so-called inner and outer sites in the Chevrel phase material, which correspond to intercalation of the first and second Mg^{2+} ions per Mo_6S_8 . Coin cells constructed with these materials exhibited >2000 discharge/charge cycles at 100% depth of discharge at practical rates (0.1–1 mA/cm²) over a wide temperature range from –20 °C to +80 °C with <15% capacity fade. This indicates that these cathode materials, while not necessarily providing energy densities similar to those of Li-ion batteries, can be used in long cycle life Mg batteries potentially suitable for applications such as stationary energy storage.

A number of features of these compounds which impact their electrochemical behavior were identified in these studies. Unlike most previously identified Mg^{2+} intercalation cathode materials, these Chevrel phase compounds were found to exhibit rapid Mg^{2+} diffusivity, which was attributed to the presence of a large number of vacant sites and relatively short distances between these sites. In addition, the octahedral Mo clusters with delocalized electrons permitted rapid redistribution of the two electrons needed to balance the charge of each Mg^{2+} -ion inserted.¹⁴¹ However, Levi et al. found that the initial

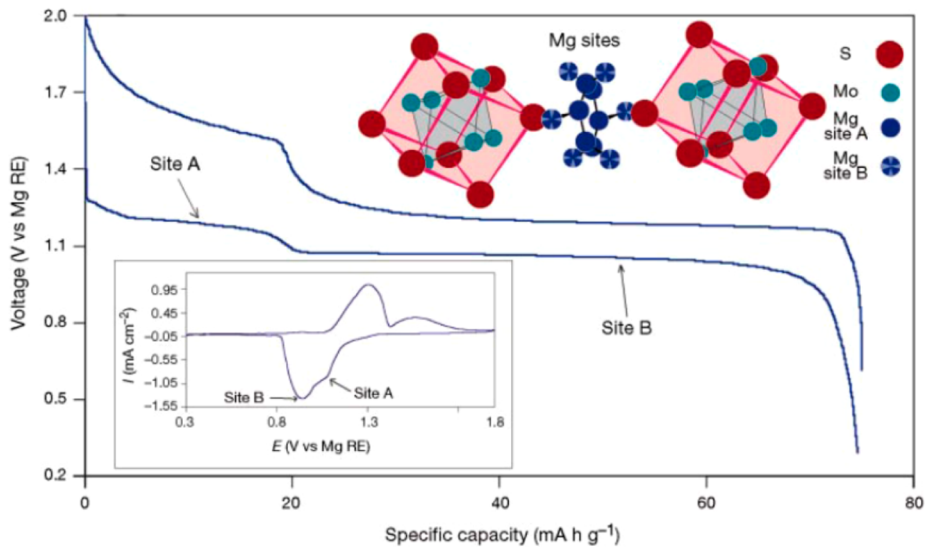


Figure 26. Electrochemical characteristics of Mg^{2+} intercalation into Mo_3S_4 . Cell discharge current density was 0.3 mA/cm^2 , and CV scan rate was 0.05 mV/s . Note the different response to intercalation into site A vs site B. Reprinted with permission from ref 140. Copyright 2000 Nature Publishing Group.

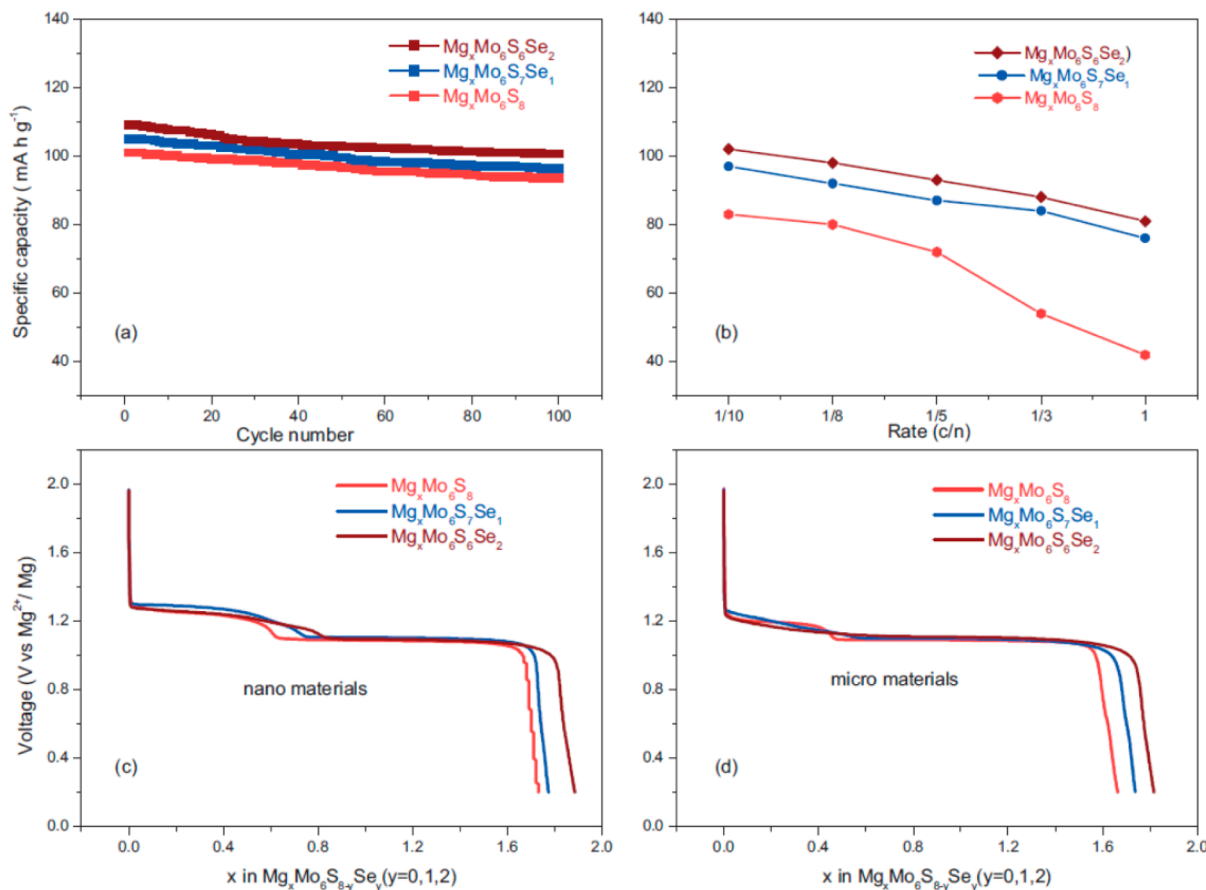


Figure 27. Effect of substitution of Se for S in Mo_6S_8 . Reprinted with permission from ref 48. Copyright 2007 WILEY-VCH Verlag GmbH & Co. KGaA, Weinheim.

Mg^{2+} insertion (and final Mg^{2+} deinsertion during cell recharge) was relatively slow at room temperature, which was attributed to low ionic conductivity (low mobility and low concentration) in the solid.¹⁴² Also, some irreversible capacity loss was noted in this work which was attributed to Mg^{2+} -ion trapping in the Chevrel phase materials. Both of these

phenomena were much less evident at elevated temperature, as might be expected based on increased ionic conductivity and diffusivity with increased temperature. Substitution of Se for S was also found to enhance ionic diffusivity and substantially eliminate this ion trapping phenomenon.^{48,143} Substitution of up to 2 S atoms by Se in Mo_6S_8 was found to result in an

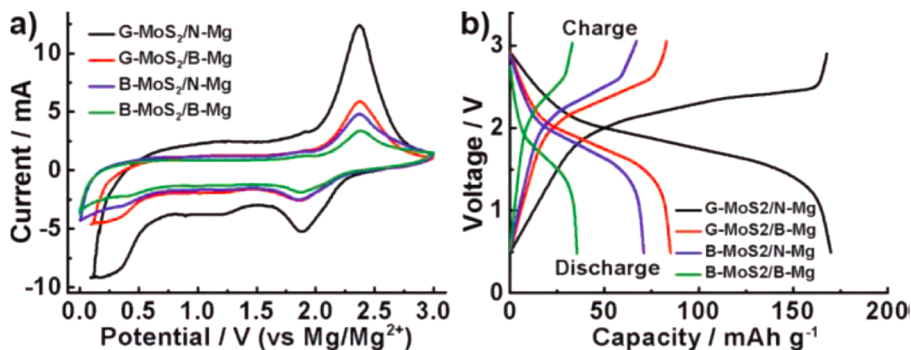


Figure 28. (a) Cyclic voltammograms of the electrodes made from B- and G-MoS₂ with B- and N-Mg as the counter and reference electrodes, measured at a scan rate of 1 mV/s. (b) Typical galvanostatic discharge–charge voltage profiles of the cells fabricated with B- or G-MoS₂ cathode and B- or N-Mg anode measured at a current density of 20 mA/g. Reprinted with permission from ref 148. Copyright 2011 WILEY-VCH Verlag GmbH & Co. KGaA, Weinheim.

increase in the moles of Mg inserted per mole of host material during the first discharge plateau, total moles of Mg inserted per mole host material over the entire discharge cycle, higher delivered specific capacity over at least 100 cycles (despite the fact that substitution of heavier Se for S results in a decrease in theoretical capacity), and improved rate capability. Figure 27 illustrates these factors.

Substitution of Se for some of the S in the Chevrel phase material was found to result in crystallographic changes in the material which changes the geometry of the Mg²⁺ insertion sites and prevents ion trapping in the inner ring sites. Increased polarizability of the anion framework was also cited as improving Mg²⁺ transport in the material. These factors improve the kinetics of Mg²⁺ insertion/deinsertion. The authors also indicated that the thermodynamics of the Mg²⁺ insertion process are also impacted by substitution of Se for S due to differing interactions between Mg and Se vs Mg and S.

Lancry et al. noted that the surface of Chevrel-phase materials was stable in electrolytes capable of reversible Mg deposition/dissolution and did not form surface films.¹⁴⁴ Thus, it was speculated that synthesis of these materials as nanoparticles could further enhance electrode kinetics through increased specific surface area and shorter diffusion distances without resulting in increased electrolyte decomposition. Milling was evaluated for nanoparticle formation; characteristics of milled materials depended strongly on milling conditions. Milling in air caused oxidation of the particle surfaces including formation of molybdenum sulfate, which resulted in a reduction in material performance. Milling under argon resulted in material with improved discharge characteristics as long as the milling time was relatively short (~5 min), but longer milling times caused amorphitization of the material and a reduction in useful capacity. Attempts to achieve improved electrochemical performance through synthesis of Chevrel-phase materials in nanostructures such as electrospun nanofibers with diameters in the 100–300 nm range have also been reported.¹⁴⁵ Another method which has been demonstrated to improve the performance of these materials is to allow at least a portion of the Cu used in the Cu_xMo₆S₈ precursor synthesis to remain in the material after the leaching step. Use of CuMo₆S₈ was found to yield improved capacities vs fully leached Mo₆S₈ due at least in part to the lack of charge trapping in this material.¹³⁹ An important feature of this material is that Cu⁺ apparently exchanges with Mg²⁺ during the initial stages of Mg insertion, eliminating the slow kinetics observed when Mg²⁺ is intercalated into Cu-free Mo₆S₈. One consideration, however,

is the possible deposition of Cu at the negative electrode during cell recharge.

The composition of the electrolyte was also found to have a substantial impact on the electrochemical behavior of Chevrel-phase materials. Organohaloaluminate electrolytes such as DCC were found to allow Mg²⁺ intercalation into Chevrel-phase cathodes as well as reversible Mg metal deposition/dissolution and thus allow construction of a rechargeable Mg battery. Addition of 0.5 M LiCl increased the specific conductivity of the electrolyte nearly 3-fold; Li⁺ was expected to be nonreducible at the operating conditions of the cell, and the added LiCl was found to influence the ionic equilibria in the solution. The specific capacity of the Chevrel-phase material increased from 92 to 113 mAh/g when LiCl was added to the electrolyte, and this improvement was sustained during extended cycling.¹⁴⁶ The biggest drawback to this system is that the cell operating voltage was only ~1.1 V.¹⁴⁰ The cathodic properties of Mo₆S₈ in 0.25 M Mg(ClO₄)₂/ACN were inferior to those achieved in the DCC electrolytes, with a capacity of 87 mAh/g, decreased faradaic efficiency, and poor cycling ability. Similar experiments with a Mg(ClO₄)₂/PC electrolyte resulted in no observations of reversible Mg²⁺ intercalation.¹⁴²

While Chevrel-phase materials have been shown to allow rapid, reversible Mg²⁺ intercalation using electrolytes capable of reversible Mg deposition/dissolution, their relatively low operating voltage and specific capacity are drawbacks to their use in practical secondary Mg batteries. Since the Mo₆ cluster structural component of these materials appears to be crucial to this intercalation behavior, two classes of materials have been proposed to take advantage of this structural element: Chevrel-type materials with stoichiometries such as Mo₆T₆ and Mo₁₅T₁₉ and cluster-containing Mo oxides such as NaMo₄O₆ and Mn_{1.5}Mo₈O₁₁. The authors also speculate that other metal clusters which may be useful in this application include Fe₆, Co₆, and Cr₆, although electrochemical data to support this is not available.¹⁴⁷

Layered MoS₂ has also been evaluated for use in secondary Mg batteries. Liang et al. prepared highly exfoliated (“Graphene-like”) MoS₂ via a solvothermal synthesis by reacting MoO₃ and thioacetamide in pyridine and reported an operating voltage of about 1.8 V and a reversible capacity of about 170 mAh/g when coupled with a nanoparticulate Mg negative electrode and an electrolyte of Mg(AlCl₃Bu)₂/THF.¹⁴⁸ Figure 28 shows cyclic voltammograms and charge/discharge curves for cells using both bulk (B) and highly exfoliated (G) MoS₂ cathodes and bulk (B) and nano-

particulate (N) Mg anodes. The combination of G-MoS₂ and N-Mg clearly exhibited the highest discharge capacity and also retained 95% of the first cycle capacity after 50 cycles. An estimated capacity of 223 mAh/g for fully exfoliated MoS₂ was determined using density functional theory calculations.

Liu et al. used hydrothermal synthesis to produce a series of MoS₂/carbon composites where the carbon was interspersed with the MoS₂ layers.¹⁴⁹ Figure 29 shows specific capacity vs

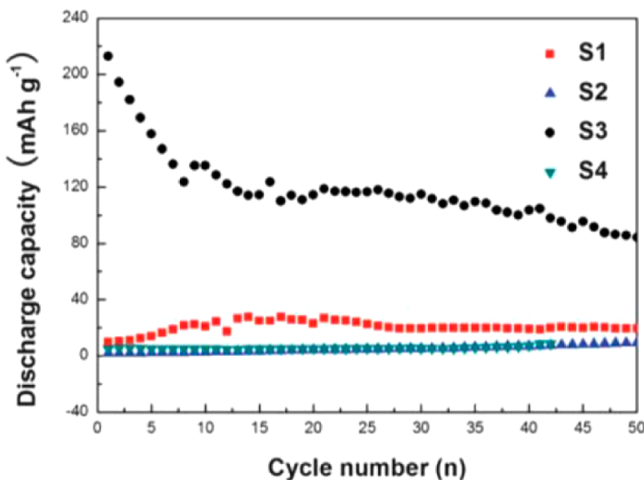


Figure 29. Cycling behavior of MoS₂/C composites. Reprinted with permission from ref 149. Copyright 2013 Royal Society of Chemistry.

cycle number for the different forms of MoS₂/C synthesized in this work at a discharge current density of 50 mA/g. The material designated as S3 (microspheres of highly exfoliated MoS₂, 0.5–1 μm diameter with curled nanosheets dispersed on the surface, 46.04% C) exhibited the most favorable electrochemical performance in the cell AZ31 Mg alloy|APC|MoS₂–C. The superior performance of the S3 composite was attributed to a synergistic effect of the carbon coating which imparts electronic conductivity and the highly exfoliated MoS₂ structure which allows electrolyte penetration throughout the material. Although capacities reported in this work were less than those reported by Liang,¹⁴⁸ the discharge current density was also significantly higher, and thus, it is difficult to directly compare the two sets of results. Nevertheless, highly exfoliated MoS₂ appears to hold promise as a cathode material for rechargeable Mg batteries.

2.2.1.4. Other Sulfides and Selenides. Previously cited work^{44,113,114} with various crystalline forms of TiS₂ yielded relatively low Mg²⁺ intercalation capacity and poor electrochemical performance. Tao et al. evaluated electrochemical Mg²⁺ intercalation from 1 M Mg(ClO₄)₂/ACN in TiS₂ nanotubes prepared by a gas-phase reaction and observed significantly improved performance vs polycrystalline TiS₂.¹⁵⁰ The first cycle discharge capacity of 236 mAh/g at 10 mA/g for TiS₂ nanotubes corresponds to a Mg loading of 0.49 per TiS₂ unit, while the first cycle Mg loading for polycrystalline TiS₂ was only about 0.2, which is consistent with previously reported values. The TiS₂ nanotubes also retained capacity > 180 mAh/g even after 80 cycles at 100% DOD. The improved capacity measured for these multiwall TiS₂ nanotubes vs polycrystalline material was attributed to the more orderly structure of the nanotubes, which led to a higher proportion of active sites for Mg²⁺ intercalation. It was speculated that small-grain bulk TiS₂ with platelet morphology should also exhibit similar capacities.

This invites conjecture as to whether exfoliation of bulk TiS₂ could produce a material with high capacity, similar to that cited above for highly exfoliated MoS₂.

Monoclinic NbS₃ prepared by high-temperature and -pressure reaction of a stoichiometric mixture of Nb and S was found to reversibly intercalate Mg²⁺ when coupled with Mg powder negative electrode and a complex montmorillonite solid electrolyte.¹⁵¹ Open-circuit voltage was 1.82 V, and the first cycle discharge capacity was 170 mAh/g NbS₃, corresponding to a Mg loading of 0.6 per NbS₃ unit. Two discharge voltage plateaus at about 1.5 and 1.2 V were observed in the first discharge, with compositions corresponding to Mg_{0.48}NbS₃ at the end of the first plateau and Mg_{0.58}NbS₃ at the end of the second plateau. However, the second plateau disappeared in subsequent cycles, and the capacity decreased to about 85 mAh/g after 5 cycles. Possible amorphization of the NbS₃ was noted as a possible explanation for this capacity fade.

Another chalcogenide compound with a layered structure which can be synthesized as a nanostructured material is WSe₂. Electrochemical Mg²⁺ intercalation into WSe₂ nanowires was evaluated by Liu et al.¹⁵² The positive electrode consisted of single-crystal WSe₂ nanowires with an average diameter of about 100 nm on W substrate prepared via CVD involving the use of Se powder and W film. Charge/discharge curves for the cell Mg|DCC|WSe₂–W at a current density of 50 mA/g are shown in Figure 30.

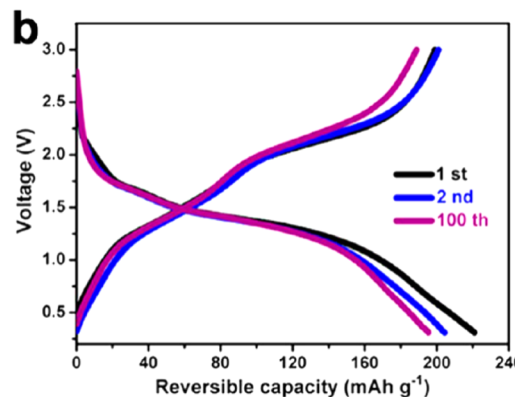


Figure 30. Charge/discharge curves for the cell Mg|DCC|WSe₂–W. Reprinted with permission from ref 152. Copyright 2013 American Chemical Society.

The claimed reversible capacity ~200 mAh/g appears to be inconsistent, however, with the claimed Mg loading of 0.67 per WSe₂ unit, which would indicate a capacity of 105 mAh/g WSe₂. Intercalation of Mg²⁺ beyond one per WSe₂ unit would likely result in (possibly irreversible) MgSe formation, which would have had an obvious impact on cell performance and electrode structure. A capacity retention of 83.5% at a current density of 800 mA/g is claimed; this impressive rate capability is likely due to the nanowire structure of the active material. DFT calculations were also presented to support the performance of this material. It is also noteworthy that the oxidative stability of DCC is 2.2 V vs Mg. Thus, these cells were charged above the voltage stability of the electrolyte.

Amir et al. synthesized and evaluated a series of metal chalcogenides including CuS, CuFeS₂, CuRe₂S₃, Cu_xS_y, Cu₂S, NiS, cubic Ti₂S₄, layered Ti₂S₄, TiSSe, and NiS_xSe_y (solid solutions with varying ratios of x:y).¹⁵³ Electrochemical Mg²⁺

intercalation capacity was evaluated using DCC electrolytes. Cubic TiS_2 delivered a first cycle discharge capacity of about 90 mAh/g (Mg loading of about 0.2 per TiS_2 unit, consistent with previous work) but also showed rapid capacity decline. CuS_x , NiS_x , and NiSSe behaved like conversion cathodes instead of intercalation cathodes, displacing Cu or Ni with Mg during discharge but only at elevated temperature (except for NiSSe , which was active at room temperature). It was concluded that none of these compounds are suitable for practical rechargeable Mg batteries.

2.2.1.5. Mg^{2+} Intercalation into Polyanion Compounds.

Polyanion compounds such as phospho-olivines have received substantial attention for use as positive electrode active materials in lithium-ion batteries, but significantly less attention has been paid to their possible use in magnesium batteries. NuLi et al. evaluated the electrochemical behavior of MgMnSiO_4 materials using DCC electrolytes.^{154,155} Dense particles of this cathode material were synthesized via reaction between stoichiometric quantities of MgO , MnCO_3 , and SiO_2 in molten KCl, and structure and composition were confirmed via XRD and ICP-AES. Particle size was strongly impacted by reaction temperature; at 1000 °C microparticles 1–2 μm average particle size were produced, but at 800 °C nanoparticles of about 80–90 nm average size were obtained. Particle size was found to have a significant impact on electrochemical performance, with nanoparticles exhibiting improved capacity retention vs microparticles (Figure 31).

At C/20 rate, a discharge capacity of 253.8 mAh/g was reported, corresponding to 0.81 mol of Mg per unit formula, while at the higher rate used to generate the data in Figure 29 only about one-half as much Mg is utilized. Note that the first

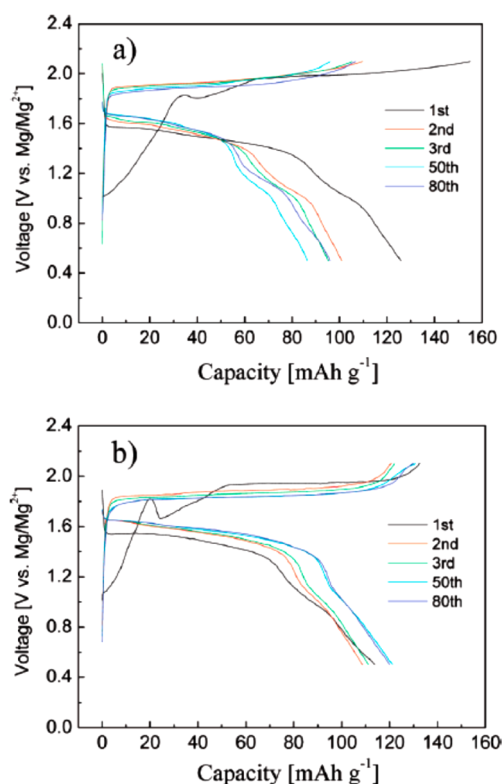


Figure 31. Charge–discharge curves for $\text{Mg}/\text{Mg}_{1.03}\text{Mn}_{0.97}\text{SiO}_4$ (a) micro- and (b) nanoparticles at C/5 rates. Reprinted with permission from ref 154. Copyright 2009 American Chemical Society.

discharge plateau at about 1.6–1.4 V corresponds to the bulk of the material's delivered capacity. This was attributed to preferential insertion of Mg^{2+} ions into one particular type of site in the cathode material, and the second lower voltage (and lower capacity) plateau was attributed to the existence of a second type of insertion site. The anomalous voltage curve obtained in the first charge cycle was attributed to intersite exchange between Mn and Mg ions which apparently only occurred during that initial charge. The authors also demonstrated that improvement in the delivered capacity could be realized by replacing dense SiO_2 in the material synthesis procedure with mesoporous SiO_2 . Depending on the specific type of mesoporous silica used, the discharge capacity at C/5 rates increased up to 301.4 mAh/g, and sustained capacities of about 200 mAh/g over 20 cycles were obtained at a discharge voltage of about 1.65 V.

Alman et al. prepared $\text{Mg}_{1.03}\text{Mn}_{0.97}\text{SiO}_4$ using a sol–gel synthesis and mesoporous SiO_2 .¹⁵⁶ Utilizing the same electrolyte as NuLi, a discharge capacity of only ~50 mAh/g was obtained which was substantially lower than the charge capacity. The difference between the results of the two groups was attributed to possible structural inhomogeneity and conductivity differences in the cathode material. The authors proposed that partially substituting other transition metals for Mn, improving the conductivity of the cathode matrix by incorporating conductive carbon in the material synthesis, use of Mg–Al alloys instead of pure Mg, and use of new electrolytes including ionic liquids could be possible routes to improve this technology.

Ling et al. used density functional theory (DFT) calculations to attempt to elucidate the behavior of MgMnSiO_4 and other polyanion cathode materials from first principles.¹⁵⁷ It was found that intercalation of 0.5 Mg per host unit would be expected to result in structural changes in the host material similar to that experienced with Li^+ intercalation, but insertion of one Mg per host unit could cause structural instabilities. Another issue was the fact that many of the compounds evaluated had potentials outside of the stability range of current secondary Mg battery electrolytes. Exceptions to this which appeared to be compatible with these electrolytes included Mn and Fe silicates where the Mg loading was varied between 0.5 and 1.0 per unit and Mn and Fe phosphates where the Mg loading was varied between 0 and 0.5 per unit. Kinetic and transport processes were not evaluated in this work; it was concluded however that the electronic conductivity of the Mg-containing compounds is likely to be similar to corresponding Li compounds with poor electronic conductivity. Thus, batteries using these cathode materials would likely need to use techniques to reduce the impact of poor conductivity and ionic diffusion akin to what is utilized with Li phospho-olivine cathode materials such as use of nanoparticles and carbon coatings.

Magnesium cobalt silicate (MgCoSiO_4) was synthesized by three different techniques and evaluated for its ability to intercalate/deintercalate Mg^{2+} by Zheng et al.¹⁵⁸ High-temperature solid-state (HTSS), molten salt (MS), and solvothermal (ST) techniques were used to synthesize the materials. ST synthesis was found to produce mesoporous material which exhibited better rate capability, higher specific capacity, and a higher discharge voltage than material obtained with the other techniques. Figure 32 illustrates this behavior.

The ST material also was the only one of the three that showed a distinct (albeit very short) second voltage plateau,

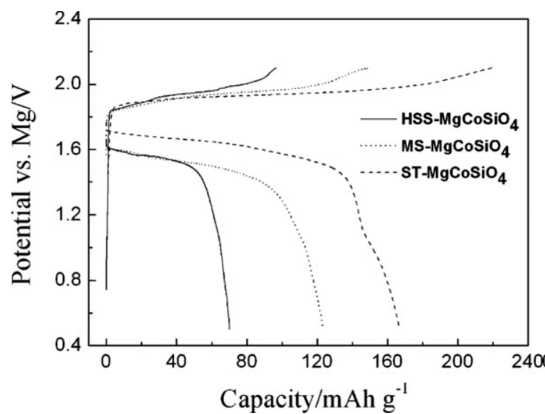


Figure 32. Typical charge/discharge curves of HSS, MS, and ST MgCoSiO_4 at 0.1 C rate. Reprinted with permission from ref 158. Copyright 2012 Elsevier.

similar to that observed above for MgMnSiO_4 . The improved performance of the ST- MgCoSiO_4 was attributed to a larger specific surface area which allowed access to more active sites as well as thin pore walls which provided shorter paths for both electron and ion transport vs the other materials.

The iron analog of these materials, MgFeSiO_4 , was synthesized via a molten salt technique by Li et al.¹⁵⁹ Electrochemical evaluation utilized $\text{Mg}|\text{GEN1}||\text{MgFeSiO}_4$ cells. Discharge curves were similar to those reported above for other Mg metal silicate cathode materials: first plateau at about 1.6 V with a second smaller plateau at about 1.2 V. Reported capacities were about 110 mAh/g for material synthesized at 900 °C, which is similar to that reported above for molten salt synthesized MgCoSiO_4 . Thus, it may be reasonable to speculate that a solvothermal synthesis of MgFeSiO_4 could potentially result in material with improved performance and a lower cost than the cobalt-containing silicate.

Makino et al. utilized sol-gel techniques to synthesize $\text{Mg}_{0.5}\text{Ti}_2(\text{PO}_4)_3$, which was found to be capable of intercalating up to one Mg^{2+} ion per host unit, corresponding to reduction of Ti from IV to III valence and a specific capacity of 136 mAh/g.¹⁶⁰ Electrochemical Mg^{2+} intercalation from 1 M $\text{Mg}(\text{ClO}_4)_2$ -PC electrolyte exhibited relatively poor rate capability, however, and the cathode potential vs Mg was estimated at only about 0.5 V based on measurements with a Ag/AgClO_4 -PC reference electrode. Substitution of up to one-half of the Ti with Fe or Cr resulted in a reduction in both specific capacity and rate capability.^{161,162} Substitution of Ca, Sr, or Ba for Mg in the host material was reported to increase the size of the unit cell and appeared to improve rate capability and capacity.¹⁶³ Thus, it was concluded that unit cell volume is an important parameter which influences Mg^{2+} intercalation and that the capacity was limited by poor Mg^{2+} mobility in the host structure rather than the availability of sites for Mg^{2+} intercalation. Direct comparison between the performance of these phosphate compounds with the analogous silicates discussed above is difficult due to the use of different synthesis methodologies which could lead to different material properties as well as use of different electrolytes. Thus, it would be instructive to prepare and evaluate both phosphates and silicates using, for example, the solvothermal method found to be optimum for the silicate cathode and an electrolyte capable of reversible Mg electrochemistry.

2.2.1.6. Mg^{2+} Intercalation into Organic Materials. A significant limitation of many inorganic intercalation materials for Mg^{2+} insertion and deinsertion is the relatively slow diffusion of Mg^{2+} in such structures which along with low intrinsic conductivity limits rate capability and results in low effective capacity at acceptable charge and discharge rates. An alternative approach which has been investigated is to use redox-active organic materials in which intermolecular forces may be weaker than those in inorganic materials and thus may interact less strongly with Mg^{2+} . An example of such a material is polypyrrole, which is both intrinsically conductive and has been shown to function as a cathode in an aqueous primary Mg battery with a discharge capacity of 565 mAh/g.¹⁶⁴

Organosulfur compounds, which are capable of undergoing redox reactions involving cleavage and recombination of S-S bonds, have been evaluated as possible secondary Mg battery positive electrode active materials.¹⁶⁵ Cathodes consisting of 2,5-dimercapto-1,3,4-dithiazole (DMcT), polyaniline, copper oxalate, carbon black, and PVDF were constructed and placed in coin cells with Mg anodes, microporous polyethylene separators, and electrolytes such as DCC. Polyaniline provided both conductivity and catalyzed DMcT electrochemical oxidation. Figure 33 shows electrochemical redox reactions of DMcT.¹⁶⁶

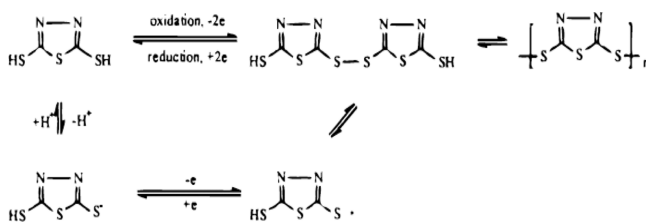


Figure 33. Electrochemical redox processes of DMcT. Reprinted with permission from ref 166. Copyright 1999 The Electrochemical Society.

Copper oxalate was added to introduce copper ions into the cathode, which were believed to improve the performance of the electrode through multiple mechanisms. In particular, addition of Cu(II) to DMcT has been shown to improve the performance of the material as a cathode for Li-ion batteries through redox chemistry between Cu(II) and thioamide groups, forming an electroactive Cu(I)/DMcT complex.¹⁶⁷ A similar mechanism may give rise to Mg^{2+} storage in this material. Discharge capacity was found to increase over the first few cycles and stabilize at ~27 mAh/g after 25 cycles. Two discharge plateaus were observed at about 1.4 (major plateau; attributed to DMcT reduction) and 0.9 V (minor plateau; attributed to polyaniline reduction). Although the polyaniline contributed little to the capacity of the composite electrode through direct electrochemical reaction, electrodes without it delivered significantly less capacity and were lower in conductivity than electrodes with polyaniline. Poly-2,2'-dithiodianiline (PDTDA; Figure 34a) was found to deliver higher specific capacity than DMcT (~78 mAh/g after 2 cycles, slowly decreasing over 30 cycles but remaining significantly above 50 mAh/g) with a sloping discharge curve between 1.4 and 0.4 V.

A composite cathode material consisting of a conductive sulfur-containing material (Figure 34b) prepared via reaction between sulfur and polyacrylonitrile, polyaniline, and copper oxalate delivered ~73 mAh/g reversible capacity after 22 cycles with a relatively flat discharge plateau at 1.35 V and a very

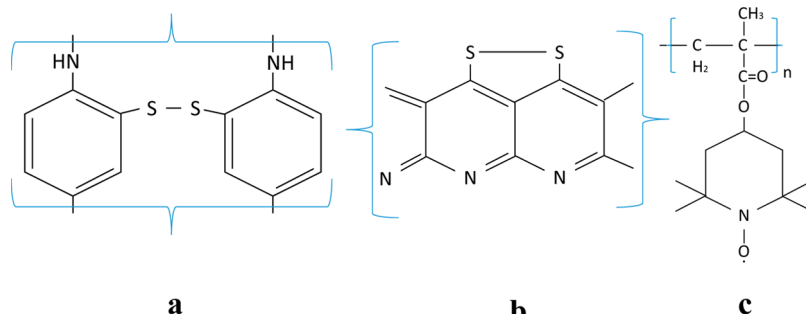


Figure 34. (a) Poly-2,2'-dithioaniline. (b) Structure of conductive sulfur-containing material. (c) Poly(2,2,6,6-tetramethylpiperidinyloxy-4-yl methacrylate) (PTMA).

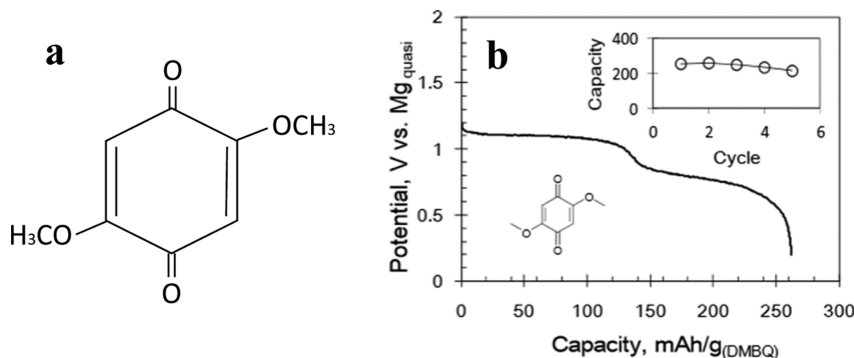


Figure 35. (a) DMBQ. (b) Discharge behavior of the cell Mg|0.5 M Mg(ClO₄)₂- γ -butyrolactone|DMBQ-acetylene black-PTFE (Discharge rate not specified). Reprinted with permission from ref 170. Copyright 2012 Chemical Society of Japan.

minor plateau at 0.8 V attributed to the polyaniline component. It was speculated that further improvements in these types of cathodes could possibly be achieved by identifying an improved catalyst system to enhance the redox process in disulfide compounds, increasing the S–S bond density in disulfides or using tri-, tetra-, etc., sulfides, or designing electrically conductive organosulfides. The authors did not speculate on the nature of improved catalyst systems. However, solid iron metal–organic framework materials have been shown to catalyze aerobic oxidation of thiols to disulfides, and this may suggest a pathway to develop improved catalysts for battery electrodes using this chemistry.¹⁶⁸ Poly(2,2,6,6-tetramethylpiperidinyloxy-4-yl methacrylate) (PTMA; Figure 34c) has been evaluated as a cathode material for both Li and Mg secondary batteries.¹⁶⁹ Evaluation in Mg cells utilized DCC electrolyte. A single pair of redox reactions was identified in cyclic voltammograms of the PTMA electrode, which were ascribed to the reversible reduction of PTMA to aminoxy anion. When coupled with a Mg anode, first cycle discharge capacity was measured as 81.2 mAh/g at a discharge rate of 22.8 mA/g. The discharge capacity decreased rapidly, stabilizing at ~20 mAh/g after 5 cycles, and remained relatively constant through 20 cycles. Cells were charged to 1.8 V; discharge voltage declined rapidly until a brief plateau occurred at about 1.05 V, which was followed by declining voltage until the cutoff voltage of 0.3 V was reached. It was speculated that other redox polymers could be incorporated into polymer–graphene composites to improve the electronic conductivity of the matrix and thus be evaluated as cathode materials in rechargeable batteries.

Another organic compound capable of reversible redox reactions which has been evaluated for use in both Li and Mg batteries is 2,5-dimethoxy-1,4-benzoquinone (DMBQ, Figure 35a).¹⁷⁰ This compound was evaluated for Mg²⁺ storage

capability in the cell Mg|0.5 M Mg(ClO₄)₂- γ -butyrolactone|DMBQ-acetylene black-PTFE (cathode weight ratio 4:5:1). A Mg wire was used as a quasi-reference electrode, and cathode potentials were reported vs that reference, which was found to be about 0.7 V positive of the reversible potential for Mg/Mg²⁺. A first cycle discharge capacity of about 250 mAh/g was measured which remained at about 200 mAh/g after 5 cycles. The discharge curve displayed two voltage plateaus at about 1.1 and 0.8 V vs the Mg wire quasi-reference electrode. The DMBQ was determined to undergo 2-electron redox reactions with insertion and deinsertion of one Mg²⁺ ion per DMBQ molecule. Figure 35b shows the discharge behavior of DMBQ.

The two voltage plateaus presumably correspond to the successive one-electron reduction steps of DMBQ to first the semiquinone anion and then the quinone dianion, with charge compensation provided by Mg²⁺. The authors noted that their Mg quasi-reference electrode exhibited a potential approximately 0.7 V positive of the reversible potential for Mg/Mg²⁺, and thus, the potential of an actual Mg battery using DMBQ may be significantly higher than that obtained in the cell used in this work. In order to determine the usefulness of DMBQ or similar compounds in rechargeable Mg batteries, its electrochemical behavior with an electrolyte capable of reversible Mg deposition and dissolution must be evaluated, but the high capacity measured for this compound is a promising development which should be explored further.

2.2. Conversion Cathodes. **2.2.1. Oxygen.** Despite considerable efforts to develop and commercialize primary and mechanically rechargeable Mg/air batteries, very little work has been published on electrically rechargeable Mg–O₂ batteries. Conceptual Mg/O₂ battery architectures are similar to those of rechargeable Li/O₂ batteries: (1) aqueous electrolytes with a metal-ion conducting membrane to protect the negative

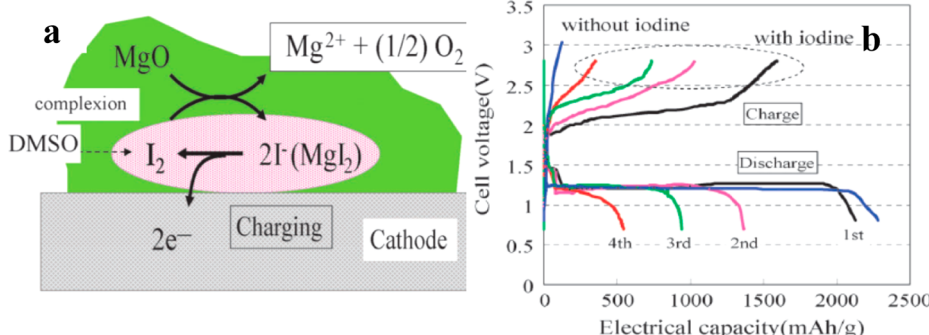


Figure 36. (a) Catalytic cycle for Mg–O₂ battery recharge. (b) Charge/discharge curves for the I₂-mediated Mg/O₂ battery. Reprinted with permission from ref 175. Copyright 2013 Royal Society of Chemistry.

electrode from corrosion by the electrolyte or (2) use of nonaqueous electrolytes capable of supporting reversible oxygen electrochemistry.^{8,171–174} Demonstration of the first concept has been hampered by the lack of a Mg²⁺ conducting solid which is stable in contact with aqueous electrolytes. The second concept may not be feasible due to the fact that the probable discharge product, MgO, is considered to be electrochemically irreversible at ambient temperature and is also nonconductive and insoluble in organic electrolytes. Shiga et al.¹⁷⁵ demonstrated that an iodine/DMSO complex decomposes MgO with visible evolution of oxygen and proposed a catalytic cycle for recharge of a Mg–O₂ battery as shown in Figure 36a.

Discharge of a Mg–O₂ cell utilizing an electrolyte containing this complex would involve formation of both MgO and MgI₂; during recharge the electrochemically active species at the positive electrode would be I⁻, which would result in regeneration of the I₂/DMSO complex. This complex would then react with MgO to form MgI₂ and O₂.¹⁷⁵ Figure 36b shows charge/discharge curves for the Mg/O₂ battery at 60 °C. The brief discharge plateau at about 1.5 V was attributed to formation of MgI₂, and the longer plateau at about 1.25 V was attributed to MgO formation.

Reactivity of the iodine/DMSO complex with the Mg electrode could result in self-discharge of the cell, but this was not discussed.

2.2.2. Sulfur. A very attractive cathode material to couple with magnesium is sulfur, which has a high theoretical capacity of 1671 mAh/g. Unfortunately, the in-situ-generated magnesium organohaloaluminate electrolyte components which show high Coulombic efficiency and compatibility with magnesium are nucleophilic and therefore preclude use of electrophilic cathodes such as sulfur. Kim et al. recently demonstrated that crystallization is a critical step in the synthesis of non-nucleophilic electrolytes such as GEN1, GEN2, crystallized APC, and crystallized DCC.^{9,52} Development of these non-nucleophilic electrolytes has allowed the demonstration of secondary Mg/S batteries. The first cycle discharge capacity was 1200 mAh/g S (vs 1675 mAh/g theoretical capacity based on a 2-electron reduction to form MgS), but the capacity declined to 394 mAh/g in the second cycle. Cell voltage increased from 0.55 to 0.89 V from the first to the second cycle, which was attributed to removal of a surface film from the Mg anode during the first discharge, similar to the delay phenomenon in Mg primary batteries. Charge capacity was significantly higher than discharge capacity, likely due to a shuttling mechanism caused by soluble polysulfide species in the electrolyte. This was supported by postmortem cell analysis

which revealed a yellow discoloration of the separator, indicative of the presence of polysulfide species similar to that observed in Li–S batteries. XPS analysis of the cathode surface also supported this conclusion. The authors of this study concluded that incorporation of an electrolyte solvent or solvent blend that minimizes or eliminates polysulfide solubility would significantly improve the performance of Mg–S batteries.

2.2.2.3. Other Conversion Cathodes. The only reported attempt to use a metal halide conversion cathode in an ambient-temperature secondary magnesium battery was that of Chilton.¹⁷⁶ The cell Mg|MgBr₂|diethyl CuBr₂,Cu was constructed. Electrolyte conductivity was reported as only 0.5 mS/cm, and no measured open-circuit potential was reported. Mg electrode Coulombic efficiencies were only 40% for discharge and 33% for the charge cycle. Solubility of the cathode material in the electrolyte was cited as an issue for this cell. Graphite fluorides have been demonstrated as cathode materials in nonaqueous primary batteries with Mg anodes in Mg(ClO₄)₂ solutions of various organic solvents but not secondary batteries.¹⁷⁷ Specific energies based on the electrode materials up to 618 Wh/kg were obtained, but discharge potentials were only in the 0.7–1.2 V range. MgF₂ was identified as a discharge product, and thus, rechargeability may not be possible, unlike rechargeable Li/CF_x batteries. WS₂ has also been shown to function as a conversion cathode in primary Mg batteries with solid polymer electrolytes, but reversibility was not demonstrated.¹⁷⁸

Use of molten salt electrolytes has also been explored with Mg/conversion cathode systems.¹⁷⁹ Ag/AgCl, Cu/CuCl, Ni/NiCl₂, Ni/NiO, and Cu/Cu₂O cathode materials were evaluated using an electrolyte of 48 mol % MgCl₂/52 mol % NaCl (sulfate salts were used in the catholytes of cells with oxide cathodes). A Na⁺ conductive ceramic separator was used, and the normal operating temperature was 500 °C. Charge/discharge behavior was obtained with the cell Mg|Ag_xAgCl at discharge voltages of about 1.7 V or less depending on current density, but rate capability was not good. Only discharge data was shown for Mg|Ni,NiCl₂; Mg|Cu,CuCl cycled successfully at low current density. Mg|Ni,NiO cycled but cell voltage was low, and Mg|Cu,Cu₂O also cycled but polarized severely.

2.2.3. Mg Cathode Summary. In summary, direct comparison of the results obtained in the Mg battery cathode studies discussed here is difficult due to the fact that a wide variety of experimental conditions were used in the cited work: different electrolytes, different physical and structural forms of compositionally similar materials, different electrode preparation techniques, different binders and conductive additives, and

different electrochemical test conditions among others. However, there are a few commonalities and conclusions that may be inferred from the existing body of work. In general, relatively low capacities and cell potentials (vs theoretical values) have been typically obtained, especially for intercalation cathodes, along with substantial capacity fade over relatively few cycles. Factors which appear to impact these results include slow solid-state diffusion of Mg^{2+} ions which increases electrode polarization and can also result in ion trapping, possible cointercalation of solvent molecules which may help shield the charge on the Mg^{2+} ion but also cause severe structural distortion as well as decompose within the cathode material, and chemical and physical instability of some intercalates. In addition, passivation of Mg anodes due to formation of SEI layers with poor Mg^{2+} transport properties in at least some electrolytes also hampers cell performance. Poor electronic conductivity of some cathode materials is another issue that reduces performance. Apparent minimal cathode surface film formation allows the use of nanostructured cathode materials and appears to improve this situation but at the cost of reduced volumetric capacity. Future research directions which involve structural modifications of intercalation cathodes may be fruitful. For example, doping with other metal ions and/or use of multimetal compositions are techniques which have been very successful in lithium-ion battery cathode development and may be useful avenues to explore for Mg batteries as well. Blending of different cathode materials may also prove advantageous. Fundamental studies such as elucidation of the intercalation mechanism including identification of the exact intercalating Mg species would be very useful in terms of both cathode and electrolyte development. Conversion cathode performance also suffers from a number of problems, including irreversibility of high-voltage conversion reactions due to formation of stable, nonconductive discharge products. Thermodynamic limitations may render this situation very difficult to overcome, and materials which undergo a 2-electron transfer per redox center appear to be preferable to preserve the advantages of using divalent Mg.

3. CALCIUM

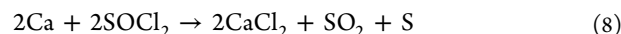
Calcium is a multivalent metal which is less reactive than lithium, has a high volumetric capacity of 2073 mAh/mL, and is the fifth most abundant element in the earth's crust. In addition, its reduction potential is very attractive, only 0.17 V more positive than lithium (-2.87 V vs SHE for calcium). While development of electrolytes for other multivalent metals (such as magnesium, aluminum, or zinc) benefits from a long electroplating history, the chemistry of calcium electrolytes has received far less attention. It would be desirable to apply the lessons learned in the development of magnesium electrolytes toward the discovery of a new, high-voltage calcium electrolyte which would allow its reversible deposition. Such a breakthrough could open the gates toward a rechargeable battery with a calcium metal anode.

3.1. Electrochemistry of Ca Electrodes in $SOCl_2$

Despite their superior energy density and excellent shelf life and power density, a major obstacle to the commercialization of high-rate Li/ $SOCl_2$ primary batteries is the explosion hazard during undesired charging or deep discharge which can occur in cells arranged in a parallel configuration. The culprit was determined to be facile lithium deposition which occurs with low overpotentials on the lithium metal anode or on the

passivated cathode. High deposition rates and the dendritic deposition characteristic of lithium lead to formation of powder-like lithium deposits and can lead to internal sparks and exothermic reactions with the electrolyte which can rapidly melt the lithium. This can result in thermal runaway leading to an explosion.¹⁸⁰ In addition to the dendritic problem associated with the Li metal anode, it also has a very low melting point of 180.5 °C. Batteries used on oil and geothermal energy drilling rigs can experience temperatures in excess of 200 °C; thus, lithium would exist in a molten state in such batteries. Containment of the molten Li metal anode to prevent contact with the cathode is difficult in an environment where shocks and vibrations are common, so use of high melting point lithium–magnesium alloys or calcium metal (mp of 838 °C) was suggested for negative electrodes in applications which required operating temperatures above the melting point of Li.¹⁸¹ The journey toward the use of calcium as an anode begins with attempts to improve the performance of Li/ $SOCl_2$ primary batteries used on oil and geothermal energy drilling rigs. The safety advantages calcium holds over lithium are the higher melting point and a lack of deposition during limited cathode cell reversal.

In the 1980s, an extensive amount of research was devoted to the study of the electrochemistry of the Ca anode in inorganic polar aprotic solvents such as $SOCl_2$, SO_2 , and SO_2Cl_2 . The anodes of both calcium– and lithium–thionyl chloride cells are always covered by a solid electrolyte interphase (SEI) which protects them from direct contact with the solution. In the case of a lithium anode, the SEI has the properties of a solid electrolyte which exhibits very poor electronic but good ionic conductivity. The ionic resistivity of the SEI (composed of LiCl) in a lithium–thionyl chloride cell is about 10^7 – 10^8 Ω·cm and depends on its thickness. Interestingly, the resistivity of the SEI (composed of $CaCl_2$) in a calcium–thionyl chloride cell was 2 orders of magnitude higher.¹⁸⁰ A possible explanation for this observation is the fact the LiCl is an ionic salt while $CaCl_2$ exhibits substantial covalent character, thus limiting its ionic mobility. Equations 8 and 9 show how the predominant component in the SEI, $CaCl_2$, is formed on the surface of the anode.



In addition, while the transference number of Li^+ through its SEI is unity, Peled and Staniewicz independently suggested that the poor deposition of metals from bivalent cations such as Ca^{2+} was governed by their poor diffusion through their SEIs.^{182,183} In addition, Derrington suggested that these SEIs are a mixed ionic conductor for anions and cations (t^- , $t^+ > 0$) which could account for the difficulty in the migration of calcium cations.¹⁸⁴ Since calcium cannot be deposited on the carbon cathode or on calcium metal but dissolution of Ca^{2+} can occur in $Ca(AlCl_4)_2$, preliminary results suggested that construction of a $Ca/Ca(AlCl_4)_2/SOCl_2$ cell with a carbon cathode current collector was feasible and this cell could possess an inherent safety advantage due to avoidance of undesired charge or overdischarge. Thus, a high-rate battery with a Ca anode and a $SOCl_2$ cathode should not suffer from the inherent safety issues associated with Li dendrite formation. Unfortunately, Ca/ $SOCl_2$ cells suffered from a shorter cathode life (when compared with analogous Li/ $SOCl_2$ cells) and unacceptably high calcium corrosion levels. Staniewicz found

that precoating calcium with calcium oxide improved the stability, but 20% of the calcium was still lost through corrosion.¹⁸³ In addition, Walker and Binder used SO_2 as a cosolvent to improve the cell capacity as well as raise cell voltages under load due to preferential solvation of Ca^{2+} by SO_2 .¹⁸⁵ Also, Peled and Binder showed that use of $\text{Sr}(\text{AlCl}_4)_2$ in thionyl chloride instead of $\text{Ca}(\text{AlCl}_4)_2$ resulted in reduced Ca corrosion.^{186,187} Corrosion of Mg electrodes in SOCl_2 solutions is apparently also highly dependent on the electrolyte solute; use of AlCl_3 was found to result in rapid Mg corrosion, but saturation with MgCl_2 effectively suppressed Mg corrosion with either AlCl_3 or FeCl_3 .^{188,189} Interestingly, reversible Mg deposition was reported on a Ni cathode in $\text{SOCl}_2/\text{Mg}(\text{FeCl}_4)_2$ solutions; however, deposition did not occur until a passivating layer consisting of SOCl_2 breakdown products was formed on the cathode surface. The estimated specific energy density of a $\text{Ca}/\text{Ca}(\text{AlCl}_4)_2/\text{SOCl}_2$ battery is around 250–300 Wh/kg; because it is practically impossible to charge or overdischarge these cells this results in superior safety vs their Li/ SOCl_2 counterpart.¹⁸⁰ However, as noted rechargeability has not been demonstrated in Ca/SOCl_2 cells.

3.2. Organic Solvents and Salts

While the electrochemistry of $\text{Ca}(\text{AlCl}_4)_2$ in SOCl_2 has been extensively studied there has been virtually no progress reported in the area of using calcium electrolytes in organic solvents with the goal of developing a rechargeable calcium battery. In 1991, Aurbach et al. investigated the behavior of calcium electrodes in electrolytes containing several organic solvents and salts.¹⁰² Analysis by infrared spectroscopy, scanning electron microscopy, X-ray microanalysis, and cyclic voltammetry suggested that the surface chemical composition of the calcium anode was highly dependent on both the salt and the solvent used in the electrolyte. In solvents such as γ -butyrolactone (BL) and methyl formate (MF) the surface species include calcium butyrate derivatives of the γ -hydroxyl butyrate and cyclic β -ketone ester calcium salts. However, in acetonitrile, the calcium surface is covered by products formed from condensation of acetonitrile. In the case of $\text{Ca}(\text{ClO}_4)_2$ the calcium anode reduces the anion ClO_4^- to form CaCl_2 . On the other hand, Aurbach claims that the TBABF_4 salt is stable against reduction by the calcium anode and reports the conductivity of the corresponding $\text{Ca}(\text{BF}_4)_2$ salt. The stability of the BF_4^- anion against reduction by a calcium anode suggests that use of a salt such as $\text{Ca}(\text{BF}_4)_2$ could allow deposition of Ca in a stable solvent such as tetrahydrofuran (THF) or *n*-methyl-2-pyrrolidone (NMP).¹⁹⁰ However, no electrochemistry has been reported for organic solutions of the $\text{Ca}(\text{BF}_4)_2$ salt.

In conclusion, calcium deposition (even at high negative potentials of -2.0 V vs Ca) has not been observed in any electrolyte systems comprising $\text{Ca}(\text{ClO}_4)_2$ in organic solvents such as acetonitrile (AN), dimethylformamide (DMF), propylene carbonate (PC), BL, THF, and MF.¹⁰² This is presumably due to formation of a passivating layer formed by reduction of the salt and/or solvent which is apparently nonconductive with respect to calcium ions. Figure 37a shows a typical cyclic voltammogram with no deposition observed even at high negative potentials vs Ca; in Figure 37b dissolution of Ca in a solution of TBABF_4 /BL can be assumed since Faradaic currents appear as early as 0 V vs Ca (no Ca deposition is observed because the Ca^{2+} cation is absent from the

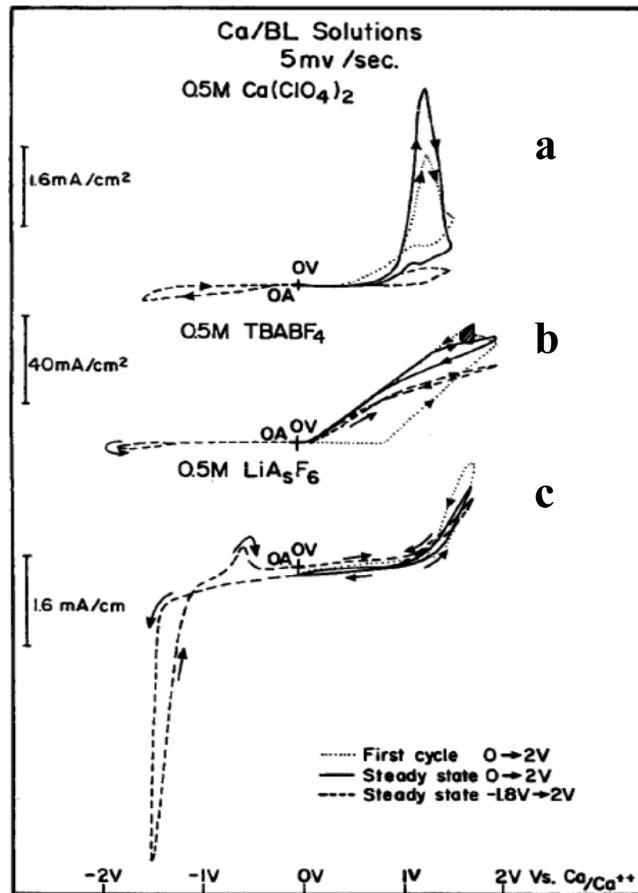
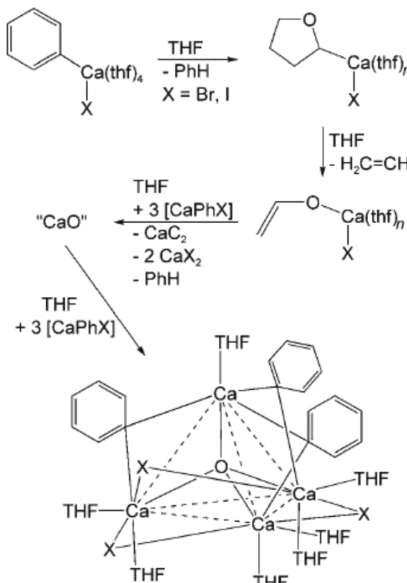


Figure 37. Comparison of typical voltammograms obtained with calcium electrodes and BL solutions of three different salts: (A) $\text{Ca}(\text{ClO}_4)_2$, (B) TBABF_4 , and (C) LiAsF_6 . Sweep rate: 5 mV/s. Reprinted with permission from ref 102. Copyright 1991 The Electrochemical Society.

electrolyte), whereas in Figure 37c, in a LiAsF_6 /BL solution, deposition and dissolution of Li is observed on a Ca electrode.

3.3. Challenges in Developing New Calcium Electrolytes

In the quest to develop a new calcium electrolyte one could envision exploring synthetic pathways which have been successful in obtaining electrolytes for another bivalent metal, namely, magnesium. Many of these synthetic approaches are based on Grignard reagents or organomagnesium compounds derived from Grignard reagents and are discussed extensively in section 2.1.^{9,191} This suggests that the corresponding calcium derivatives known as heavy Grignard reagents (RCaX , where R is alkyl or phenyl and X is iodide or bromide) would be an interesting starting point for investigating calcium electrolytes. In contrast to magnesium, where PhMgCl is commercially available and a precursor for numerous magnesium electrolytes,^{9,191} it has been reported that calcium powder shows no reactivity with chlorobenzene, so the corresponding heavy Grignard PhCaCl cannot be synthesized.¹⁹² This is unexpected since calcium is more reductive than magnesium. However, heavy Grignards such as PhCaI can be readily synthesized at low temperatures by reaction of calcium powder with iodobenzene in good yields.^{192–194} Maintaining a low temperature during synthesis is important to avoid the degradation reaction of PhCaI as shown in Scheme 2.

Scheme 2. Degradation Reaction of PhCaI^a

^aReprinted with permission from ref 192. Copyright 2007 WILEY-VCH Verlag GmbH & Co. KGaA, Weinheim.

The electrochemistry of PhCaI or the degraded product has not yet been investigated. Reactions of the heavy Grignards PhCaX (where X is I or Br) at low temperatures with Lewis acids (such as AlCl₃ or B(C₆F₅)₃) used for obtaining magnesium organohaloaluminate or magnesium organoborates^{9,52,191} have also not been reported but might be of interest. Another potentially feasible approach toward the synthesis of calcium electrolytes may be based on ion-exchange reactions where a silver salt can be converted to a calcium salt by reaction with CaCl₂. Our group has recently exploited this strategy to synthesize magnesium electrolytes.⁶⁷ Since it has been reported that no successful deposition of Ca occurs through passivating films formed from the reduction of the electrolyte, it is important to note that both the solvent and the salt of a viable calcium battery electrolyte would have to be stable against reduction at potentials 0.5 V more negative than that encountered by magnesium battery electrolytes.

The current evolutionary level of a rechargeable calcium battery is rather primitive due to the primordial state of electrolyte development. The lack of useful calcium battery electrolytes limits the investigation of cathodes for a rechargeable calcium battery. However, Tsuchida et al. reported a calcium primary battery with Ca(ClO₄)₂ in AN as an electrolyte and MnO₂ as the cathode active material.¹⁹⁵ A sloping discharge curve between 2.5 and 1 V was obtained. Given the development of a viable calcium battery electrolyte which is stable against reduction by a calcium metal anode, a rechargeable calcium battery with a cathode such as MnO₂ can be envisioned. However, development of feasible high-voltage cathodes with metal centers capable of undergoing two-electron transfer will be of paramount importance for all multivalent metal batteries. As noted in section 1, the larger ionic radius of Ca²⁺ vs Mg²⁺ may result in improved ionic mobility in solid-state cathode materials due to reduced charge density which is additional incentive to continue the search for a viable calcium electrolyte.

4. ALUMINUM

After oxygen and silicon, aluminum is the third most abundant element in the earth's crust. An aluminum metal anode is a superior multivalent candidate in terms of volumetric capacity (8040 mAh/cm³). Its multivalent nature (it can provide three electrons per cation for reduction of a cathode), low atomic weight (26.98 g/mol), and high density (2.7 g/cm³) endow aluminum with a volumetric capacity twice as large as that offered by magnesium. However, aluminum suffers from a standard reduction potential 0.7 V more positive (−1.67 V vs SHE) than magnesium. As a result, given cathodes with similar discharge voltages and similar anodic polarization, a battery with an aluminum anode would operate 0.7 V lower than one with a magnesium anode. Surprisingly, the first attempts at using aluminum as a battery electrode by Hulot in 1855 do not describe the use of aluminum as an anode but as a cathode in combination with zinc (mercury) anode and dilute sulfuric acid as the electrolyte.¹⁹⁶ Aluminum was first utilized as an anode in the Buff cell in 1857.¹⁹⁷ A century later, aqueous electrolytes were considered for use in Leclanche battery cells with an aluminum anode and a MnO₂ cathode by Sargent and Ruben.^{198–202} These batteries are plagued by the intrinsic formation of an oxide layer which passivates the aluminum metal anode and decreases the battery voltage and efficiency. This protective layer can be removed chemically by addition of potent corrosive agents, such as concentrated alkali solutions, to eliminate this blocking layer. This approach is capable of restoring the anode potential to its thermodynamic value but also results in an accelerated rate of wasteful corrosion and limits the battery shelf life.²⁰³ With a reduction potential more negative than the hydrogen electrode, nonpassivated aluminum metal causes hydrogen evolution when exposed to a protic electrolyte solution. In addition, this renders deposition of aluminum impossible in aqueous electrolytes. The only primary aluminum battery which has received serious attention for potential widespread application is the aluminum air battery.^{204,205} Al-air batteries have been proposed for applications including vehicular propulsion, a recent example being Phinergy's demonstration of its Al-air battery for range extension in a vehicle which utilizes a lithium battery as the primary energy source.²⁰⁶ These efforts have been targeted at primary Al-air batteries, however, with rechargeability in some cases being accomplished by mechanical replacement of the anode and electrolyte rather than by application of an electrical current to reverse the electrochemical reactions.

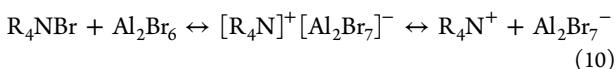
Therefore, in order to develop a rechargeable aluminum battery where both aluminum deposition and dissolution is required, it is essential to develop electrolytes based on aprotic solvents stable against reduction by aluminum. As with magnesium electrolytes the other two stringent requirements are a noncorrosive nature and a high resistance against oxidation. Since oxidation occurs at the positive electrode during discharge, it is the ability of the electrolyte to resist oxidation which governs the choice of cathodes.

4.1. Electroplating Baths as Aluminum Electrolytes

Nonaqueous aluminum electrolytes utilized to date for battery evaluations are derived from those used for aluminum electroplating baths. Electrodeposition is a well-established aluminum coating method in the corrosion protection, electronics, and telecommunications industries.²⁰⁷ Here, aluminum electrodeposition from aluminum halides/organo-aluminum compounds in organic solvents and ionic liquids will

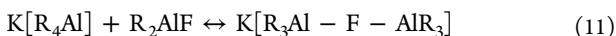
be summarized. The components of the plating baths have changed little since 1899 when Plotnikov was the first to attempt aluminum deposition from aromatic hydrocarbon solutions.²⁰⁸ The weak coordination centers of these solvents solvate some aluminum halides well despite their low dielectric constants. Noncomplexed aluminum halides (AlX_3 , where X is a halide) were the first salts to be dissolved in aromatic hydrocarbons such as benzene, toluene, or xylene to achieve solutions capable of electroplating aluminum.^{209–211} In particular, acceptable deposition of aluminum was achieved from solutions of AlBr_3 . Additives such as MBr (M is an alkali metal such as K) were used to increase the conductivities (1–6 mS/cm) of these bromide baths.^{212,213} Use of such additives improved the electroplating bath throwing power (uniformity of aluminum deposits). In these solutions, the electrochemically active aluminum species are the anions formed by addition of the metal bromides: Al_2Br_7^- and AlBr_4^- . Aluminum deposits from these baths on copper, brass, and steel were smooth, homogeneous, and microcrystalline and 99.5% pure.²⁰⁷ Coulombic efficiencies were as high as 100% at both electrodes at current densities of 10 A/dm². HBr was also utilized as a conductivity boosting additive (3–4 mS/cm).²¹¹ This bath provided excellent aluminum dissolution from the anode, but the deposition efficiency (80% at currents of 1 A/dm²) was reduced, which resulted in an enrichment of the bath with aluminum over time. Bath life was excellent (up to 1 year), but unfortunately introduction of hydrogen into the bath composition also caused undesired hydrogen evolution upon depletion of aluminum from the electrolyte.²⁰⁷

Complexation of AlBr_3 with tertiary ammonium halide compounds has also been investigated as a means of improving Al deposition uniformity and rate.²¹⁴ In the presence of a quaternary ammonium compound AlBr_3 can form an ionized complex as in eq 10

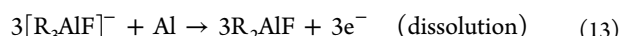


Optimal aluminum coatings were obtained with current densities of 2–15 A/dm² from solutions of AlBr_3 complexed with triethylisobutylammonium bromide.

While solutions of AlBr_3 and complexes were the first practical aluminum electrodeposition baths to be developed, the most advanced electroplating baths in use today are those composed of organoaluminum compounds proposed by Lehmkuhl et al.¹⁹⁰ This electrolyte system provides very pure aluminum deposits (99.9999% Al at current densities of 1–1.5 A/dm² and 90–100 °C) and is also used for electrorefining of aluminum. In the case of all other aluminum electrolyte baths used for electrochemical plating, the AlCl_4^- anion was the source of electrodeposited aluminum. However, in the case of organoaluminums (such as trimethylaluminum) in the presence of metal fluorides in a 2:1 ratio, the species $\text{K}[\text{Et}_3\text{Al}-\text{F}-\text{AlEt}_3]$ forms which has been structurally characterized by single-crystal X-ray diffraction. Due to the high price of high-grade alkyl metal fluorides an alternative synthetic approach is necessary to obtain $\text{K}[\text{Et}_3\text{Al}-\text{F}-\text{AlEt}_3]$ on a commercial scale. As a result, reaction of a crystallized metal tetraalkylaluminate with distilled dialkylaluminumfluoride was utilized (eq 11).



Lehmkuhl proposes the following mechanism for dissolution and deposition of aluminum



Progress toward smoother deposits at higher current densities primarily resulted from solvent improvements. Ethereal solvents such as diethyl ether provided a good compromise between a higher coordination affinity to aluminum and a higher dielectric constant.²¹⁵ Unfortunately, an electrodeposition bath based on ethers (developed at NBS) is plagued by the high flammability of ether and hydrogen evolution due to hydride additives present in the bath mixture.^{216,217} An improvement to the NBS baths was utilization of THF as a solvent.^{218,219} THF is less flammable and has a lower vapor pressure than diethyl ether and improved the anode dissolution efficiency. Current densities above 10 A/dm provided excellent aluminum deposits from agitated baths consisting of THF/benzene (40:60) with $\text{AlCl}_3:\text{LiAlH}_4$ in mole ratios of 3:1. Another solvent with a dielectric constant higher than ethers is dimethylsulfone (DMSO₂).^{220–222} Solutions containing salts such as $\text{AlCl}_3:\text{LiCl}$ in a 2:1 mole ratio in DMSO₂ have exhibited reversible aluminum deposition and dissolution (see Figure 38). ²⁷Al NMR and Raman spectro-

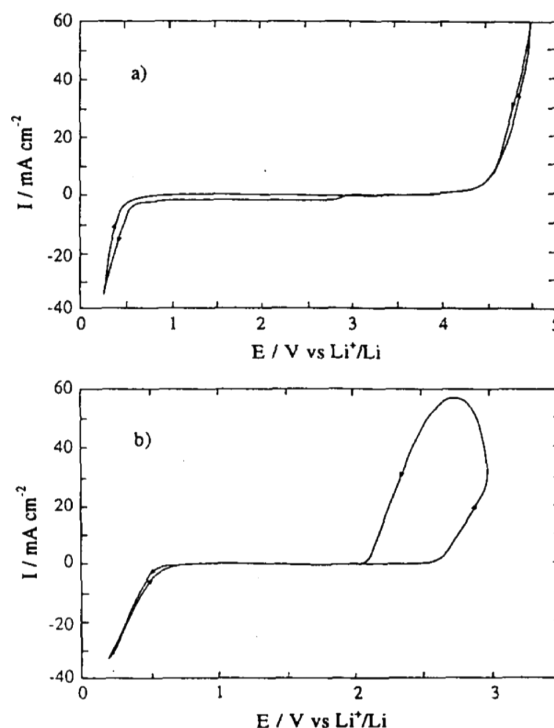


Figure 38. Voltammograms obtained at a scan rate of 10 mV/s in LiAlCl_4 1 mol/kg/DMSO₂ electrolyte at 130 °C on tungsten (a) and aluminum (b) electrodes. Reprinted with permission from ref 221. Copyright 1994 Elsevier.

copy indicate there are two major soluble aluminum species, namely, AlCl_4^- and $\text{Al}(\text{DMSO}_2)_3^{3+}$, formed according to the following reaction



RTILs have been evaluated as solvents for aluminum plating electrolytes. Ionic liquids possess several attractive features such as improved chemical and thermal stability, negligible vapor

pressure at elevated temperatures, and high intrinsic electrical conductivities. In addition, the Lewis acidity of an AlCl_3 :molten salt mixture can be adjusted by varying the molar ratio of the components.²⁰⁷ When an aluminum halide (AlX_3) is combined with an organic salt (R^+X^-), a dominant anionic equilibrium is reached and can be described as



The Al_2X_7^- ion is a strong Lewis acid, while the X^- ion is the conjugate Lewis base. When the X^- ion exists in excess, the mixture is described as basic. Similarly, when the Al_2X_7^- is the principal constituent, the mixture is acidic. Both aluminum containing anions are electrochemically active and allow for aluminum reduction to its metallic form.

In the 1940s, Hurley and Wier paved the way for use of ionic liquids such as ethylpyridinium bromide (EPB)- AlCl_3 mixtures as electrolytes for aluminum electroplating baths.^{223,224} Unfortunately, it was commonplace to observe reduction of the EP^+ cation during electroplating. In addition to coreduction of the cation, EPB- AlCl_3 melts also suffer from rapid photodecomposition and possess a narrow electrochemical window of 1.8 V due to oxidation of bromide. In order to develop an Al plating bath with an expanded electrochemical window, *N*-(1-butyl)pyridinium chloride (BPC)- AlCl_3 mixtures were investigated for electrodeposition of aluminum.^{225–228} These mixtures were found to have a wider electrochemical window (>2 V) than EPB- AlCl_3 ; however, they possess high viscosities, and practical electroplating can only be achieved by addition of up to 50% aromatic hydrocarbons such as benzene and toluene. Freshly deposited Al from (BPC)- AlCl_3 mixtures was shown to corrode slowly, possibly reacting with the BP^+ cation or being corroded by the Cl^- anion. In addition, in basic BPC: AlCl_3 melts the BP^+ cation is more readily reduced on the cathode than the AlCl_4^- anions. In order for electrodeposition of aluminum to occur with high efficiencies and purities from basic melts, a cation which reduces at a potential more negative than aluminum was required.

Hussey et al. calculated the electron affinities of a number of organic cations using molecular orbital theory.^{229,230} Alkylimidazolium cations were found to have higher reductive stability than alkylpyridinium cations. The most favorable cation was 1-methyl-3-ethylimidazolium (MEI^+), which formed a very low melting point mixture when combined in excess with AlCl_3 . In addition, this melt could be formulated in a more basic composition than BPC melts. MEIC: AlCl_3 melts allow for smooth aluminum deposition with some of the highest current densities (25 A dm⁻² have been reported) with high efficiencies (>99%). Although the MEI^+ cation is more stable against reduction than BP^+ , it suffers from high rates of decomposition during preparation.²²⁹ In the search for reductively stable cations with easily scalable preparation procedures, quaternary ammonium species were evaluated based on an expectation of superior electrochemical stabilities. Commercial salts with fully substituted quaternary ammonium groups such as trimethylphenylammonium chloride (TMPAC) form low-melting ionic liquids when mixed with AlCl_3 . TMPAC- AlCl_3 melts are easy to prepare and have an electrochemical stability (Figure 39) equal to that of MEIC- AlCl_3 melts as well as good conductivities.²³¹

In addition to satisfying the requirements for electroplating baths, a battery electrolyte also requires resistance toward oxidation at even higher potentials. This additional requirement

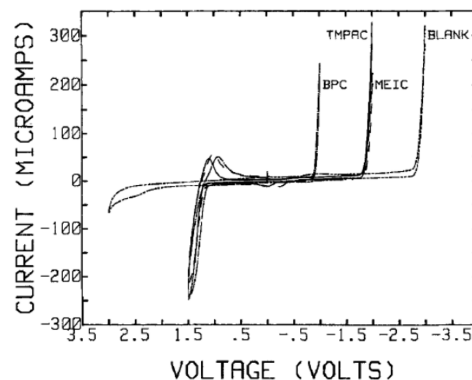


Figure 39. Cyclic voltammetry results for 20 mM solutions of TMPAC, MEIC, and BPC in acetonitrile solution with 0.1 M TMAP as background salt. Glassy carbon was used as the working and counter electrodes, and the reference electrode was a silver wire in 0.1 M TMAP in acetonitrile. Scan rates were 50 mV/s. Reprinted with permission from ref 231. Copyright 1989 The Electrochemical Society.

defines the characteristics of a wide electrochemically inert window inside which no corrosion should occur in order to maximize battery voltage. Ionic liquid AlCl_3 melts have been shown to undergo reversible aluminum stripping and plating and have been extensively evaluated as aluminum electrolytes in secondary aluminum batteries. Among the ionic liquid-based electrolytes the combination of aluminum chloride with 1-ethyl-3-methylimidazolium chloride has been considered the most promising electrolyte.^{232–235} One of the major advantages of this melt is that it is a liquid at room temperature without addition of cosolvents and has a maximum voltage stability of 2.7 V vs Al. According to Jiang et al., AlCl_4^- oxidizes around 2.7 V vs Al and a substantial amount of chlorine gas is evolved (due to oxidation of Cl^- anion) if the potential is scanned to 3.0 V vs Al. The challenge of moving beyond 2.7 V vs Al will require a shift away from aluminum electrolytes where Al_2Cl_7^- is the electrochemically active species because it is in equilibrium with AlCl_4^- and free Cl^- anions. On the basis of previous work in the area of magnesium battery electrolyte development where free chlorides render magnesium electrolytes containing the electrochemically active cation $\text{Mg}_2\text{Cl}_3\cdot 6\text{THF}^+$ corrosive in nature,^{9,67} it would be appropriate to evaluate the oxidative stability of these aluminum electrolytes on less inert working electrodes such as stainless steel, nickel, or copper to evaluate their corrosive nature.

An interesting aluminum electrolyte $\text{K}[\text{R}_3\text{Al}-\text{F}-\text{R}_3\text{Al}]$:toluene was proposed as an electrolyte for electrochemical aluminum plating at 90 °C by Lehmkuhl et al.¹⁹⁰ On the basis of the proposed mechanism of deposition and dissolution there should be no free halide anions present in this electrolyte. However, these electrolytes lack high oxidative stability due to the presence of the substituted alkyl groups on the aluminum which break by β -H elimination. The electrochemical stability window could be improved by substituting the alkyl functionality on the aluminum with phenyl groups, and further improvements in oxidative stability could be achieved by fluorination of the phenyl groups. However, it has been previously reported that some fluorinated aluminates are explosive in nature.^{58,236} All previously discussed aluminum electrolytes contain aluminum in an electrochemically active anion. A unique and thus far untested approach would follow the example set by previously reported magnesium electrolytes where the electroactive species resides in the cation.

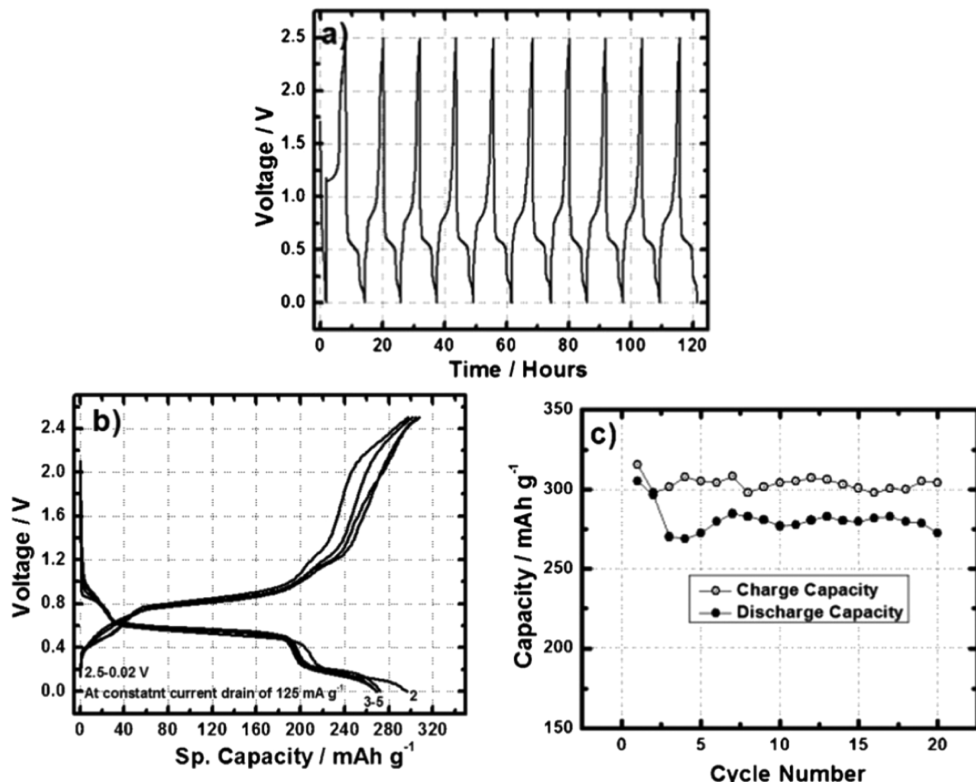


Figure 40. (a) Voltage vs time, (b) voltage vs specific capacity, and (c) cycle life plot of Al-ion battery containing aluminum anode, V_2O_5 nanowire cathode in ionic liquid under the potential window 2.5–0.02 V and at a constant current drain of 125 mA/g. Reprinted with permission from ref 234. Copyright 2011 Royal Society of Chemistry.

4.2. Cathodes for Rechargeable Aluminum Batteries

Reports of positive electrode materials which operate by reversible electrochemical intercalation of Al^{3+} have been scarce. Interestingly, many of the cathode materials demonstrated in secondary aluminum batteries, including Chevrel-phase Mo_6Se_8 , V_2O_5 , Ag halides, and various manganese oxides, have also been demonstrated as cathodes for magnesium batteries. Unfortunately, aluminum batteries containing these cathodes are plagued by low open-circuit potentials when compared to their magnesium counterparts. For example, the first rechargeable battery with a magnesium metal anode and a Chevrel-phase cathode was demonstrated in 2000.¹⁴⁰ It showed impressive cycle life (>3500 cycles measured), low capacity fading, negligible self-discharge, and a wide operating temperature range. The cathode specific capacity was 75 mAh/g, and the cell discharged at 1.1 V. However, in the case of the aluminum counterpart, while the cathode specific capacity was similar to that obtained with magnesium, the operating potential was below 0.5 V.²³⁷ Improvements in terms of voltage and capacity were reported by Archer et al., who observed a capacity of 273 mAh/g for V_2O_5 nanowire cathodes at an average discharge voltage of 0.5 V with good cyclability (20 cycles) (Figure 40).²³⁴ This represents 62% of the theoretical capacity of V_2O_5 for Al^{3+} intercalation, which is estimated to be 442 mAh/g considering a three-electron transfer reaction. The battery electrolyte consisted of AlCl_3 dissolved in 1-ethyl-3-methylimidazolium chloride. However, no electrochemical activity was reported when the same cell was constructed utilizing an electrolyte of aluminum trifluoromethansulfonate dissolved in an aprotic liquid mixture of 1:1 PC:THF.

Use of amorphous V_2O_5 was reported by Chiku et al. with a similar discharge voltage vs Al/Al^{3+} .²³⁸ A capacity of 150 mAh/g with an operating voltage of 2.2 V for $\text{Mg}/\text{V}_2\text{O}_5$ cells was reported by Aurbach et al.,¹²³ thus, it appears that $\text{Mg}/\text{V}_2\text{O}_5$ cells polarize less severely than $\text{Al}/\text{V}_2\text{O}_5$ cells but also deliver lower specific cathode capacity. VO_2 nanowires were also cycled with AlCl_3 and 1-butyl-3-methylimidazolium chloride (1:1 molar ratio) ionic liquid electrolyte and an Al metal anode. Capacities of 116 mAh/g with an average voltage of 0.3 V were reported after 100 cycles. XPS analysis shows a one-electron reduction of V^{4+} to V^{3+} .²³⁹ V_2O_5 has also been extensively investigated as a cathode for magnesium batteries as indicated above and in section 2.2.1.2.1.

Other cathodes reported for aluminum batteries are conversion materials such as metal halides (Hg_2Cl_2 , AgBr , NiCl_2 , CuF_2 , and FeCl_3).²⁴⁰ These cathodes offer voltages slightly below 1 V with Al, but their solubility in the electrolyte results in direct reaction with the aluminum anode which limits cell cyclability. It is interesting to note that when the same class of cathode is utilized, the operating voltages of the aluminum and magnesium cells typically differ by more than the difference in reduction potentials of their metal anodes, possibly indicating increased polarization of Al vs Mg anodes and/or the cathodes in the Al cells. Other conversion cathode materials such as Ni_2S_3 and FeS_2 were also reported to discharge at voltages as high as 1.3 V vs Al/Al^{3+} .²⁴¹ Conductive polymers have also been studied as anion-insertion positive electrodes for secondary aluminum batteries in chloroaluminate ionic liquid electrolytes. For example, a polythiophene cathode discharged at 1.2 V vs Al/Al^{3+} with Coulombic efficiencies greater than 95% (50 cycles were reported).²⁴² Higher cell voltages were reported when a cathode material based on Cl-intercalated

carbon was utilized.²⁴³ In an electrolyte composed of 1.5:1 AlCl₃/1,2-dimethyl-3-propyl imidazolium chloride a discharge potential of 1.7 V was obtained; 100% depth of discharge was achieved in cathode-limited cells (150 cycles reported). Aluminum has a volumetric capacity three times higher than lithium, but in order for an aluminum battery to offer a substantially higher energy density than a lithium-ion battery, it requires the reversible transfer of three electrons between Al³⁺ and a single cathode metal center as well as a high operating voltage. This has not been reported to date.

5. CLOSING REMARKS

One of the greatest electrochemistry success stories in recent years has been the commercialization of the lithium-ion battery, which has changed the world we live in. Lithium-ion batteries now power cell phones, computers, power tools, and EVs. However, in order to develop an EV with a range and cost competitive with a conventional combustion engine vehicle, development of new high-energy, low-cost batteries will be desirable. This requirement has led to increasing interest and research and development activity in post-lithium-ion battery technologies. The major advantage of multivalent systems such as magnesium is a higher volumetric capacity and the apparent lack of dendrite formation during charging which overcomes major safety and performance challenges encountered with the use of a lithium metal anode. However, the nonaqueous and solid-state chemistry and electrochemistry of multivalent metals is substantially more complex than that of the monovalent alkali metals, which leads to greater difficulty in identifying and implementing a practical battery chemistry based on multivalent metals. As highlighted throughout this review, the major developments for a high-energy multivalent metal battery are rooted in material discovery of both high-voltage cathodes and electrolytes. The most significant issues for development of multivalent metal batteries include the compatibility of the electrolyte with both the anode and the cathode and the discovery of high-voltage cathodes capable of undergoing multiple electron transfers to the same metal center with rapid diffusion of the multivalent ion in the solid state. The opportunity to utilize cathode materials in nanostructured forms will help reduce the impact of slow solid-state diffusion as well as structural distortion during intercalation/deintercalation but also tends to reduce the volumetric capacity of the cathode structure. It is important to note that formation of passivation layers on the cathode by oxidation of the electrolyte might impede the search for cathodes capable of intercalating magnesium. Such trade-offs must be identified and optimized in the quest to develop practical rechargeable multivalent metal batteries.

AUTHOR INFORMATION

Corresponding Author

*Phone: 734-995-4403. E-mail: john.muldoon@tema.toyota.com.

Notes

The authors declare no competing financial interest.

Biographies



John Muldoon received his B.Sc. (Hons) degree in Chemistry from Queens University of Belfast. He completed his Ph.D degree at the University of Notre Dame under the direction of Professor Brown studying air oxidation of organics using terminal oxo complexes of late transition metals. He worked as Research Associate at The Scripps Research Institute under Professor Sharpless (Nobel Laureate in Chemistry 2001) and Professor Fokin, developing applications of click chemistry including in-situ click chemistry to discover HIV protease inhibitors and acceleration for chemical reactions on water. He is currently a principal scientist at Toyota Research Institute of North America. His research interests include future energy solutions such as multivalent batteries, lithium/sulfur batteries, Li-ion batteries, and fuel cells. He has numerous patents in the area of new battery chemistry and fuel cell.



Claudiu B. Bucur obtained his Ph.D degree in 2008 from Florida State University under the mentorship of Professor Schlenoff. He strived to understand the manner in which polyelectrolyte multilayers assemble and how doping them with ions changes their mechanical and thermodynamic properties. Several manuscripts and a book were published with his findings. In 2010 he completed postdoctoral studies at the USDA Agricultural Research Service, where he investigated corrosion inhibition by biomembranes. Currently, he is a research associate for the Post Lithium Ion Research Group at the Toyota Research Institute of North America. He is fascinated by energy storage, namely the synthesis and characterization of innovative materials for batteries with multivalent anodes or sulfur cathodes.



Thomas D. Gregory received his B.S. and M.S. degrees in Chemical Engineering in 1978 and 1979, respectively, from Case Western Reserve University. He spent 34 years in a variety of R&D roles at The Dow Chemical Co. in Midland, MI, retiring in 2013 as a Principal Research Scientist in Dow's Energy Materials Business. His work at Dow encompassed a wide variety of technology areas, including electrochemical engineering, process development and scale up, polymer processing, and process economic analysis. He is widely recognized for his pioneering work in rechargeable magnesium battery electrochemistry. He is currently the owner of Borealis Technology Solutions LLC and consults in the areas of electrochemical energy generation and storage and chemical and electrochemical process technology.

ACKNOWLEDGMENTS

We thank our colleagues and collaborators for their support: Dr. Gary D. Allred, Dr. Timothy S. Arthur, Dr. William C. Boggess, Dr. Jack Chen, Dr. Paul Fanson, Dr. Hideki Iba, Mr. Toshihiko Inoue, Mr. Yasutoshi Jagawa, Prof. Noboru Kikuchi, Dr. Hee Soo Kim, Dr. Angela Knapp, Mr. Yukinari Kotani, Mr. Takashi Kuzuya, Dr. Chen Ling, Dr. Masaki Matsui, Dr. Fuminori Mizuno, Dr. Rana Mohtadi, Dr. John G. Newman, Dr. Allen G. Oliver, Dr. Alexander E. Rodnyansky, Mr. Kazuaki Sato, Dr. Nikhilendra Singh, Mrs. Wei Song, Mr. Tsuyoshi Sugimoto, Dr. Kensuki Takechi, Dr. Oscar Tutusaus, Dr. Ruigang Zhang, and Dr. Jaroslav Zajicek. We dedicate this review to Professor Aurbach and Mr. Kazuaki Sato.

GLOSSARY

APC	1:2 AlCl ₃ –phenyl magnesium chloride
ACN	acetonitrile
BL	γ-butyrolactone
DMF	dimethylformamide
DMSO	dimethyl sulfoxide
DMSO ₂	dimethyl sulfone
THF	tetrahydrofuran
MF	methyl formate
NMP	<i>N</i> -methyl-2-pyrrolidone
PC	propylene carbonate
PAN	polyacrylonitrile
PEG	polyethylene glycol
PEO	poly(ethylene oxide)
PVDF	polyvinylidene fluoride
HFP	hexafluoropropylene
MWCNT	multiwall carbon nanotube
Z31	Mg alloy containing 3% Al and 1% Zn
Bu	butyl (C ₄ H ₉)
Et	ethyl (C ₂ H ₅)

Me	methyl (CH ₃)
Ph	phenyl (C ₆ H ₅)
TBA	tetrabutylammonium
EMI	ethyl methyl imidazolium
R	organic group (unspecified; typically alkyl or aryl)
T	chalcogen such as S or Se
X	halogen such as Cl or Br
DCC	Mg(AlCl ₂ BuEt) ₂
HMDS	hexamethyldisilazide
BARF	tetrakis[3,5-bis(trifluoromethyl)phenyl]borate
TFSI	trifluoromethane sulfonimide
GEN1	(Mg ₂ (μ-Cl) ₃ ·6THF)(HMDS _n AlCl _{4-n}) (<i>n</i> = 1, 2)
GEN2	(Mg ₂ (μ-Cl) ₃ ·6THF)(BPh ₄)
GEN3	(Mg ₂ (μ-Cl) ₃ ·6THF)[B(C ₆ F ₅) ₃ Ph]
RTIL	room-temperature ionic liquid
EPB	tthylopyridinium bromide
PLIB	post lithium-ion battery
SHE	standard hydrogen electrode
DOD	depth of discharge
EV	electric vehicle
ORTEP	Oak Ridge thermal ellipsoid plot
XANES	X-ray absorption near edge structure
XPS	X-ray photoelectron spectroscopy (also known as ESCA)
XRD	X-ray diffraction
EDS	energy-dispersive X-ray analysis
ICP-AES	inductively coupled plasma atomic emission spectroscopy
DFT	density functional theory
IEPCM	integral equation formalism polarizable continuum model
HOMO	highest occupied molecular orbital
LUMO	lowest unoccupied molecular orbital
OCV	open-circuit voltage
SEI	solid electrolyte interphase (or interface)
NBS	National Bureau of Standards (now NIST, National Institute of Standards and Technology)

REFERENCES

- (1) Armand, M.; Tarascon, J. M. *Nature* **2008**, *451*, 652.
- (2) Chan, C. K.; Peng, H.; Liu, G.; McIlwraith, K.; Zhang, X. F.; Huggins, R. A.; Cui, Y. *Nat. Nanotechnol.* **2008**, *3*, 31.
- (3) Scrosati, B.; Hassoun, J.; Sun, Y. K. *Energy Environ. Sci.* **2011**, *4*, 3287.
- (4) Toyota Motor Corp. Sustainability Report 2011 CP-1108-E, 2011.
- (5) Manthiram, A.; Fu, Y.; Su, Y. S. *Acc. Chem. Res.* **2013**, *46*, 1125.
- (6) Li, W.; Zheng, G.; Yang, Y.; Seh, Z. W.; Liu, N.; Cui, Y. *Proc. Natl. Acad. Sci. U.S.A.* **2013**, 201220992.
- (7) Bucur, C. B.; Muldoon, J.; Lita, A.; Schlenoff, J. B.; Ghostine, R. A.; Dietz, S.; Allred, G. *Energy Environ. Sci.* **2013**, *6*, 3286.
- (8) Bruce, P. G.; Freunberger, S. A.; Hardwick, L. J.; Tarascon, J. M. *Nat. Mater.* **2012**, *11*, 172.
- (9) Muldoon, J.; Bucur, C. B.; Oliver, A. G.; Sugimoto, T.; Matsui, M.; Kim, H. S.; Allred, G. D.; Zajicek, J.; Kotani, Y. *Energy Environ. Sci.* **2012**, *5*, 5941.
- (10) Crowther, O.; West, A. C. *J. Electrochem. Soc.* **2008**, *155*, A806.
- (11) Xu, K. *Chem. Rev.* **2004**, *104*, 4303.
- (12) Ding, F.; Xu, W.; Graff, G. L.; Zhang, J.; Sushko, M. L.; Chen, X.; Shao, Y.; Engelhard, M. H.; Nie, Z.; Xiao, J.; Liu, X.; Sushko, P. V.; Liu, J.; Zhang, J. G. *J. Am. Chem. Soc.* **2013**, *135*, 4450.
- (13) Aurbach, D.; Zinigrad, E.; Cohen, Y.; Teller, H. *Solid State Ionics* **2002**, *148*, 405.
- (14) Gireaud, L.; Grugeon, S.; Laruelle, S.; Yrieix, B.; Tarascon, J. M. *Electrochim. Commun.* **2006**, *8*, 1639.

- (15) Yamaki, J.; Tobishima, S.; Hayashi, K.; Saito, Keiichi; Nemoto, Y.; Arakawa, M. *J. Power Sources* **1998**, *74*, 219.
- (16) Thompson, R. S.; Schroeder, D. J.; López, C. M.; Neuhold, S.; Vaughey, J. T. *Electrochem. Commun.* **2011**, *13*, 1369.
- (17) Marchioni, F.; Star, K.; Menke, E.; Buffeteau, T.; Servant, L.; Dunn, B.; Wudl, F. *Langmuir* **2007**, *23*, 11597.
- (18) Muldoon, J.; Richard, M.; Stamm, K. L.; Nicolas, E. Method of Chemical Protection of Metal Surface. U.S. Patent 7,776,385, Aug 17, 2010.
- (19) Muldoon, J.; Richard, M.; Stamm, K. L.; Nicolas, E. E. Method of Chemical Protection of Metal Surface. U.S. Patent 8,383,190, Feb 26, 2013.
- (20) Aurbach, D.; Cohen, Y.; Moshkovich, M. *Electrochem. Solid-State Lett.* **2001**, *4*, A113.
- (21) Matsui, M. *J. Power Sources* **2011**, *196*, 7048.
- (22) Aurbach, D.; Gofer, Y.; Schechter, A.; Chusid, O.; Gizbar, H.; Cohen, Y.; Moshkovich, M.; Turgeman, R. *J. Power Sources* **2001**, *97–98*, 269.
- (23) Gaddum, L. W.; French, H. E. *J. Am. Chem. Soc.* **1927**, *49*, 1295.
- (24) Whittingham, M. S. *Chem. Rev.* **2004**, *104*, 4271.
- (25) Nyten, A.; Abouimrane, A.; Armand, M.; Gustafsson, T.; Thomas, J. O. *Electrochem. Commun.* **2005**, *7*, 156.
- (26) Ellis, B. L.; Makahnouk, W. R. M.; Makimura, Y.; Toghill, K.; Nazar, L. F. *Nat. Mater.* **2007**, *6*, 749.
- (27) Zhou, H.; Upadhyay, S.; Chernova, N. A.; Hautier, G.; Ceder, G.; Whittingham, M. S. *Chem. Mater.* **2011**, *23*, 293.
- (28) Islam, M. S.; Dominko, R.; Masquelier, C.; Sirisopanaporn, C.; Armstrong, A. R.; Bruce, P. G. *J. Mater. Chem.* **2011**, *21*, 9811.
- (29) Kozawa, A.; Yeager, J. F. *J. Electrochem. Soc.* **1965**, *112*, 959.
- (30) Xu, J. J.; Ye, H.; Huang, J. *Electrochem. Commun.* **2005**, *7*, 1309.
- (31) Kar, M.; Winther-Jensen, B.; Forsyth, M.; MacFarlane, D. R. *Phys. Chem. Chem. Phys.* **2013**, *15*, 7191.
- (32) Li, Y.; Gong, M.; Liang, Y.; Feng, J.; Kim, J. E.; Wang, H.; Hong, G.; Zhang, B.; Dai, H. *Nat. Commun.* **2013**, *4*, 1805.
- (33) Jolibois, P. C. R. *Chim.* **1912**, *155*, 353.
- (34) Jolibois, P. C. R. *Chim.* **1913**, *156*, 712.
- (35) Overcash, D. M.; Mathers, F. C. *Trans. Electrochem. Soc.* **1933**, *64*, 305.
- (36) Connor, J. H.; Reid, W. E.; Wood, G. B. *J. Electrochem. Soc.* **1957**, *104*, 38.
- (37) Brenner, A. *J. Electrochem. Soc.* **1971**, *118*, 99.
- (38) Genders, J. D.; Pletcher, D. *J. Electroanal. Chem. Interfacial Electrochem.* **1986**, *199*, 93.
- (39) Liebenow, C. *J. Appl. Electrochem.* **1997**, *27*, 221.
- (40) Feng, Z.; NuLi, Y.; Wang, J.; Yang, J. *J. Electrochem. Soc.* **2006**, *153*, C689.
- (41) Mohtadi, R.; Matsui, M.; Arthur, T. S.; Hwang, S. J. *Angew. Chem., Int. Ed.* **2012**, *51*, 9780.
- (42) Shiraga, M.; Sagane, F.; Miyazaki, K.; Fukutsuka, T.; Abe, T.; Nishio, K.; Uchimoto, Y. Electrochemical Behavior of Platinum Electrode in 2-Methyltetrahydrofuran Containing Magnesium Bromide. Presented at the 218th Meeting of The Electrochemical Society, Las Vegas, NV, 2010.
- (43) Abe, T.; Miyazaki, K.; Fukutsuka, T.; Nishio, K.; Uchimoto, Y. Fabrication of Ether-Based Electrolyte Solutions for Mg-Rechargeable Batteries. Presented at the 224th Meeting of The Electrochemical Society, San Francisco, CA, 2013.
- (44) Gregory, T. D.; Hoffman, R. J.; Winterton, R. C. *J. Electrochem. Soc.* **1990**, *137*, 775.
- (45) Mayer, A. *J. Electrochem. Soc.* **1990**, *137*, 2806.
- (46) Aurbach, D.; Weissman, I.; Gofer, Y.; Levi, E. *Chem. Rec.* **2003**, *3*, 61.
- (47) Vestfried, Y.; Chusid, O.; Goffer, Y.; Aped, P.; Aurbach, D. *Organometallics* **2007**, *26*, 3130.
- (48) Aurbach, D.; Suresh, G. S.; Levi, E.; Mitelman, A.; Mizrahi, O.; Chusid, O.; Brunelli, M. *Adv. Mater.* **2007**, *19*, 4260.
- (49) Gizbar, H.; Vestfrid, Y.; Chusid, O.; Gofer, Y.; Gottlieb, H. E.; Marks, V.; Aurbach, D. *Organometallics* **2004**, *23*, 3826.
- (50) Aurbach, D.; Gizbar, H.; Schechter, A.; Chusid, O.; Gottlieb, H. E.; Gofer, Y.; Goldberg, I. *J. Electrochem. Soc.* **2002**, *149*, A115.
- (51) Pour, N.; Gofer, Y.; Major, D. T.; Aurbach, D. *J. Am. Chem. Soc.* **2011**, *133*, 6270.
- (52) Kim, H. S.; Arthur, T. S.; Allred, G. D.; Zajicek, J.; Newman, J. G.; Rodnyansky, A. E.; Oliver, A. G.; Boggess, W. C.; Muldoon, J. *Nat. Commun.* **2011**, *2*, 427.
- (53) Liebenow, C.; Yang, Z.; Lobitz, P. *Electrochem. Commun.* **2000**, *2*, 641.
- (54) Arthur, T. S.; Glans, P. A.; Matsui, M.; Zhang, R.; Ma, B.; Guo, J. *Electrochem. Commun.* **2012**, *24*, 43.
- (55) Zhao-Karger, Z.; Zhao, X.; Fuhr, O.; Fichtner, M. *RSC Adv.* **2013**, *3*, 16330.
- (56) Doe, R. E.; Han, R.; Hwang, J.; Gmitter, A. J.; Shertenberg, I.; Yoo, H. D.; Pour, N.; Aurbach, D. *Chem. Commun.* **2013**, *50*, 243.
- (57) Liu, T.; Shao, Y.; Li, G.; Gu, M.; Hu, J.; Xu, S.; Nie, Z.; Chen, X.; Wang, C.; Liu, J. *J. Mater. Chem. A* **2013**.
- (58) Bochmann; Sarsfield, M. *J. Organometallics* **1998**, *17*, 5908.
- (59) Hocking, R. K.; Deeth, R. J.; Hambley, T. W. *Inorg. Chem.* **2007**, *46*, 8238.
- (60) Crystal data for $C_{48}H_{53}BCl_3F_{15}Mg_2O_6$; $M_r = 1176.68$; triclinic; space group $P\bar{1}$; $a = 13.2768(6)$ Å; $b = 16.0377(7)$ Å; $c = 24.4450(12)$ Å; $\alpha = 98.923(2)^\circ$; $\beta = 90.129(2)^\circ$; $\gamma = 91.139(2)^\circ$; $V = 5141.0(4)$ Å³; $Z = 4$; $T = 100(2)$ K; $\lambda(Cu\text{K}\alpha) = 1.54178$ Å; $\mu(Cu\text{K}\alpha) = 2.772$ mm⁻¹; $d_{\text{calcd}} = 1.520$ g·cm⁻³; 27 681 reflections collected; 14 674 unique ($R_{\text{int}} = 0.0449$), giving $R_1 = 0.0686$, $wR_2 = 0.1751$ for 10 002 data with [$I > 2\sigma(I)$] and $R_1 = 0.1037$, $wR_2 = 0.1970$ for all 14 674 data. Residual electron density ($e^{-}\cdot\text{\AA}^{-3}$) max/min 0.877/-0.397.
- (61) Guo, Y.; Zhang, F.; Yang, J.; Wang, F.; NuLi, Y.; Hirano, S. *Energy Environ. Sci.* **2012**, *5*, 9100.
- (62) Wang, F.; Guo, Y.; Yang, J.; Nuli, Y.; Hirano, S. *Chem. Commun.* **2012**, *48*, 10763.
- (63) Zhao, Q. S.; NuLi, Y. N.; Guo, Y. S.; Yang, J.; Wang, J. L. *Electrochim. Acta* **2011**, *56*, 6530.
- (64) Doe, R. E.; Blomgren, G. E.; Persson, K. A. Rechargeable Magnesium Ion Cell Components and Assembly. U.S. Patent Application 20110159381, June 30, 2011.
- (65) Lv, D.; Xu, T.; Saha, P.; Datta, M. K.; Gordin, M. L.; Manivannan, A.; Kumta, P. N.; Wang, D. *J. Electrochem. Soc.* **2013**, *160*, A351.
- (66) Yagi, S.; Tanaka, A.; Ichikawa, Y.; Ichitsubo, T.; Matsubara, E. *J. Electrochem. Soc.* **2013**, *160*, C83.
- (67) Muldoon, J.; Bucur, C. B.; Oliver, A. G.; Zajicek, J.; Allred, G. D.; Boggess, W. C. *Energy Environ. Sci.* **2013**, *6*, 482.
- (68) Nishida, H.; Takada, N.; Yoshimura, M.; Sonoda, T.; Kobayashi, H. *Bull. Chem. Soc. Jpn.* **1984**, *57*, 2600.
- (69) Yakelis, N. A.; Bergman, R. G. *Organometallics* **2005**, *24*, 3579.
- (70) Cheng, Y.; Liu, T.; Shao, Y.; Engelhard, M. H.; Liu, J.; Li, G. *J. Mater. Chem. A* **2014**, *2*, 2473.
- (71) Arthur, T. S.; Singh, N.; Matsui, M. *Electrochem. Commun.* **2012**, *16*, 103.
- (72) Shao, Y.; Gu, M.; Li, X.; Nie, Z.; Zuo, P.; Li, G.; Liu, T.; Xiao, J.; Cheng, Y.; Wang, C.; Zhang, J. G.; Liu, J. *Nano Lett.* **2014**, *14*, 255.
- (73) Singh, N.; Arthur, T. S.; Ling, C.; Matsui, M.; Mizuno, F. *Chem. Commun.* **2012**, *49*, 149.
- (74) Asaka, K.; Miyazaki, K.; Fukutuka, T.; Abe, T.; Niho, K.; Uchimoto, Y. MgBr₂/Ether-Based Electrolyte Solutions for Mg-Rechargeable Batteries. PRIME 2012; The Electrochemical Society Inc.: Honolulu, HI, Oct 8, 2012.
- (75) Fenton, D. E.; Parker, J. M.; Wright, P. V. *Polymer* **1973**, *14*, 589.
- (76) Vashishta, P.; Mundy, J. N.; Shenoy, G. K., Eds.; Proceedings of the International Conference on Fast Ion Transport in Solids, Electrodes, and Electrolytes, Lake Geneva, WI, USA, May 21–25, 1979, North Holland: New York, 1979.
- (77) Patrick, A.; Glassee, M.; Latham, R.; Linford, R. *Solid State Ion.* **1986**, *18–19* (Part 2), 1063.
- (78) Yang, L. L.; McGhie, A. R.; Farrington, G. C. *J. Electrochem. Soc.* **1986**, *133*, 1380.

- (79) Yang, L. L.; Huq, R.; Farrington, G. C.; Chiodelli, G. *Solid State Ionics* **1986**, *18–19* (Part 1), 291.
- (80) Martins, M. A. G.; Sequeira, C. A. C. *J. Power Sources* **1990**, *32*, 107.
- (81) Abraham, K. M.; Alamgir, M.; Hoffman, D. K. *J. Electrochem. Soc.* **1995**, *142*, 683.
- (82) Ikeda, S.; Mori, Y.; Furuhashi, Y.; Masuda, H.; Yamamoto, O. J. *Power Sources* **1999**, *81–82*, 720.
- (83) Masayuki Morita, N. Y. *Electrochim. Solid State Lett.* **2001**, *4*, A177.
- (84) Morita, M.; Shirai, T.; Yoshimoto, N.; Ishikawa, M. *J. Power Sources* **2005**, *139*, 351.
- (85) Saito, M.; Ikuta, H.; Uchimoto, Y.; Wakihara, M.; Yokoyama, S.; Yabe, T.; Yamamoto, M. *J. Electrochim. Soc.* **2003**, *150*, A477.
- (86) Saito, M.; Ikuta, H.; Uchimoto, Y.; Wakihara, M.; Yokoyama, S.; Yabe, T.; Yamamoto, M. *J. Electrochim. Soc.* **2003**, *150*, A726.
- (87) Saito, M.; Ikuta, H.; Uchimoto, Y.; Wakihara, M.; Yokoyama, S.; Yabe, T.; Yamamoto, M. *J. Phys. Chem. B* **2003**, *107*, 11608.
- (88) Di Noto, V.; Lavina, S.; Longo, D.; Vidali, M. *Electrochim. Acta* **1998**, *43*, 1225.
- (89) Di Noto, V.; Vittadello, M.; Pace, G.; Biscazzo, S.; Lavina, S. *Macromol. Chem. Phys.* **2002**, *203*, 1201.
- (90) Di Noto, V. *J. Phys. Chem. B* **2002**, *106*, 11139.
- (91) Piccolo, M.; Giffin, G. A.; Vezzù, K.; Bertasi, F.; Alotto, P.; Guarneri, M.; Di Noto, V. *ChemSusChem* **2013**, *6*, 2157.
- (92) Liebenow, C. *Electrochim. Acta* **1998**, *43*, 1253.
- (93) Liebenow, C. *Solid State Ionics* **2000**, *136–137*, 1211.
- (94) Liebenow, C.; Mantey, S. J. *Solid State Electrochem.* **2003**, *7*, 313.
- (95) Oh, J. S.; Ko, J. M.; Kim, D. W. *Electrochim. Acta* **2004**, *50*, 903.
- (96) Pandey, G. P.; Agrawal, R. C.; Hashmi, S. A. *J. Phys. Chem. Solids* **2011**, *72*, 1408.
- (97) Pandey, G. P.; Agrawal, R. C.; Hashmi, S. A. *J. Solid State Electrochem.* **2011**, *15*, 2253.
- (98) Pandey, G. P.; Hashmi, S. A. *J. Power Sources* **2009**, *187*, 627.
- (99) Aurbach, D.; Chasid, O.; Gofer, Y.; Gizbar, C. High Energy Rechargeable Electrochemical Cells. U.S. Patent 6,713,212, Mar 30, 2004.
- (100) Kumar, G. G.; Munichandraiah, N. *Electrochim. Acta* **1999**, *44*, 2663.
- (101) Kumar, G. G.; Munichandraiah, N. *Solid State Ionics* **2000**, *128*, 203.
- (102) Aurbach, D.; Skaletsky, R.; Gofer, Y. *J. Electrochim. Soc.* **1991**, *138*, 3536.
- (103) NuLi, Y.; Yang, J.; Wu, R. *Electrochim. Commun.* **2005**, *7*, 1105.
- (104) Cheek, G. T.; O’Grady, W. E.; Abedin, S. Z. E.; Moustafa, E. M.; Endres, F. J. *J. Electrochim. Soc.* **2008**, *155*, D91.
- (105) NuLi, Y.; Yang, J.; Wang, J.; Xu, J.; Wang, P. *Electrochim. Solid-State Lett.* **2005**, *8*, C166.
- (106) Yoshimoto, N.; Matsumoto, M.; Egashira, M.; Morita, M. *J. Power Sources* **2010**, *195*, 2096.
- (107) Kakibe, T.; Yoshimoto, N.; Egashira, M.; Morita, M. *Electrochim. Commun.* **2010**, *12*, 1630.
- (108) Kakibe, T.; Hishii, J.; Yoshimoto, N.; Egashira, M.; Morita, M. *J. Power Sources* **2012**, *203*, 195.
- (109) Venkata Narayanan, N. S.; Ashok Raj, B. V.; Sampath, S. *Electrochim. Commun.* **2009**, *11*, 2027.
- (110) Khoo, T.; Howlett, P. C.; Tsagouria, M.; MacFarlane, D. R.; Forsyth, M. *Electrochim. Acta* **2011**, *58*, 583.
- (111) Higashi, S.; Miwa, K.; Aoki, M.; Takechi, K. *Chem. Commun.* **2014**, *50*, 1320.
- (112) Aubrey, M. L.; Ameloot, R.; Wiers, B. M.; Long, J. R. *Energy Environ. Sci.* **2014**.
- (113) Bruce, P. G.; Krok, F.; Nowinski, J.; Gibson, V. C.; Tavakkoli, K. *J. Mater. Chem.* **1991**, *1*, 705.
- (114) Novák, P.; Desilvestro, J. *J. Electrochim. Soc.* **1993**, *140*, 140.
- (115) Novák, P.; Scheifele, W.; Haas, O. *J. Power Sources* **1995**, *54*, 479.
- (116) Novák, P.; Scheifele, W.; Joho, F.; Haas, O. *J. Electrochim. Soc.* **1995**, *142*, 2544.
- (117) Novák, P.; Imhof, R.; Haas, O. *Electrochim. Acta* **1999**, *45*, 351.
- (118) Yu, L.; Zhang, X. *J. Colloid Interface Sci.* **2004**, *278*, 160.
- (119) Jiao, L. F.; Yuan, H. T.; Si, Y. C.; Wang, Y. J.; Wang, Y. M. *Electrochim. Commun.* **2006**, *8*, 1041.
- (120) Amatucci, G. G.; Badway, F.; Singhal, A.; Beaudoin, B.; Skandan, G.; Bowmer, T.; Plitz, I.; Pereira, N.; Chapman, T.; Jaworski, R. *J. Electrochim. Soc.* **2001**, *148*, A940.
- (121) Le, D. B.; Passerini, S.; Coustier, F.; Guo, J.; Soderstrom, T.; Owens, B. B.; Smyrl, W. H. *Chem. Mater.* **1998**, *10*, 682.
- (122) Yoshimoto, N.; Yakushiji, S.; Ishikawa, M.; Morita, M. *Electrochim. Acta* **2003**, *48*, 2317.
- (123) Gershinsky, G.; Yoo, H. D.; Gofer, Y.; Aurbach, D. *Langmuir* **2013**, *29*, 10964.
- (124) Inamoto, M.; Kurihara, H.; Yajima, T. *Materials* **2013**, *6*, 4514.
- (125) Kumar, G. G.; Munichandraiah, N. *J. Power Sources* **2000**, *91*, 157.
- (126) Girish Kumar, G.; Munichandraiah, N. *Electrochim. Acta* **2002**, *47*, 1013.
- (127) Rasul, S.; Suzuki, S.; Yamaguchi, S.; Miyayama, M. Microstructural Effects on the Mg-ion Intercalation Mechanism in MnO_2 /Acetylene Black Composite Cathodes for Magnesium-ion Rechargeable Batteries. Presented at the 220th Meeting of the Electrochemical Society, Boston, MA, 2011.
- (128) Rasul, S.; Suzuki, S.; Yamaguchi, S.; Miyayama, M. *Solid State Ionics* **2012**, *225*, 542.
- (129) Zhang, R.; Yu, X.; Nam, K. W.; Ling, C.; Arthur, T. S.; Song, W.; Knapp, A. M.; Ehrlich, S. N.; Yang, X. Q.; Matsui, M. *Electrochim. Commun.* **2012**, *23*, 110.
- (130) Sánchez, L.; Pereira-Ramos, J. P. *J. Mater. Chem.* **1997**, *7*, 471.
- (131) Spahr, M. E.; Novák, P.; Haas, O.; Nesper, R. *J. Power Sources* **1995**, *54*, 346.
- (132) KochV. R.NanjundiahC.OrsiniM.Rechargeable Magnesium Power Cells, NASA Technical Support Package MSC-22293; National Aeronautics and Space Administration: Houston, TX, 1995.
- (133) Sutto, T. E.; Duncan, T. T. *Electrochim. Acta* **2012**, *79*, 170.
- (134) Sutto, T. E.; Duncan, T. T. *Electrochim. Acta* **2012**, *80*, 413.
- (135) Kamioka, N.; Ichitsubo, T.; Uda, T.; Imashuku, S.; Taninouchi, Y.; Matsubara, E. *Mater. Trans.* **2008**, *49*, 824.
- (136) Ichitsubo, T.; Adachi, T.; Yagi, S.; Doi, T. *J. Mater. Chem.* **2011**, *21*, 11764.
- (137) <http://www.predmaterials.com/products/3478/magnesium-complex-oxide-magnesium-ion-battery> (accessed July 5, 2014).
- (138) Mitelman, A.; Levi, M. D.; Lancry, E.; Levi, E.; Aurbach, D. *Chem. Commun.* **2007**, *41*, 4212.
- (139) Levi, E.; Gofer, Y.; Vestfreed, Y.; Lancry, E.; Aurbach, D. *Chem. Mater.* **2002**, *14*, 2767.
- (140) Aurbach, D.; Lu, Z.; Schechter, A.; Gofer, Y.; Gizbar, H.; Turgeman, R.; Cohen, Y.; Moshkovich, M.; Levi, E. *Nature* **2000**, *407*, 724.
- (141) Aurbach, D.; Weissman, I.; Gofer, Y.; Levi, E. *Chem. Rec.* **2003**, *3*, 61.
- (142) Levi, M. D.; Lancry, E.; Gizbar, H.; Lu, Z.; Levi, E.; Gofer, Y.; Aurbach, D. *J. Electrochim. Soc.* **2004**, *151*, A1044.
- (143) Suresh, G. S.; Levi, M. D.; Aurbach, D. *Electrochim. Acta* **2008**, *53*, 3889.
- (144) Lancry, E.; Levi, E.; Gofer, Y.; Levi, M. D.; Aurbach, D. *J. Solid State Electrochim. Acta* **2005**, *9*, 259.
- (145) Woan, K. V.; Scheffler, R. H.; Bell, N. S.; Sigmund, W. M. *J. Mater. Chem.* **2011**, *21*, 8537.
- (146) Gofer, Y.; Chusid, O.; Gizbar, H.; Viestfrid, Y.; Gottlieb, H. E.; Marks, V.; Aurbach, D. *Electrochim. Solid-State Lett.* **2006**, *9*, A257.
- (147) Levi, E.; Gofer, Y.; Aurbach, D. *Chem. Mater.* **2010**, *22*, 860.
- (148) Liang, Y.; Feng, R.; Yang, S.; Ma, H.; Liang, J.; Chen, J. *Adv. Mater.* **2011**, *23*, 640.
- (149) Liu, Y.; Jiao, L.; Wu, Q.; Du, J.; Zhao, Y.; Si, Y.; Wang, Y.; Yuan, H. *J. Mater. Chem. A* **2013**, *1*, 5822.
- (150) Tao, Z. L.; Xu, L. N.; Gou, X. L.; Chen, J.; Yuan, H. T. *Chem. Commun.* **2004**, *18*, 2080.
- (151) Yuan, W.; Günter, J. R. *Solid State Ionics* **1995**, *76*, 253.

- (152) Liu, B.; Luo, T.; Mu, G.; Wang, X.; Chen, D.; Shen, G. *ACS Nano* **2013**, *7*, 8051.
- (153) Amir, N.; Vestfrid, Y.; Chusid, O.; Gofer, Y.; Aurbach, D. J. *Power Sources* **2007**, *174*, 1234.
- (154) NuLi, Y.; Yang, J.; Wang, J.; Li, Y. *J. Phys. Chem. C* **2009**, *113*, 12594.
- (155) NuLi, Y.; Yang, J.; Li, Y.; Wang, J. *Chem. Commun.* **2010**, *46*, 3794.
- (156) Alman, D. New High Energy Density Mg Battery Concepts for Stationary Power Electrical Grids. Presented at the *25th Annual Conference on Fossil Energy Materials*, U.S. Department of Energy: Portland, OR, 2011.
- (157) Ling, C.; Banerjee, D.; Song, W.; Zhang, M.; Matsui, M. J. *Mater. Chem.* **2012**, *22*, 13517.
- (158) Zheng, Y.; NuLi, Y.; Chen, Q.; Wang, Y.; Yang, J.; Wang, J. *Electrochim. Acta* **2012**, *66*, 75.
- (159) Li, Y.; Nuli, Y.; Yang, J.; Yilinuer, T.; Wang, J. *Chin. Sci. Bull.* **2011**, *56*, 386.
- (160) Makino, K.; Katayama, Y.; Miura, T.; Kishi, T. *J. Power Sources* **2001**, *99*, 66.
- (161) Makino, K.; Katayama, Y.; Miura, T.; Kishi, T. *J. Power Sources* **2001**, *97*, 512.
- (162) Makino, K.; Katayama, Y.; Miura, T.; Kishi, T. *J. Power Sources* **2002**, *112*, 85.
- (163) Makino, K.; Katayama, Y.; Miura, T.; Kishi, T. Electrochemical Magnesium Insertion to $A_{0.5}Ti_2(PO_4)_3$ ($A = Mg, Ca, Sr, Ba$). Presented at the *200th Meeting of The Electrochemical Society*, San Francisco, CA, 2011.
- (164) Kong, Y.; Wang, C.; Yang, Y.; Too, C. O.; Wallace, G. G. *Synth. Met.* **2012**, *162*, 584.
- (165) NuLi, Y.; Guo, Z.; Liu, H.; Yang, J. *Electrochim. Commun.* **2007**, *9*, 1913.
- (166) Yu, L.; Wang, X.; Li, J.; Jing, X.; Wang, F. *J. Electrochim. Soc.* **1999**, *146*, 1712.
- (167) Oyama, N.; Pope, J. M.; Sotomura, T. *J. Electrochim. Soc.* **1997**, *144*, L47.
- (168) Dhakshinamoorthy, A.; Alvaro, M.; Garcia, H. *Chem. Commun.* **2010**, *46*, 6476.
- (169) Chen, Q.; NuLi, Y. N.; Guo, W.; Yang, J.; Wang, J. L.; Guo, Y. G. *Acta Phys. Chim. Sin.* **2013**, *29*, 2295.
- (170) Sano, H.; Senoh, H.; Yao, M.; Sakaebe, H.; Kiyobayashi, T. *Chem. Lett.* **2012**, *41*, 1594.
- (171) Sharon, D.; Etacheri, V.; Garsuch, A.; Afri, M.; Frimer, A. A.; Aurbach, D. *J. Phys. Chem. Lett.* **2013**, *4*, 127.
- (172) McCloskey, B. D.; Speidel, A.; Scheffler, R.; Miller, D. C.; Viswanathan, V.; Hummelshøj, J. S.; Nørskov, J. K.; Luntz, A. C. J. *Phys. Chem. Lett.* **2012**, *3*, 997.
- (173) Peng, Z.; Freunberger, S. A.; Chen, Y.; Bruce, P. G. *Science* **2012**, *337*, 563.
- (174) Jung, H. G.; Hassoun, J.; Park, J. B.; Sun, Y. K.; Scrosati, B. *Nat. Chem.* **2012**, *4*, 579.
- (175) Shiga, T.; Hase, Y.; Kato, Y.; Inoue, M.; Takechi, K. *Chem. Commun.* **2013**, *49*, 9152.
- (176) Chilton, J. E. J. *New Cathode-anode Couples Using Nonaqueous Electrolytes*; Flight Accessories Laboratory, Aeronautical Systems Division, Air Force Systems Command, United States Air Force: Dayton, OH, 1962.
- (177) Giraudet, J.; Claves, D.; Guérin, K.; Dubois, M.; Houdayer, A.; Masin, F.; Hamwi, A. *J. Power Sources* **2007**, *173*, 592.
- (178) Gregory, T. D.; Hoffman, R. J. Electrochemical Generator Utilizing Solid Polymer-Salt Complex. U.S. Patent 4,702,974, Oct 27, 1987.
- (179) Uhler, E. F. Investigation of new cathode-anode couples for secondary batteries using molten salt electrolytes. U.S. Air Force Systems Command Technical Documentary Report ASD-TDR-63-115, Jan 1963.
- (180) Meitav, A.; Peled, E. *J. Electrochim. Soc.* **1982**, *129*, 451.
- (181) Babai, M.; Pallivathikal, M. *J. Power Sources* **1989**, *28*, 325.
- (182) Peled, E.; Meitav, A.; Brand, M. *J. Electrochim. Soc.* **1981**, *128*, 1936.
- (183) Staniewicz, R. J. *J. Electrochim. Soc.* **1980**, *127*, 782.
- (184) Derrington, C. E.; Lindner, A.; O'Keeffe, M. *J. Solid State Chem.* **1975**, *15*, 171.
- (185) Walker, C. W., Jr.; Wade, W. L., Jr.; Binder, M. *J. Power Sources* **1989**, *25*, 187.
- (186) Wade, W. L., Jr.; Walker, C. W., Jr.; Binder, M. *J. Power Sources* **1989**, *28*, 295.
- (187) Peled, E.; Elster, E.; Kimel, J.; Brand, M. *Electrochemical Cells*. U.K. Patent GB2187590, Jan 10, 1990.
- (188) Peled, E.; Straze, H. *J. Electrochim. Soc.* **1977**, *124*, 1030.
- (189) Meitav, A.; Peled, E. *J. Electrochim. Soc.* **1981**, *128*, 825.
- (190) Lehmkuhl, H.; Mehler, K.; Landau, U. In *Advances in Electrochemical Science and Engineering*; Gerischer, H.; Tobias, C. W., Eds.; Wiley-VCH Verlag GmbH: Weinheim, Germany, 2008; pp 163–226.
- (191) Yoo, H. D.; Shterenberg, I.; Gofer, Y.; Gershinsky, G.; Pour, N.; Aurbach, D. *Energy Environ. Sci.* **2013**, *6*, 2265.
- (192) Westerhausen, M.; Gärtner, M.; Fischer, R.; Langer, J.; Yu, L.; Reiher, M. *Chem. Eur. J.* **2007**, *13*, 6292.
- (193) Fischer, R.; Gärtner, M.; Görsls, H.; Westerhausen, M. *Organometallics* **2006**, *25*, 3496.
- (194) Fischer, R.; Gärtner, M.; Görsls, H.; Westerhausen, M. *Angew. Chem., Int. Ed.* **2006**, *45*, 609.
- (195) Tsuchida, T.; Nakanishi, M.; Takayanagi, H.; Yamamoto, K. *Proceedings of the 2nd Battery Material Symposium*, Graz, Austria, International Battery Material Association: Strongsville, OH, 1985, p 417.
- (196) Hulot, M. R. *Acad. Sci.* **1855**, *40*, 148.
- (197) Tomassi, D. In *Traité des Piles Électriques*; George Carré: Paris, 1889; p 131.
- (198) Sargent, D. E. Voltaic Cell. U.S. Patent 2,554,447, May 22, 1951.
- (199) Ruben, S. Primary Cell. U.S. Patent 2,638,489, May 12, 1953.
- (200) Stokes, J. J., Jr. Primary Cell Anode. U.S. Patent 2,796,456, June 18, 1957.
- (201) Stokes, J. J., Jr. Primary Cell. U.S. Patent 2,838,591, June 10, 1958.
- (202) Stokes, J. J., Jr. Primary Cell. U.S. Patent 3,307,976, March 7, 1967.
- (203) Li, Q.; Bjerrum, N. *J. J. Power Sources* **2002**, *110*, 1.
- (204) Bockstie, L.; Trevethan, D.; Zaromb, S. *J. Electrochim. Soc.* **1963**, *110*, 267.
- (205) Zaromb, S. *J. Electrochim. Soc.* **1962**, *109*, 1125.
- (206) Voelcker, J. Phinergy 1000-Mile Aluminum-Air Battery: On The Road In 2017? http://www.greencarreports.com/news/1083111_phinergy-1000-mile-aluminum-air-battery-on-the-road-in-2017 (accessed Sept 24, 2013).
- (207) Zhao, Y.; VanderNoot, T. *J. Electrochim. Acta* **1997**, *42*, 3.
- (208) Plotnikov, V. A. *J. Russ. Phys. Chem. Soc.* **1899**, *31*, 1020.
- (209) Brown, H. C.; Wallace, W. J. *J. Am. Chem. Soc.* **1953**, *75*, 6265.
- (210) Eley, D. D.; King, P. J. *J. Chem. Soc.* **1952**, 2517.
- (211) Peled, E.; Gileadi, E. *J. Electrochim. Soc.* **1976**, *123*, 15.
- (212) Simanavicius, L. E.; Dobrovoskis, P. P. *Issled. Obe. Elektroosazhd. Met.* **1971**, *2*, 192.
- (213) Simanavicius, L. E., Dobrovoskis, P. P. USSR Patent 382,761, 1972.
- (214) Simanavicius, L. E. *Chemija* **1990**, *178*, 3.
- (215) Gálová, M. *Surf. Technol.* **1980**, *11*, 357.
- (216) Couch, D. E.; Brenner, A. *J. Electrochim. Soc.* **1952**, *99*, 234.
- (217) Brenner, A.; Couch, D. E. Electrodeposition of Aluminum from Nonaqueous Solutions. U.S. Patent 2,651,608, Sept 8, 1953.
- (218) Ishibashi, N.; Yoshio, M. *Electrochim. Acta* **1972**, *17*, 1343.
- (219) Yoshio, M.; Ishibashi, N. *J. Appl. Electrochim.* **1973**, *3*, 321.
- (220) Pereira-Ramos, J. P.; Messina, R.; Perichon, J. *J. Electroanal. Chem. Interfacial Electrochim.* **1986**, *209*, 283.
- (221) Legrand, L.; Tranchant, A.; Messina, R. *Electrochim. Acta* **1994**, *39*, 1427.

- (222) Legrand, L.; Tranchant, A.; Messina, R. *J. Electrochem. Soc.* **1994**, *141*, 378.
- (223) Hurley, F. H.; Wier, T. P. Electrodeposition of Aluminum. U.S. Patent 2,446,349, Aug 3, 1948.
- (224) Hurley, F. H.; Wier, T. P. *J. Electrochem. Soc.* **1951**, *98*, 203.
- (225) Gale, R. J.; Osteryoung, R. A. *Inorg. Chem.* **1979**, *18*, 1603.
- (226) Gale, R. J.; Osteryoung, R. A. *J. Electrochem. Soc.* **1980**, *127*, 2167.
- (227) Robinson, J.; Osteryoung, R. A. *J. Am. Chem. Soc.* **1979**, *101*, 323.
- (228) Robinson, J.; Osteryoung, R. A. *J. Am. Chem. Soc.* **1980**, *102*, 4415.
- (229) Wilkes, J. S.; Hussey, C. L. The Frank J. Seiler Research Laboratory Technical Report; FJSRL-TR-820002; 1982.
- (230) Wilkes, J.S.; Leviski, J. A.; Hussey, C. L.; Druelinger, M. Abstract 648, *158th Meeting of the Electrochemical Society*, Hollywood, FL; The Electrochemical Society: Pennington, NJ, 1980.
- (231) Jones, S. D.; Blomgren, G. E. *J. Electrochem. Soc.* **1989**, *136*, 424.
- (232) Jiang, T.; Chollier Brym, M. J.; Dubé, G.; Lasia, A.; Brisard, G. M. *Surf. Coat. Technol.* **2006**, *201*, 1.
- (233) Simka, W.; Puszczyk, D.; Nawrat, G. *Electrochim. Acta* **2009**, *54*, 5307.
- (234) Jayaprakash, N.; Das, S. K.; Archer, L. A. *Chem. Commun.* **2011**, *47*, 12610.
- (235) Schaltin, S.; Ganapathi, M.; Binnemans, K.; Fransaer, J. *J. Electrochem. Soc.* **2011**, *158*, D634.
- (236) Biagini, P.; Luigli, G.; Andeussi, P.; Abis, L. Organometallic Derivatives of Group IIIA and Process for their Preparation. U.S. Patent 5,602,269, Feb. 11, 1997.
- (237) Rogosic, J.; Sadoway, D. R. Experimental Considerations Involving Aluminum and Beryllium Battery Development. Presented at the *224th Meeting of The Electrochemical Society*, San Francisco, CA, 2013.
- (238) Chiku, M.; Takeda, H.; Kunisawa, T.; Higuchi, E.; Inoue, H. Construction of Aluminum Rechargeable Batteries and Investigation of their Positive Electrode Materials. Presented at the *224th Meeting of The Electrochemical Society*, San Francisco, CA, 2013.
- (239) Wang, W.; Jiang, B.; Xiong, W.; Sun, H.; Lin, Z.; Hu, L.; Tu, J.; Hou, J.; Zhu, H.; Jiao, S. *Sci. Rep.* **2013**, *3*, 3383.
- (240) Donahue, F. M.; Mancini, S. E.; Simonsen, L. *J. Appl. Electrochem.* **1992**, *22*, 230.
- (241) Hjuler, H. A.; Winbush, S.; von Berg, R. W.; Bjerrum, N. *J. J. Electrochem. Soc.* **1989**, *136*, 901.
- (242) Hudak, N.; Ingersoll, D. Conductive Polymers as Positive Electrodes in Rechargeable Aluminum Batteries. Presented at the *222nd Meeting of The Electrochemical Society*, Toronto, Canada, 2013.
- (243) Gifford, P. R.; Palmisano, J. B. *J. Electrochem. Soc.* **1988**, *135*, 650.